

ÉCOLE DE TECHNOLOGIE SUPÉRIEURE
UNIVERSITÉ DU QUÉBEC

DISSERTATION PRESENTED TO
ÉCOLE DE TECHNOLOGIE SUPÉRIEURE

IN PARTIAL FULFILLMENT OF THE REQUIREMENTS FOR
A MASTER'S DEGREE IN MECHANICAL ENGINEERING
M. Eng.

BY
Roger GARCIA BARCELÓ

MESH SENSITIVITY ANALYSIS ON WIND FARMS USING CFD WIND FLOW
MODELS AND CFD WAKE MODELS

MONTREAL, AUGUST 28 2012



Roger Garcia Barceló 2012



This Creative Commons license allows readers to download this work and share it with others as long as the author is credited. The content of this work cannot be modified in any way or used commercially.

BOARD OF EXAMINERS

THIS THESIS HAS BEEN EVALUATED

BY THE FOLLOWING BOARD OF EXAMINERS :

Mr. Christian Masson, Thesis director
Département de génie mécanique à l'École de technologie supérieure

Mr. Daniel Cabezón Martinez, Thesis Co-director
National Renewable Energy Center of Spain (CENER)

Mr. Robert Benoit, Committee President
Département de génie mécanique à l'École de technologie supérieure

Mr. Louis Dufresne, Examiner
Département de génie mécanique à l'École de technologie supérieure

THIS THESIS WAS PRESENTED AND DEFENDED

IN THE PRESENCE OF A BOARD OF EXAMINERS AND PUBLIC

ON JULY 23 2012

AT ÉCOLE DE TECHNOLOGIE SUPÉRIEURE

ACKNOWLEDGEMENTS

This Master thesis was carried out within the Canada Research Chair on the Nordic Environment Aerodynamics of Wind turbines at the Mechanical Engineering Department of ÉTS, in Montréal, Canada and at the Wind Energy Department of the National Renewable Energy Centre (CENER), in Madrid, Spain. The project was supervised by Christian Masson, Chair holder and professor at ÉTS and Daniel Cabezón, CFD wind engineer at CENER.

I owe my deepest gratitude to Christian Masson for his confidence in me and my project from the beginning, for his valuable advices and for guiding me during the difficult first year of the project. I would like to specially thank Daniel Cabezón for his confidence too, his infinite patience and for having solved all my daily doubts. I do not want to forget professor Alan Carter for giving me the opportunity of working at LCMB parallely with my master project. I would also have a thank you for all the members of the Chair research students at ÉTS and CENER members at the office of Madrid for creating a great work ambience. Specially thank to Jonathon Sumner and Nicolas Lussier for having shared their knowledge on OpenFOAM with me and Mohammadreza Majlesi for having shared complete days working and talking at ÉTS. Thanks for that incredible iranian dinner with your wife. That was a wonderful experience!

I am grateful to Anne Réglain, Sylvain Fléchais and specially to Joan Hereter, friends and roommates for their incredible daily support and encouragement during tough times. Moltes gràcies, merci beaucoup!

Last but not least I would like to thank Laura, my parents Conrad and Montserrat and my sister Núria for the tranquility they have transmit me over the last two years. Without this oasis of calm and energy, this thesis would not have been possible. Gràcies a tots quatre!

ANALYSE DE SENSIBILITÉ DE MAILLAGE POUR LA MODÉLISATION DE PARCS ÉOLIENS

Roger GARCIA BARCELÓ

RÉSUMÉ

Actuellement, les énergies renouvelables semblent prendre au jour le jour plus de poids dans les politiques énergétiques actuelles. Entre les multiples formes, l'énergie éolienne, ayant une grande présence de nos jours, est celle qui présente des prévisions de majeure croissance lors des prochaines décennies.

Un outil très efficace pour la prédiction de la ressource éolienne sont les simulations CFD. Cette technique permet de résoudre les équations qui gouvernent le mouvement d'écoulement en tenant compte des effets de recirculation et de séparation. Evidemment, les résultats d'une simulation CFD pour la prédiction de la ressource éolienne dépendent de la modélisation que l'on effectue mais aussi du maillage.

Le maillage du domaine d'étude doit être le résultat d'une fonction optimisée tenant en compte deux paramètres: la qualité des résultats et les coûts de simulation. Visant cette fonction, deux analyses de sensibilité de maillage à travers une batterie de cas. Les paramètres géométriques visés sont la résolution des différentes zones d'études, l'extension des zones, hauteur du domaine, etc.

L'objectif principal est de recommander un guide de paramètres de maillage aux usagers de CFDWind1.0 lors de l'étude de l'écoulement du vent en CFD sur terrain complexe puis off-shore, tout en ayant atteint la convergence de maillage. Les résultats obtenus lors du maillage en terrain complexe sont très satisfaisant alors que lors de l'étude de l'écoulement en sillage, la modélisation doit être améliorée. Plusieurs voies d'amélioration sont proposées en visant des futures études.

Mots-clés: Modèles de vent CFD, modèles de sillage CFD, Analyse de sensibilité, OpenFOAM

MESH SENSITIVITY ANALYSIS ON WIND FARMS USING CFD WIND FLOW MODELS AND CFD WAKE MODELS

Roger GARCIA BARCELÓ

ABSTRACT

In the present framework, renewables seem to take every day more weight in the current energy policies. Among many types, wind energy, has already a great presence within green energies with great perspectives for the coming decades.

A very effective tool for wind resource estimation is computational fluid dynamics (CFD). This technique solves the flow motion governing equations taking into account the recirculation effects and flow separation. Obviously, CFD results depend not only on modeling set up but also on achieving mesh independance.

Meshing the computational domain must be the result of an optimized function taking into account two parameters: results accuracy and computational costs. In order to optimize the mesh, two sensitivity analysis are done through different battery cases. The geometrical parameters defining the mesh such as horizontal resolution, expansion of the different areas, height of the computational domain among others are analyzed.

The main objective is to furnish a guideline of meshing parameters for CFDWind1.0 users through studies of wind flow over complex terrain and offshore. The results obtained over complex terrain shown very good accuracy and the grid geometry is optimized enough. Nevertheless, for wake model studies, the current modelisation can be improved and some further works are proposed.

Keywords: CFD wind flow model,CFD wake model, Mesh sensitivity analysis, OpenFOAM, grid independence

TABLE OF CONTENTS

| | Page |
|---|------|
| INTRODUCTION | 1 |
| CHAPTER 1 LITERATURE REVIEW | 5 |
| 1.1 Atmospheric and Surface Boundary Layer | 5 |
| 1.2 Numerical modelling | 6 |
| 1.2.1 Governing Equations | 6 |
| 1.2.2 Turbulence modelling | 8 |
| 1.2.2.1 Description and characteristics | 8 |
| 1.2.2.2 RANS models: $k - \epsilon$ | 9 |
| 1.2.2.3 More Turbulence Models | 10 |
| 1.2.3 Wind flow model: CFDWind 1.0 | 12 |
| 1.2.3.1 General Features | 12 |
| 1.2.3.2 Boundary conditions | 12 |
| 1.3 CFD software: OpenFOAM 1.7.1 | 19 |
| 1.3.1 Execution of OpenFOAM | 20 |
| 1.3.2 Selected solver (from the options offered by OpenFOAM) | 20 |
| 1.3.3 Selected turbulence model (from the options offered by OpenFOAM) .. | 22 |
| CHAPTER 2 THE BOLUND EXPERIMENT: BLIND COMPARISON OF FLOW MOD- ELS | 23 |
| 2.1 The experiment setup | 23 |
| 2.2 The blind comparison | 24 |
| 2.3 Computational domain | 25 |
| 2.4 Verification of CFDWind1 using OpenFOAM 1.7 | 26 |
| 2.4.1 Graphics | 27 |
| 2.4.2 Errors and discussion | 29 |
| CHAPTER 3 MESH SENSITIVITY ANALYSIS OF CFD WIND FLOW MODEL FOR COMPLEX TERRAIN | 31 |
| 3.1 Definition and choice of the Sensitivity Analysis Method | 31 |
| 3.2 Test case | 33 |
| 3.3 Sensitivity Analysis | 35 |
| 3.3.1 Base case | 35 |
| 3.3.2 Other cases | 37 |
| 3.4 Sensitivity results | 38 |
| 3.4.1 Criteria | 38 |
| 3.4.2 Average relative error | 39 |
| 3.4.3 Discussion on the selection of input parameters | 39 |

| | | |
|--|---|----|
| 3.5 | Validation results..... | 48 |
| CHAPTER 4 MESH SENSITIVITY ANALYSIS OF CFD WAKE MODEL OVER OFFSHORE WIND FARM | | |
| 4.1 | Offshore wind farms: Advantages and disadvantages | 53 |
| 4.2 | Horns Rev Wind Farm..... | 54 |
| 4.3 | Computational Domain..... | 55 |
| 4.4 | Limitations of the numerical model and <i>simpleWindFoam</i> solver..... | 55 |
| | 4.4.1 Actuator Disk Model..... | 56 |
| | 4.4.2 Iterative algorithm of <i>simpleWindFoam</i> | 57 |
| 4.5 | Sensitivity Analysis..... | 58 |
| | 4.5.1 Base case | 58 |
| | 4.5.2 Other cases | 60 |
| 4.6 | Sensitivity results | 60 |
| | 4.6.1 Discussion on the selection of input parameters..... | 61 |
| 4.7 | Validation results..... | 67 |
| CONCLUSION..... | | 69 |
| APPENDIX I | FOLDERS STRUCTURE FOR AN ABL SIMULATION USING <i>SIM- PLEFOAM</i> SOLVER | 73 |
| APPENDIX II | WINDMESH | 77 |
| APPENDIX III | RESULTS I: MESH CONVERGENCE OF CFDWIND1 FOR COM- PLEX TERRAIN. WIND SPEED RATIOS AT WIND TURBINE PO- SITIONS..... | 81 |
| APPENDIX IV | RESULTS II: MESH CONVERGENCE OF CFDWAKE1 FOR OFF- SHORE. WIND SPEED RATIOS AT REFERENCE POSITIONS (U_{REF}) FOR THE CENTRAL ROW | 87 |

LIST OF TABLES

| | Page |
|-----------|--|
| Table 2.1 | Physics parameters for Bolund experiment 25 |
| Table 2.2 | Speed-up percentage error 29 |
| Table 2.3 | Normalized TKE percentage error 29 |
| Table 3.1 | Table for Sensitivity Analysis of Wind Flow Model over complex terrain.... 37 |
| Table 3.2 | Results of Sensitivity Analysis for Wind Flow model 39 |
| Table 3.3 | Guideline of geometric parameters for CFD wind simulations over complex terrain 49 |
| Table 4.1 | Table for Sensitivity Analysis of Wake Model over offshore wind farm 60 |
| Table 4.2 | Results of Sensitivity Analysis for Wake Flow model 60 |
| Table 4.3 | Guideline of geometric parameters for CFD wake simulations over an offshore wind farm..... 67 |
| Table 4.4 | Guideline of geometric parameters for CFD wind simulations over complex terrain 70 |
| Table 4.5 | Guideline of geometric parameters for CFD wake simulations over an offshore wind farm..... 70 |

LIST OF FIGURES

| | Page |
|------------|--|
| Figure 1.1 | Different types and scales of turbulent models (here, DES is VLES) 11 |
| Figure 1.2 | Law of the wall for smooth and sand-grain roughened surfaces with the dimensionless sand-grain roughness k_s^+ as a parameter 17 |
| Figure 1.3 | Graphical representation of fitting the mean-velocity ABL log-law inlet profile to the wall function for mean velocity in the centre point P of the wall-adjacent cell..... 18 |
| Figure 1.4 | Overview of OpenFOAM's structure 19 |
| Figure 2.1 | The Bolund orography and the positions of the ten masts 24 |
| Figure 2.2 | Definition of surface roughness and terrain height for the blind comparison 24 |
| Figure 2.3 | Bolund ground grid resolution 26 |
| Figure 2.4 | TKE at 2 meters high along line B 27 |
| Figure 2.5 | TKE at 5 meters high along line B 27 |
| Figure 2.6 | Speed-up at 2 meters high along line B 28 |
| Figure 2.7 | Speed-up at 5 meters high along line B 28 |
| Figure 3.1 | Decision framework for selecting an appropriate sensitivity analysis method 32 |
| Figure 3.2 | Complex terrain wind farm orography and wind turbine positions..... 34 |
| Figure 3.3 | Complex terrain wind farm wind roses 35 |
| Figure 3.4 | Plane along the SSW direction over wind farm 36 |
| Figure 3.5 | Details on the three zones of the computational domain and their resolution 36 |
| Figure 3.6 | Wind speed profile at the wind farm center depending on vertical levels 41 |
| Figure 3.7 | TKE profile at the wind farm center depending on vertical levels..... 41 |
| Figure 3.8 | Wind flow along main energetic directions for three different height of the domain 42 |

| | | |
|-------------|--|----|
| Figure 3.9 | TKE profiles at the entrance of the buffer zone depending on λ ratio | 44 |
| Figure 3.10 | TKE profiles at the entrance of the transition zone depending on λ ratio.... | 44 |
| Figure 3.11 | Inlet wind speed profiles at the entrance of the transition zone depending on transition zone length | 45 |
| Figure 3.12 | Inlet wind speed profiles at the entrance of the wind farm zone depending on transition zone length | 46 |
| Figure 3.13 | Relative error on TKE comparing Base Case and case 5B | 48 |
| Figure 3.14 | Comparing data with different modelisation results | 50 |
| Figure 4.1 | Horns Rev Wind Farm layout | 54 |
| Figure 4.2 | Representation of the Horns Rev Offshore Wind Farm with Paraview..... | 54 |
| Figure 4.3 | Thrust coefficient curve of the wind turbine modelled: Vestas V80..... | 56 |
| Figure 4.4 | Example of <i>cellSetDict</i> file | 57 |
| Figure 4.5 | View of the computational domain from the top (above) and from south patch (beyond)..... | 59 |
| Figure 4.6 | TKE for the internal row positions depending on mesh horizontal resolution | 61 |
| Figure 4.7 | Shape of the actuator disk by vertical ratio: 20, 100, 200, 350 (from left to right and from top to bottom) | 62 |
| Figure 4.8 | Vertical expansion for a domain height of $L=12D$ (left), $10D$ (center) and $7D$ (right)..... | 64 |
| Figure 4.9 | Wind speed ratios for the internal row positions depending on domain's height | 65 |
| Figure 4.10 | TKE for the internal row positions depending on the V_o applied to the source term | 66 |
| Figure 4.11 | Comparison: Power ratio for center row. Data VS Simulation | 68 |

LIST OF ABBREVIATIONS

| | |
|----------|--|
| ABL | Atmospheric Boundary Layer |
| BSC | Barcelona Supercomputing Center |
| CENER | Centro Nacional de Energías Renovables |
| CFD | Computational Fluid Dynamics |
| DES | Detached Eddy Simulations |
| DNS | Direct Numerical Simulations |
| ÉTS | École de Technologie Supérieure |
| GCI | Grid Convergence Method |
| LES | Large Eddy Simulations |
| NRSA | Nominal Range Sensitivity Analysis |
| OpenFOAM | Open Field Operation And Manipulation |
| RANS | Reynolds Averaged Navier-Stokes |
| RSM | Reynolds-Stress Model |
| SBL | Surface Boundary Layer |
| SIMPLE | Semi-Implicit Method for Pressure Linked Equations |
| TKE | Turbulent Kinetic Energy |
| WAsP | Wind Atlas Analysis and Application Program |

LIST OF SYMBOLS

| | |
|---|--|
| $C_\mu, C_{\varepsilon 1}, C_{\varepsilon 2}$ | $k - \varepsilon$ model constants |
| δ'_{ij} | Kronecker symbol |
| E | Smooth wall constant |
| ε | Dissipation rate [m^2/s^3] |
| k | Turbulent kinetic energy [m^2/s^2] |
| g | Gravitational acceleration [m/s^2] |
| κ | Von Karman Constant |
| k_s | Equivalent sand-grain roughness length [m] |
| k_s^+ | Dimensionless equivalent sand-grain roughness length [m] |
| L | Length scale [m] |
| l_m | Mixing length [m] |
| λ | Ratio between length of the buffer zone cells and the wind farm zone cells |
| μ | Dynamic viscosity [$N.s/m^2$] |
| ν | Kinematic viscosity [m^2/s] |
| μ_t | Turbulent dynamic viscosity [$N.s/m^2$] |
| ν_t | Turbulent kinematic viscosity [m^2/s] |
| ω | Earth's rotational speed [rad/s] |
| Ω | latitude [$^\circ$] |
| ρ | Air density [kg/m^3] |

| | |
|----------------------|--|
| Re | Reynolds number |
| σ_ε | $k - \varepsilon$ model constant |
| σ_k | Turbulent Prandtl number |
| τ'_{ij} | Reynolds Stress Tensor [Pa] |
| τ_w | Shear Stress [Pa] |
| u_i | i -component of wind velocity [m/s] |
| u_i' | i -component of wind velocity fluctuation [m/s] |
| U_p | Wind speed in the near-wall cell center [m/s] |
| U_∞ | Freestream wind velocity [m/s] |
| u^* | Wall function friction velocity [m/s] |
| u^+ | Dimensionless mean streawise wind velocity [m/s] |
| x_i | i -coordinate [m] |
| y_{Gr} | Absolute height of the ground (Blocken) [m] |
| y_p | Height of the near-wall cell center [m] |
| y^+ | Dimensionless wall unit [m] |
| y_0 | Blocken's aerodynamic roughness length [m] |
| z_0 | Surface roughness [m] |
| z_{Gr} | Absolute height of the ground [m] |

INTRODUCTION

In times of climate change and energetic dependance, renewable energies appear as a suitable solution. Although gradually, green power is becoming more relevant in the energy policies of different countries and zones. By the end of 2008, the European Union has arrived to an agreement whereby 20% of the energy consumed by its members has to be renewable in 2020. Most of this percentage should be provided by wind energy. According to IEA (2010), nowadays, wind energy already represents most of this percentage in several countries as Denmark (21,9%), Portugal (17%), and Spain (16.4%).

During many years, wind resource has been predicted by the industry using Wind Atlas Analysis and Application Program (WAsP) among others, a software developed by RisøDTU working on the basis that wind statistics can be corrected for local effects from orography, roughness and obstacles (using maps) to generate standardized free flow wind statistics.

Nevertheless, the use of WAsP model is often limited to cases of straightforward terrain or low hill flows. In complex terrain flow separation and recirculation become important and WAsP has difficulties to represent these areas. At this point and for studies in complex terrain, it makes sense to use Computational Fluid Dynamics (CFD).

In the last decade, numerous comparison studies have been carried out between WAsP and CFD models. Cabezón *et al.* (2005), Theodoropoulos (2010) and Pereira *et al.* (2010) among many others have showed that the results obtained using non-linear models are more accurate, even though WAsP results are quite acceptable for moderated complex terrain.

An extensive bibliography has been written on Computational Fluid Dynamics (CFD) simulations (see Versteeg and Malalasekera (2007) and Anderson (1995)). CFD technique is the analysis of systems involving fluid flow. It is the science of giving a numerical solution to different physical equations like mass conservation, conservation of momentum or conservation of energy in the current case of study.

Eventhough CFD methods have shown more accurate results than linear models, high resolution simulations lead to high computational efforts in terms of computational time and costs.

Therefore, the optimization of CFD must be a target. A mesh sensitivity analysis on complex and offshore terrain is carried out to achieve computational grid independance and avoid unnecessary computational calculations. The main goal is to propose a guideline of recommended geometrical parameters to the users of the studied wind and wake models: CFDWind1.0 and CFDWake1.0, both of them developped at CENER. The recommended parameters values have to allow the user to build up the computational domain by ensuring grid independence. From there, the prediction errors would be due to the physical modelisation. In both cases the solver used is Open Field Operation and Manipulation (OpenFOAM), a C++ open source CFD software that presents accurate results at the well-known Askervein hill case (Martinez (2011)).

The memoir is divided into four different parts. The literature review, the previous verification of the wind flow model using OpenFOAM, the mesh sensitivity analysis over complex terrain using CFDWind1.0 and the mesh sensitivity analysis over offshore wind farm using CFDWake1.0.

Concerning sensitivity analysis, on one hand, the wind flow model developped by the National Renewable Energy Center (CENER), CFDWind 1.0 is run over a very complex terrain onshore wind farm using WindMesh, a meshing tool recently developped at Barcelona Supercomputing Center (BSC) that continue to be tested. WindMesh allows the user to simulate the ground patch of its domain doing a high resolution construction through a Delauney triangulation of the topography. On the other hand, CENER's far wake model, CFDWake 1.0 is run over Horns Rev Offshore wind farm through *blockMeshDict*, an OpenFOAM's meshing tool.

The mesh sensitivity analysis involves several geometric parameters in both cases. As it is developed in the third chapter, a Nominal Range Sensitivity Analysis (NRSA) is chosen from the wide range of option presented in the literature due to the time and computational limitations. So, in this work, the vast majority of possible parametric combinations are not simulated. Otherwise, instead of 40 cases, the study would have been over more than 3000 cases, which is equivalent to three years of simulations full-time. It is possible and very probable that within

these 3000 combinations, there is at least one better than the layout recommendation, whereas, at this level of accuracy, the results would not be significantly better.

Linked to time constraints but also to confidentiality policies, both studies are carried out just through a single wind farm each. So, there is the possibility that current wind farms do not represent future cases of study. The wind farms have been chosen to counteract this effect as much as possible by choosing two examples with quite common characteristics within the commercial wind farms in terms of number of wind turbines, location, terrain and extension. Furthermore, limitations in modeling or technical aspects are discussed when emerging throughout the thesis.

CHAPTER 1

LITERATURE REVIEW

1.1 Atmospheric and Surface Boundary Layer

The atmospheric boundary layer (ABL) is defined as the part of the troposphere directly influenced by the presence of the earth's surface and responds to its forcings such as frictional drag, evaporation, heat transfer, pollutant emission and terrain induced flow modification (Stull (2009)). These forces give rise to the main characteristic of the ABL: the TURBULENCE. Meteorological phenomena taking place at this layer have a timescale of an hour or less. Typically, the ABL is divided in three different sub-layers: The surface boundary layer (SBL), the mixed layer and the entrainment zone.

The surface boundary layer is located at the bottom of the ABL and in contact with the surface. Its height is the 10% of the total ABL. SBL is characterized by high vertical gradients of wind speed, humidity and temperature. In the mixed layer, the turbulence is mainly due to heat transfer between warm ground surface and radiative cooling from the top of the mixed layer. The entrainment zone is a stable layer at the top of the mixed layer acting as a lid restraining the domain of turbulence (Stull (2009)).

For wind energy applications, the most interesting sub-layer is the SBL, where wind turbines operate. In wind engineering, where the interaction between wind and human constructions is studied, the Coriolis effects and the buoyancy forces due to density and thermal stratification are usually neglected due to the higher importance of the surface effects (Stangroom (2004) and Martinez (2011)). This greatly simplifies the modelling of SBL.

1.2 Numerical modelling

1.2.1 Governing Equations

Due to its accurate results (Martinez (2011), Cabezón *et al.* (2011a)) and its low computational cost compared to other turbulence models as Large Eddy Simulation (LES), the most common approach in wind engineering is the Reynolds Averaged Navier-Stokes (RANS) approach. The Reynolds decomposition ($\phi = \bar{\phi} + \phi'$) is applied to the variables ϕ of the time-dependent Navier-Stokes equations (Eq. 1.1, Eq. 1.2 and Eq. 1.3). The Reynolds decomposition split the variable in two different terms, the mean term ($\bar{\phi}$) and the fluctuation (ϕ' .)

$$\rho \frac{Du}{Dt} = -\frac{\partial p}{\partial x} + \text{div}(\mu \nabla u) + S_{Mx} \quad (1.1)$$

$$\rho \frac{Dv}{Dt} = -\frac{\partial p}{\partial y} + \text{div}(\mu \nabla v) + S_{My} \quad (1.2)$$

$$\rho \frac{Dw}{Dt} = -\frac{\partial p}{\partial z} + \text{div}(\mu \nabla w) + S_{Mz} \quad (1.3)$$

with

$$\rho \frac{Du_i}{Dt} = \frac{\partial(\rho u_i)}{\partial t} + \text{div}(\rho u_i \mathbf{u}) \quad (1.4)$$

The governing equations for an incompressible fluid of density ρ and steady-state conditions with Cartesian notation are the Continuity equation (Eq.1.5) and the Momentum equation (Eq. 1.6). For the indicial notation, the Einstein summation convention will be used.

$$\frac{\partial \bar{u}_i}{\partial x_i} = 0 \quad (1.5)$$

$$\underbrace{\rho \left(\frac{\partial \bar{u}_i}{\partial t} + \bar{u}_j \frac{\partial \bar{u}_i}{\partial x_j} \right)}_{\text{Inertia}} = \underbrace{-\frac{\partial \bar{p}}{\partial x_i}}_{\text{Pressure Gradient}} + \underbrace{\rho \bar{g}_i + \frac{\partial}{\partial x_j} \left[\mu \left(\frac{\partial \bar{u}_i}{\partial x_j} + \frac{\partial \bar{u}_j}{\partial x_i} \right) \right]}_{\text{Viscosity}} - \underbrace{\frac{\partial}{\partial x_j} \rho \overline{u'_i u'_j}}_{\text{Reynolds Stress Tensor}} \quad (1.6)$$

The result of doing the Reynolds decomposition is the appearance of six new terms $\overline{u'_i u'_j}$ composing the Reynolds stress tensor. This tensor represent the average flow of momentum (for a unit area) passing through a differential volume surrounding a fluid particle due to turbulent fluctuations. The Reynolds stresses can be interpreted as turbulent diffusive forces. In order to close the system of equations, and due to its non-linear nature, the Reynolds stress tensor is modelled according to the widely adopted approach of the Boussinesq hypothesis (Versteeg and Malalasekera (2007)):

$$\tau'_{ij} = -\rho \overline{u'_i u'_j} = \mu_t \left(\frac{\partial u_i}{\partial x_j} + \frac{\partial u_j}{\partial x_i} \right) - \frac{2}{3} \rho k \delta_{ij} \quad (1.7)$$

where μ_t is the turbulent viscosity and $k = \frac{1}{2} \overline{u'_i u'_i}$ the turbulent kinetic energy.

In terms of pressure, as we are considering an incompressible flow in hydrostatic equilibrium, the gravitational force is absorbed in the pressure term (Sorensen (1995)). The term $\frac{2}{3} \rho k \delta_{ij}$ is also absorbed in the pressure term (Eq. 1.8). Besides, in turbulent regime, $\mu \ll \mu_t$ and μ is neglected.

$$\frac{\partial p}{\partial x_i} = -\frac{\partial \bar{p}}{\partial x_i} + \rho \bar{g}_i - \frac{2}{3} \rho k \delta_{ij} \quad (1.8)$$

Concerning Coriolis force, the wind turbines used are between 50 and 100 meters height and located inside SBL. Then, Coriolis forces are normally not considered in studies in SBL as they only have an effect in the outer layer. Finally, the continuity equation (eq. 1.9) and the momentum equation (eq. 1.10) became:

$$\boxed{\frac{\partial u_i}{\partial x_i} = 0} \quad (1.9)$$

$$\boxed{\rho u_j \frac{\partial u_i}{\partial x_j} = -\frac{\partial p}{\partial x_i} + \frac{\partial}{\partial x_j} \left[\mu_t \left(\frac{\partial u_i}{\partial x_j} + \frac{\partial u_j}{\partial x_i} \right) \right]} \quad (1.10)$$

dropping the overbar notation for simplification.

1.2.2 Turbulence modelling

1.2.2.1 Description and characteristics

Wilcox (1994) wrote during the nineties a reference book about turbulence modelling for CFD. Doing an overview to highlighted ideas, it could be learned that:

- a. An ideal model should introduce the minimum amount of complexity while capturing the essence of the relevant physics. (Wilcox (1994))
- b. Practical engineering flows are mostly turbulent.
- c. Turbulence has a strongly rotational nature so it must be three dimensional.
- d. Difficult to simulate the turbulence due to its complexity, multitude of length scales and its three dimensional and time dependence.
- e. The time-dependent and three-dimensional Navier-Stokes equation contains all of the physics of a given turbulent flow.
- f. A turbulent model has a wide range of possible modeling, between the simple algebraic mixing length model to a complete solution to the Navier Stokes equation.
- g. Turbulent kinetic energy is transferred on the average from larger eddies to smaller eddies until it dissipates into heat through the action of molecular viscosity.
- h. An N-equations model means a model requiring solution for n additional differential transport equations in addition to conservation of mass, momentum and energy (i.e. $k - \epsilon$ turbulence model is a two-equation model and the additional equations that must be solved are: Turbulent kinetic energy (k) and dissipation (ϵ) of turbulence).

- i. Desirable type of turbulence model: Model that can be applied by determining at most the appropriate boundary and/or initial conditions. No advance knowledge of the flow is necessary.

1.2.2.2 RANS models: $k - \varepsilon$

In wind engineering applications, $k - \varepsilon$ turbulent model is largely used (Kasmi and Masson (2010), Martinez (2011) or Sorensen (1995)) due to its robustness economy and its relative simplicity (only two equations model (Eqs. 1.11 and 1.12)) and accuracy for a wide range of turbulent flows. The first variable to consider is the turbulent kinetic energy and determines the energy in the turbulence, also called TKE or k . The second variable is the turbulent dissipation (ε) and determines the scale of turbulence. The Jones and Launder (1972) $k - \varepsilon$ model is one of the most popular for turbulence modelling. Since a neutral atmosphere will be considered and the flow is steady-state, the transport equations used have the following form:

$$\frac{\partial}{\partial x_i}(u_i \rho k) = \frac{\partial}{\partial x_j} \left(\frac{\mu_T}{\sigma_k} \frac{\partial k}{\partial x_j} \right) + P_k - \rho \varepsilon \quad (1.11)$$

$$\frac{\partial}{\partial x_i}(u_i \rho \varepsilon) = \frac{\partial}{\partial x_j} \left(\frac{\mu_T}{\sigma_\varepsilon} \frac{\partial \varepsilon}{\partial x_j} \right) + C_{\varepsilon 1} \frac{\varepsilon}{k} P_k - C_{\varepsilon 2} \frac{\varepsilon^2}{k} \rho \quad (1.12)$$

where P_k is the turbulent production term,

$$P_k = -\rho \overline{u'_i u'_j} \frac{\partial u_j}{\partial x_i} \quad (1.13)$$

k and ε are related by the above presented turbulence viscosity μ_t

$$\mu_t = \rho C_\mu \frac{k^2}{\varepsilon} \quad (1.14)$$

The constants of that model are:

$$\boxed{C_\mu = 0.09, C_{\varepsilon 1} = 1.44, C_{\varepsilon 2} = 1.92, \sigma_k = 1.0, \sigma_\varepsilon = 1.3}$$

Nevertheless, different variations of combinations of constants have been proposed. Cabezón *et al.* (2007) has compared some of them and the set of constants from Panofsky *et al.* (1977) have shown a good description of the profiles in terms of wind speed and turbulence intensity. They are given such that:

$$C_\mu = 0.0333, C_{\varepsilon 1} = 1.181, C_{\varepsilon 2} = 1.92, \sigma_k = 1.0, \sigma_\varepsilon = 1.3$$

1.2.2.3 More Turbulence Models

Besides RANS models, several turbulence models (fig. 1.1) have been built and applied along last decades in wind engineering, depending on terrain and analyzed results.

First of all, linear models as WAsP are not based on CFD. These linear analytical models can generalise a long-term meteorological data series at a (reference) site which may then be used to estimate conditions at other sites. The results are obtained in an accurate and quickly way as far as the computational domain is flat. Once the terrain became slightly irregular, the results became wrong due to the bad prediction of the separation and the flow recirculation. (Bowen and Mortensen (1996))

Large eddy simulation (LES) allow better fidelity than RANS simulations. It is a mathematical model for turbulence which resolves larges scales and models the smallest ones (Bakker (2002)). Despite showing better results than RANS, LES requires a very fine subgrid in the near-wall region of attached turbulent boundary layers. So, the computational time increases considerably and when the available computing power is limited it is not advisable.

Nowadays, Detached eddy simulation (DES) models have become very popular. DES has been described as "a three-dimensional unsteady numerical solution using a single turbulence model, which functions as a subgrid-scale model in regions where the grid density is fine enough for a large-eddy simulation, and as a Reynolds-averaged model in regions where it is not" Spalart (2009). When DES models are used, boundary layer is treated by RANS and

regions of massive separation are treated with LES, giving better results than RANS with a lower computational cost than LES.

Direct Numerical Simulation (DNS) method is based on the complete three-dimensional and time-dependent conservation equations for mass, momentum and energy. DNS are important to provide data for the development and validation of both turbulence models presented above (RANS and LES) (see Venayagamoorthy *et al.* (2003)). With this simulation, all the scales are resolved numerically without any turbulence modelling. The computational cost is extremely expensive and it is never applied excepting for research centers owning highly powerful computers.

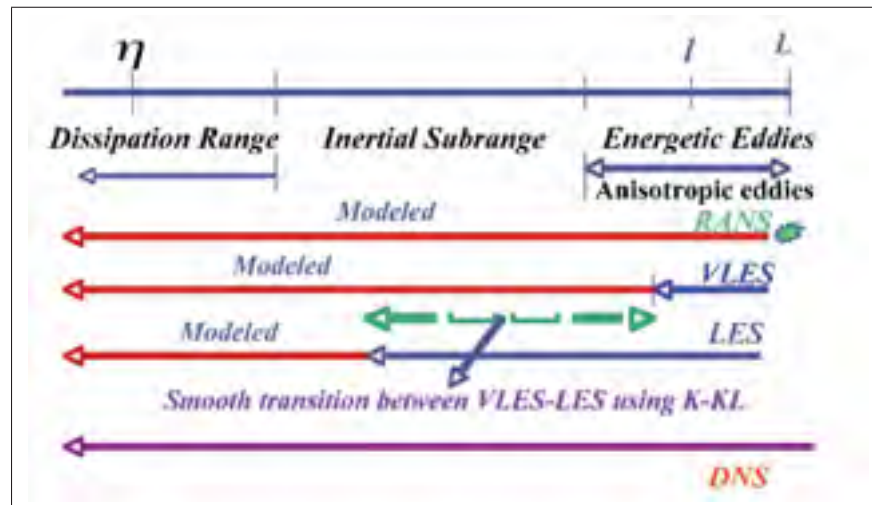


Figure 1.1 Different types and scales of turbulent models (here, DES is VLES)

In the figure 1.1, the complexity and the computational cost increase while approaching the bottom part of the graphic. In the same way, the turbulence modeling decrease while approaching the bottom until it disappears in the DNS.

1.2.3 Wind flow model: CFDWind 1.0

1.2.3.1 General Features

CFDWind 1.0 is an inhouse Surface Boundary Layer model developped at CENER since 2005 and solved through Ansys. Since 2010, CFDWind 1.0 has been adapted and solved through OpenFOAM. It has been validated over the Bolund blind test (Bechmann *et al.* (2009b)) showing very accurate results. According to Cabezón *et al.* (2011a), the model is adapted for the simulation of wind speed and turbulence based on the Monin-Obukhov theory (see Sanz *et al.* (2008)) and on Richards and Hoxey (1993) computational approach. Mixing length is considered strictly increasing with height z as $l_m = \kappa z$. In addition, the atmosphere is considered as neutral since thermal effects and Coriolis force are neglected because of the arguments presented previously.

1.2.3.2 Boundary conditions

As the air is considered as an incompressible flow, the variables in the OpenFOAM folder *incompressibleRASModels* are density independent. From now on, kinematic viscosity (Eq. 1.15) is considered instead of dynamic viscosity.

$$\nu_t = \frac{\mu_t}{\rho} \quad (1.15)$$

a. Inlet

Vertical profiles of U , k and ε (Eqs. 1.16, 1.17 and 1.18) are specified by Richards and Hoxey (1993) for the surface boundary layer and neutral conditions. The Panofsky *et al.* (1977) constants are used:

$$\frac{U}{u_*} = \frac{1}{\kappa} \ln \frac{(z - z_{Gr})}{z_0} \quad (1.16)$$

$$k = \frac{u_*^2}{\sqrt{C_\mu}} \quad (1.17)$$

$$\varepsilon = \frac{u_*^3}{\kappa(z - z_{Gr})} \quad (1.18)$$

with u_* the wall function friction velocity, z_0 the surface roughness, $\kappa = 0.4187$ the Von Karman constant, z_{Gr} the height of the cell centroid where the equations are applied and $C_\mu = 0.0333$ is part of the set of constants proposed by Panofsky *et al.* (1977).

The height of the cell centroid is subtracted in the equations 1.16 and 1.18 to adapt the profiles for complex terrain cases. Kinematic viscosity ν_t is calculated according to equations 1.14 and 1.15. ν_t will be calculated in that way for the rest of boundaries, excepting ground patch where a the wall function proposed by Blocken *et al.* (2007) is set.

b. **Outlet and lateral**

According to Franke *et al.* (2007), the outlet boundary has to be placed at least at fifteen times the height of the obstacles of our domain of interest. In the wake model study, where the presence of the objects becomes more important and the wake region has more relevance, this conditions is accomplished. When studying the freestrem (wind model study), the distance between the zone of interest and the outlet boundary is one of the studied geometrical parameters. All the variables are set as zero-gradient, excepting ν_t . The distance between the sideways of the interest zone and the lateral boundaies of the computational domain must be at least two times the wide of the zone of interest (Franke *et al.* (2007)). In this work, two patches are considered as lateral boundaries when wind flow direction is 270° , for validating CFDWind1.0 at Bolund site and for the offshore sensitivity case.

c. **Top**

The height of the top boundary is on of the geometrical parameters studied in this work. Nevertheless, in the base case of the two studies, it is located 5 times the height of the obstacles, according to Franke *et al.* (2007) recommendation. According to Richards and Hoxey (1993), to ensure the existence of an homogeneous, steady and incompressible flow, the shear stress τ_w must be constant in all the domain. Instead of fixing the shear stress directly and in order to ensure the homogeneity of the flow, the inlet profiles are applied at the top boundary imposing $z = z_{top}$. Even located above the upper limit of the SBL, where the log-law is not real, the fixed value approach produces good results when the equation 1.19 is satisfied.

$$\sigma_\varepsilon = \frac{\kappa^2}{(C_2 - C_1)\sqrt{C_\mu}} \quad (1.19)$$

with $\kappa = 0.4187$, the von Karman constant.

In addition pressure outlet conditions are set in the outlet boundary.

d. **Ground**

For the ground patch, the vertical direction is considered as y according to the notation used by Blocken *et al.* (2007) and in order to link with figures 1.2 and 1.3. No slip conditions are imposed. U is fixed as (0,0,0). The value of k remains constant in the inlet and ground boundaries. To set ε and ν_t several wall functions are offered by OpenFAOM. *epsilonWallFunction* and *nutRoughWallFunction* are chosen respectively.

(a) *epsilonWallFunction*

This wall function implement the relation between production and dissipation of TKE proposed by Sorensen (1995):

$$\varepsilon = \frac{C_\mu^{0.75} k^{1.5}}{\kappa y_p} \quad (1.20)$$

with,

$$C_\mu = 0.0333$$

$$\kappa = 0.4187$$

$$E = 9.793$$

(b) *nutRoughWallFunction*

As said above, the wall functions have a major importance for near-wall modelling. *nutRoughWallFunction* is the function used by OpenFOAM to model near-wall behaviour. These functions are based on the near-wall velocity distribution, also called law of the wall (eq. 1.21). After Blocken *et al.* (2007), the law of the wall can be modified as follows for taking into account the effects of a fully rough surface (eq. 1.22).

$$u^+ = \frac{1}{\kappa} \ln y^+ + B \quad (1.21)$$

$$u^+ = \frac{1}{\kappa} \ln y^+ + B - \Delta B(k_s^+) \quad (1.22)$$

with $u^+ = U/u^*$, $y^+ = u^*y/\nu$ and $B \approx 5.2$, where U is the mean velocity tangential to the wall, u_* is the wall function friction velocity and ν is the kinematic viscosity. The modification for rough surfaces was mainly done by Nikuradse (1933) for flow in rough surfaces introducing the equivalent sand-grain roughness (k_s). Nikuradse's

experiment show that near a rough wall, the mean velocity distribution has the same trend as a smooth wall but shows a different intercept in a semi-logarithmic scale (fig. 1.2). This difference is a function of the dimensionless sand-grain roughness height $k_s^+ = u_* k_s / \nu$.

In the current case of study, the terrain is fully rough ($k_s^+ \gg 90$) so the laminar sublayer is eliminated due to the no-influence of the molecular viscosity to the flow. Changing U and y by U_p and y_p (value at the near-wall cell centre), the wall function used (eq. 1.23 in OpenFOAM is the same as in Fluent (see Martinez (2011)):

$$\frac{U_p}{u_*} = \frac{1}{\kappa} \ln\left(\frac{E y_p^+}{1 + C_s k_s^+}\right) \quad (1.23)$$

where E is the smooth wall constant $E = e^{\kappa B} \approx 9.793$ and $(1 + C_s k_s^+)$ represents the roughness modification (see Blocken *et al.* (2007)).

In wind engineering, if $C_s k_s^+ \gg 1$, then eq. 1.23 becomes:

$$\frac{U_p}{u_*} = \frac{1}{\kappa} \ln\left(\frac{E y_p}{C_s k_s}\right) \quad (1.24)$$

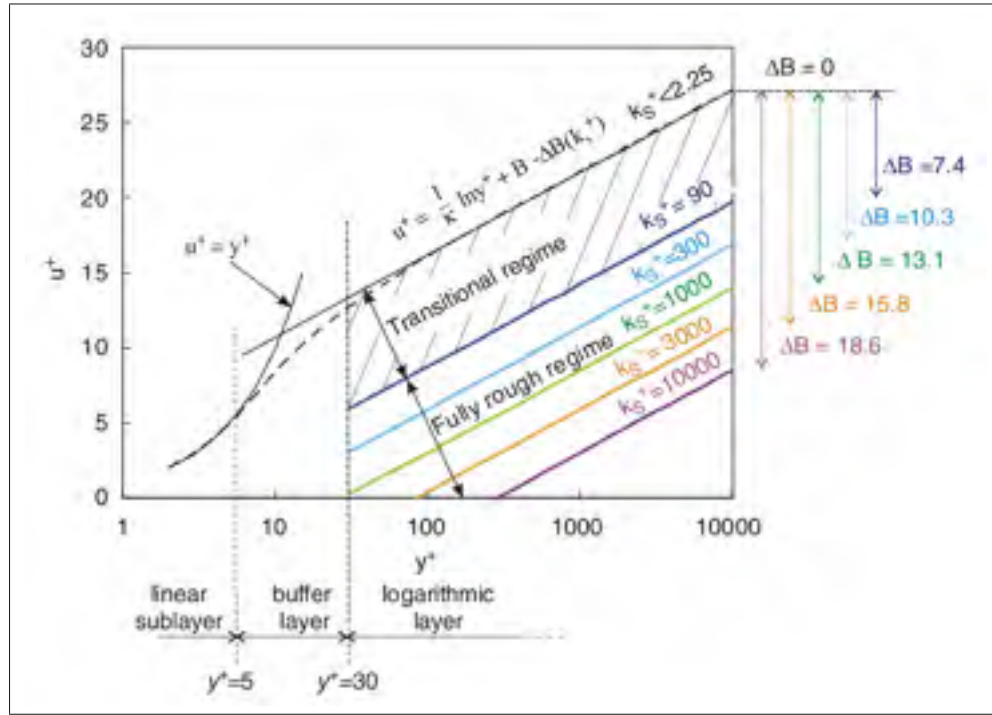


Figure 1.2 Law of the wall for smooth and sand-grain roughened surfaces with the dimensionless sand-grain roughness k_s^+ as a parameter

Finally, the velocity of the law-of-the-wall must equal the SBL log-law (see Cabezón *et al.* (2007) and Blocken *et al.* (2007)) to preserve the same roughness length and prevent the presence of an internal boundary layer that could deteriorate the flow homogeneity (see Fig. 1.3). Then, matching eqs. 1.24 and 1.16 (considering $y_{Gr} = 0$), a relationship between k_s and y_0 is obtained,

$$\frac{y_p}{y_0} = \frac{Ey_p}{C_s k_s} \quad (1.25)$$

With $k_s \leq y_p$, if k_s is maximized,

$$C_s = \frac{Ey_0}{k_s} = \frac{Ey_0}{y_p} \quad (1.26)$$

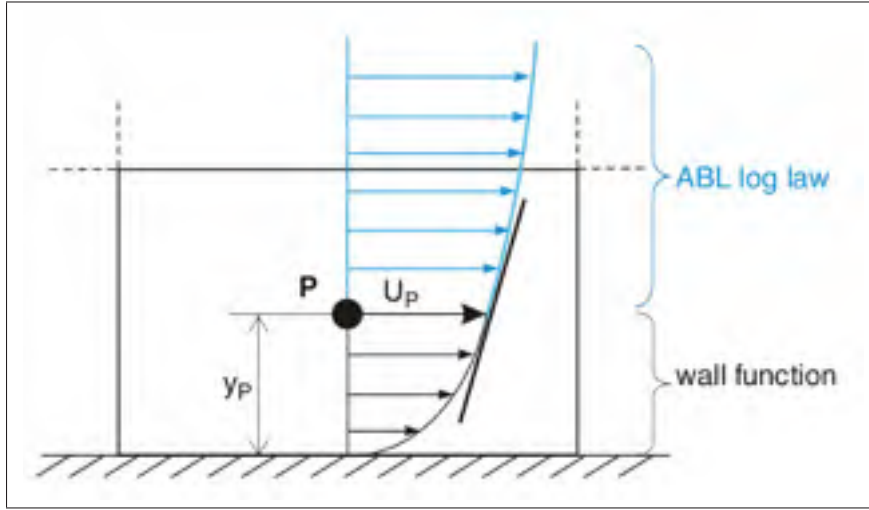


Figure 1.3 Graphical representation of fitting the mean-velocity ABL log-law inlet profile to the wall function for mean velocity in the centre point P of the wall-adjacent cell

As in the case of the top patch, the homogeneity of the flow is ensured by setting the velocity profile, not the shear stress. The details are exposed below. According to Richards and Hoxey (1993), the equations 1.27 and 1.28 have to be true in all the domain.

$$\tau_o = \rho u_*^2 \quad (1.27)$$

$$\tau_o = \mu_t \frac{\partial u}{\partial z} \quad (1.28)$$

with z being the vertical direction.

matching equations 1.27, 1.28 and 1.16, the equation 1.29 is obtained,

$$\frac{\partial u}{\partial z} = \frac{\rho}{\mu_t} u_*^2 = \frac{u_*^2}{\nu_t} = \frac{u_*}{\kappa} \frac{1}{(z - z_{Gr})} \quad (1.29)$$

Richards and Hoxey (1993) define the turbulent viscosity as $\nu_t = \frac{C_\mu k^2}{\epsilon}$. If the inlet profiles 1.17 and 1.18 are introduced in this last equation, we also obtain the equation 1.29. By setting the inlet profiles in all the domain, the homogeneity of the flow is finally ensured.

1.3 CFD software: OpenFOAM 1.7.1

Since the seventies, many CFD softwares have been created and optimized. Probably, the most significant way to separate them is between open source and commercial codes. This work is done by means of OpenFOAM 1.7.1. OpenFOAM (Open Field Operation And Manipulation) is a free, open source numerical simulation software with extensive CFD and multi-physics capabilities produced by OpenCFD Ltd. It is written under C++ language. OpenFOAM offers a wide range of components and capabilities (see figure 1.4) among which: Polyedral Finite Volume Method, second order scheme in space and time, parallelism in domain decomposition mode, incompressible flow (segregated pressure-based algorithms) and RANS for turbulent flows. All of them will be used in this work.

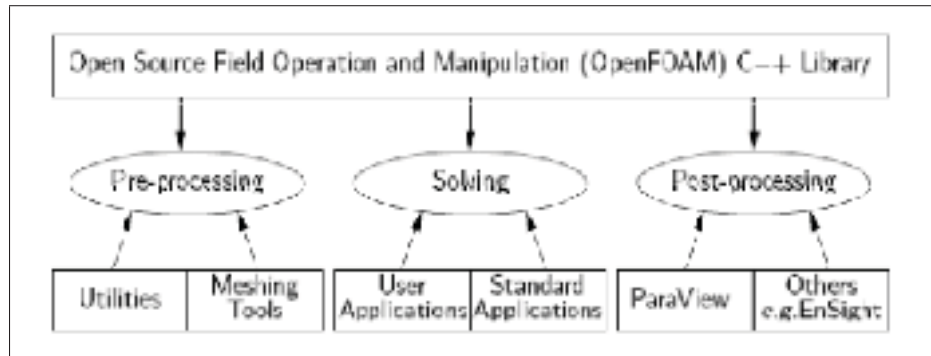


Figure 1.4 Overview of OpenFOAM's structure

It can be downloaded from the web site www.openfoam.com. Being an open source code, it allows free customising. This characteristics makes OpenFOAM very useful to research institutes and R&D departments of private companies.

1.3.1 Execution of OpenFOAM

As well as other CFD softwares, OpenFOAM is characterised by linking three main stages: pre-processor, solver, and post-processor.

During **pre-processor** the user prepares the simulation case. The computational domain has to be defined and then discretized on a finite number of elements (cells). The physical models representing wind speed or turbulence are selected and set. The fluid is chosen by defining its properties (density, viscosity). Finally, the user has to specify the boundary conditions, determine the discretization schemes used to calculate the physical fields and fix the timing of the iteration of the simulation.

The finite volume method is the numerical analysis used CFD codes as PHOENICS, FLUENT or OpenFOAM among others. After Versteeg and Malalasekera (2007) and Ansys (2009), the method presents different steps. Once the domain is divided into discrete finite control volume using the computational grid, a formal integration of the governing equations is done over all the (finite) control volumes of the solution domain to construct algebraic equations for the discrete dependent variables such as velocities, pressure, turbulence, etc. The discretized equation expresses the conservation principle for the variable inside the control volume. Finally, the discretized equations are linearized and solved by an iterative method. The solution satisfies conservation equation's at every single cell and at the whole computational domain.

During **post-processor**, visualisation tools are used to observe the results of the simulations. Grid display, vector plots, 2D and 3D plots, view manipulation, etc. Post processing is helpfull for the understanding.

1.3.2 Selected solver (from the options offered by OpenFOAM)

Since air is considered an incompressible flow, *simpleFoam* solver is chosen for the first part of this work where freestream inlet profile is developped over complex terrain. *simpleFoam* is a steady-state solver for incompressible and turbulent flow. During the second study (of

the wake model) over offshore wind farm, the solver used is *simpleWindFoam*. It has the same characteristics as *simpleFoam* and allows to add external source terms in the momentum equation to simulate wind turbines.

The key word "simple" at the beginning of both solver name's means Semi-Implicit Method for Pressure-Linked Equation. This is pressure-based segregated algorithm allowing to face the governing equations with an iterative procedure and solving them one after another. The segregated algorithm presents the advantage of being memory efficient since the discretized equations need only be stored in the memory one at a time. However, it presents an inconvenience in convergence time, inasmuch as the equations are solved in a decoupled manner Ansys (2009). The different iterative steps are:

- a. Set the boundary conditions.
- b. Solve the discretized momentum equation, one after another, using the recently updated values of pressure and face mass fluxes.
- c. Solve the pressure correction equation using the recently obtained velocity field and the mass-flux.
- d. Correct face mass fluxes, pressure, and the velocity field using the pressure correction obtained from previous step.
- e. Solve the equations for additional scalars if any, such as turbulent quantities or energy using the current values of the solution variables.
- f. Update the source terms arising from the interactions among different phases.
- g. Check for the convergence of the equations.
- h. Repeat till convergence fixed by the user in the file *fvSolution* of OpenFOAM.

The steps are continued until the convergence criteria set at *fvSolution* file are met (see Annexe I). The linear solver used is Preconditionned Bi-Conjugate Gradient (PBiCG). The preconditionner chosen, favoring convergence, is Diagonal incomplete-LU (DILU). Although those solver and preconditionner are recommended in the use of SIMPLE algorithm, an exception is done for pressure field because, due to steps c and d, it is the field with most problems to converge. In the case of the pressure, the solver used is the Geometric-Algebraic Multi-Grid (GAMG) and the preconditionner, the Faster Diagonal Incomplete-Cholesky (FDIC).

1.3.3 Selected turbulence model (from the options offered by OpenFOAM)

The *kEpsilon* turbulent model is selected within the options offered by OpenFOAM as turbulence models for incompressible fluids. Nevertheless, taking benefit of the open source nature of OpenFOAM, the turbulent model is customized limiting the turbulent kinematic viscosity to values of the order of $10^4 m^2/s$ to avoid problems during the first iterations and avoid achieving values too high.

CHAPTER 2

THE BOLUND EXPERIMENT: BLIND COMPARISON OF FLOW MODELS

The aim of this chapter is the verification of the use of OpenFOAM for the wind flow model developed by CENER, CFDWind1.0. A comparison is conducted between the behaviour of this model using Fluent 6.3 and OpenFOAM 1.7.1. CFDWind1.0 through Fluent was already validated by Cabezón *et al.* (2011a) during the well-known Bolund experiment launched by RisøDTU (see Bechmann *et al.* (2009a)).

2.1 The experiment setup

The Bolund experiment (Bechmann *et al.* (2009a)) was a field campaign providing new dataset for wind flow model validation over complex terrain. It was the basis for a blind comparison of flow models. It's had been executed during a three months period between 2007 and 2008. Bolund is a 12m high coastal hill near RisøDTU surrounded by water. A layout of ten masts M0 to M9 were installed along two lines A and B corresponding to 239° and 270° direction respectively (fig. 2.1).

Each mast was instrumented with sonic and cup anemometers at 4 different heights (2m, 5m, 9m, and 15m) in order to measure the mean velocity and turbulence profiles. The mast M0, located at the west of the hill was used as a reference. The dataset was previously filtered and averaged for this four heights.

The topography and the surface roughness were suggested as it can be observed in fig. 2.2. The land and the water were represented by a roughness length z_0 of 0.015 m and 0.0003 m respectively. At the east of the domain, roughness was also 0.015 m because the zone belongs to the land.

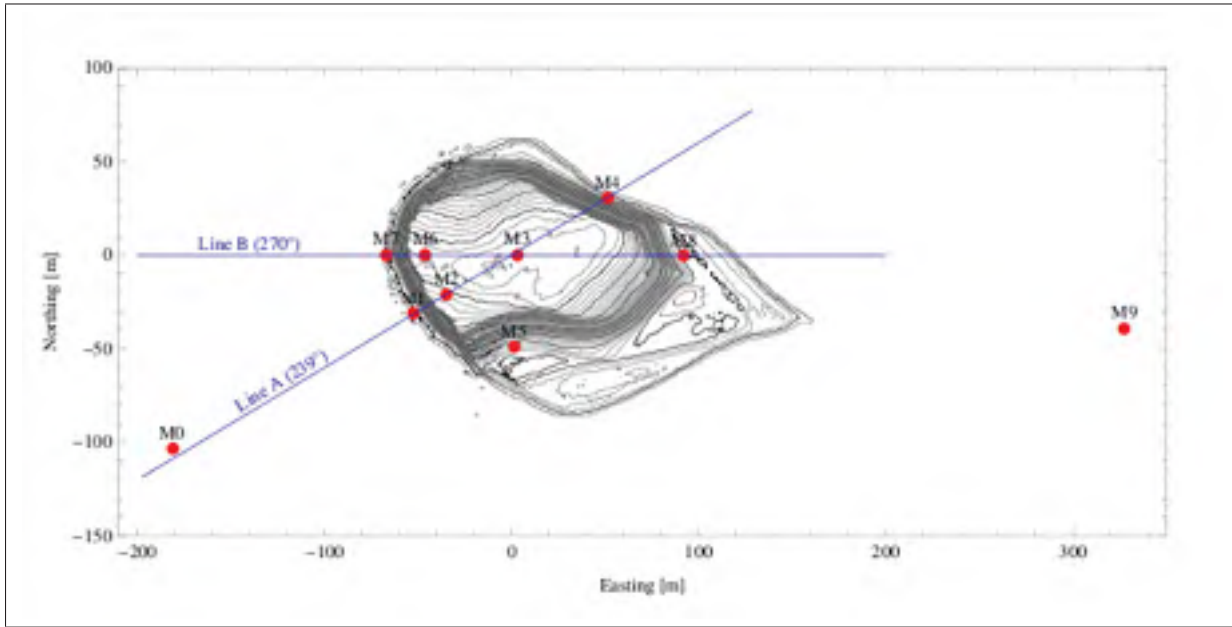


Figure 2.1 The Bolund orography and the positions of the ten masts

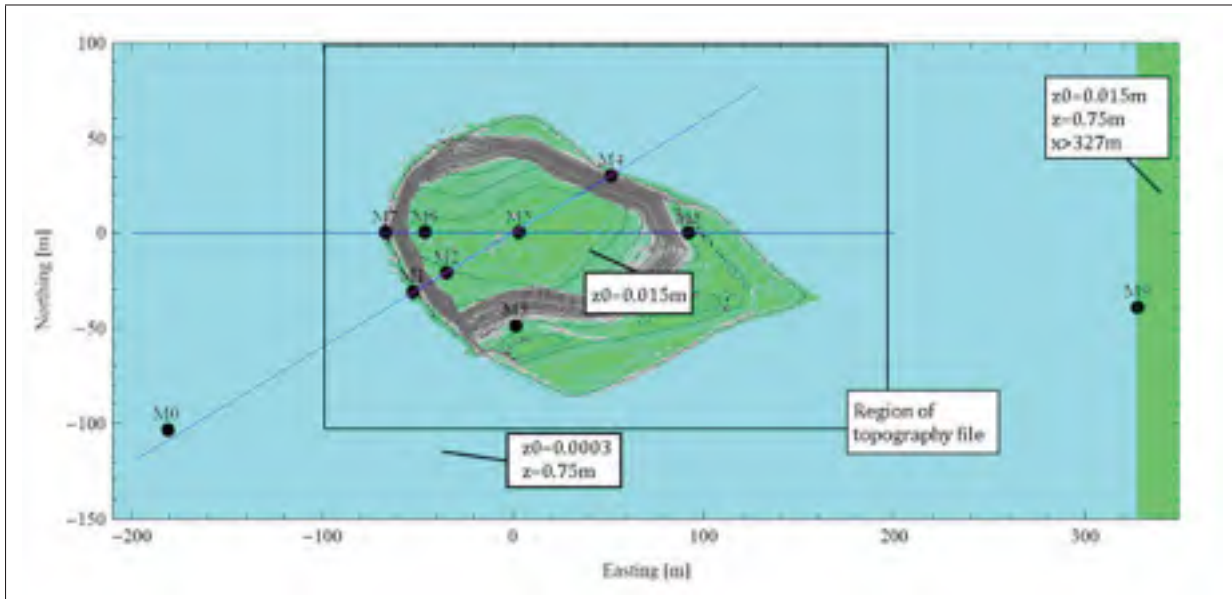


Figure 2.2 Definition of surface roughness and terrain height for the blind comparison

2.2 The blind comparison

The original blind comparison carried out by Bechmann *et al.* (2009b) for several models as linear, CFD-RANS, CFD-LES, wind tunnels, etc. on four different cases with different wind

directions: 90°, 239°, 255°, 270°. Nevertheless, the comparison done in this memoir is over west inflow direction (270°). Since the wind flow model used is the same for OpenFOAM and Fluent, boundary conditions are the same. The wind speed velocity and standard deviation are 10 minutes averaged and are respectively $U = (u, v, w)$ and $U' = (u', v', w')$.

Table 2.1 Physics parameters for Bolund experiment

| Field | Equation |
|----------------------|--|
| Total wind speed | $s = \sqrt{(u^2 + v^2 + w^2)}$ |
| TKE | $k = \frac{1}{2}(\overline{u'u'} + \overline{v'v'} + \overline{w'w'})$ |
| Friction velocity | $u_*^2 = \frac{\tau}{\rho} = \sqrt{\overline{u'w'^2} + \overline{v'w'^2}}$ |
| Monin-Obukhov length | $L = -\frac{u_*^3 \theta}{g \kappa w' \theta'}$ |

The simulation's output compared afterwards are the Speed-up ($\frac{s}{u_{ref}}$) and the normalized TKE ($\frac{TKE}{u_{ref}^2}$) with u_{ref} the wind speed at the reference meteorological mast M0.

2.3 Computational domain

The structured mesh is built up through the commercial software ICEM CFD 11.0 Hexa for OpenFOAM and Fluent. The exactly same mesh is used for both Fluent and OpenFOAM. In this way, the only difference between both simulations is the code. The dimensions are 1260 m (E-W direction), 1170 m (N-S direction) and 300 m in the vertical direction. The result is a 3 million cells mesh. As the hill is 12 m height, the minimum height, and the location of the boundaries regarding the sideways of the zone of interest are respected, as commented on the Boundary Conditions part.

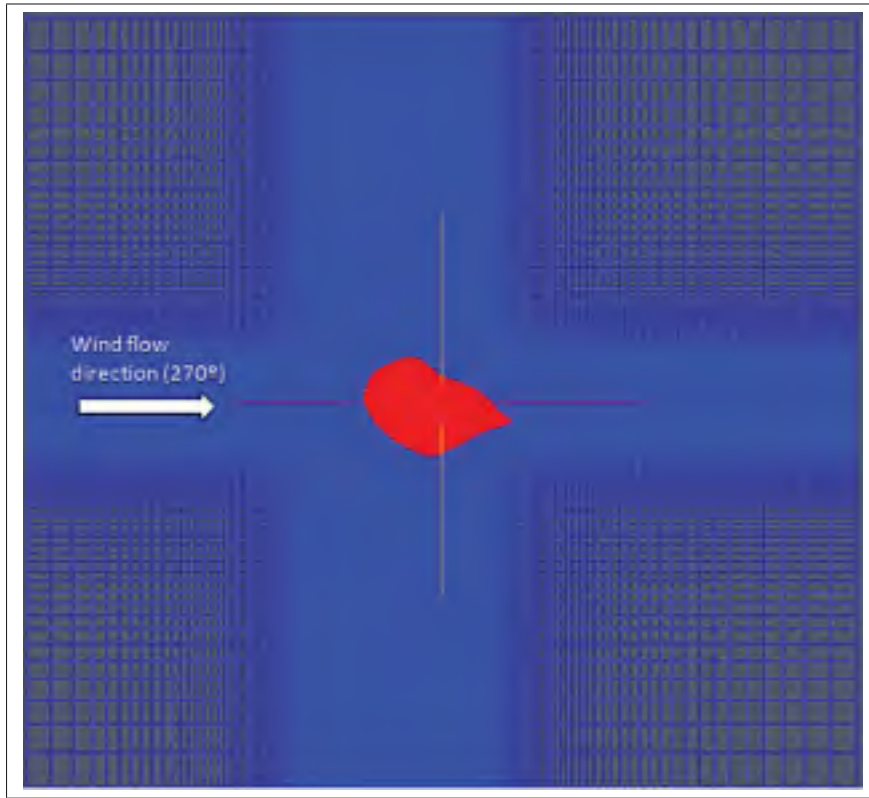


Figure 2.3 Bolund ground grid resolution

2.4 Verification of CFDWind1 using OpenFOAM 1.7

As said before, the speed-up and the turbulent kinetic energy are used to verify the use of CFDWind1.0 model through OpenFOAM. In this section, the speed-up and TKE are presented all along line B (270° direction) at 2 and 5 m above ground level. The data used for the verification was provided by RisøDTU. In all the cases, there are at least four data points corresponding to the met masts positions located along the line B, M7, M6, M3, and M8. In addition, the data obtained at the freestream (M0) and land (M9) positions are also provided (see figure 2.1)

2.4.1 Graphics

The figures 2.4 and 2.5 represent the normalized TKE obtained through simulations along the line B at 2 m and 5 m above the ground level respectively.

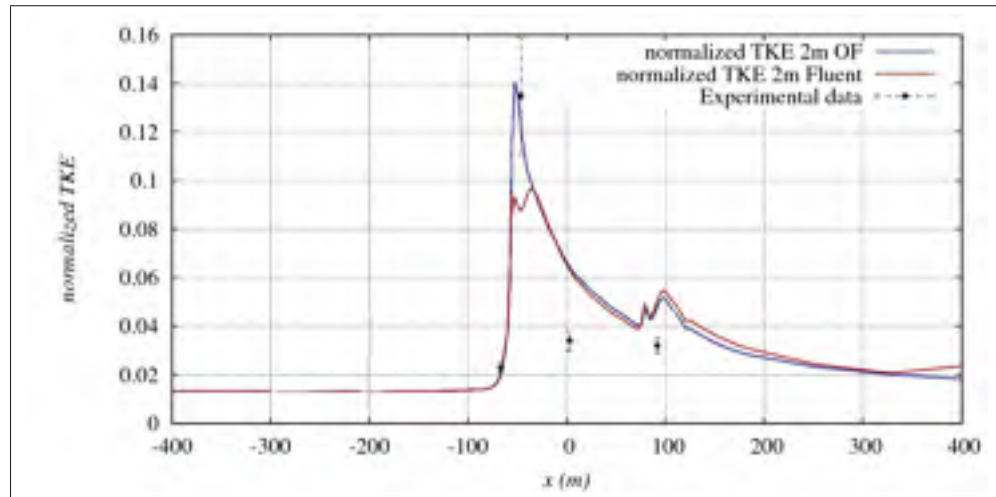


Figure 2.4 TKE at 2 meters high along line B

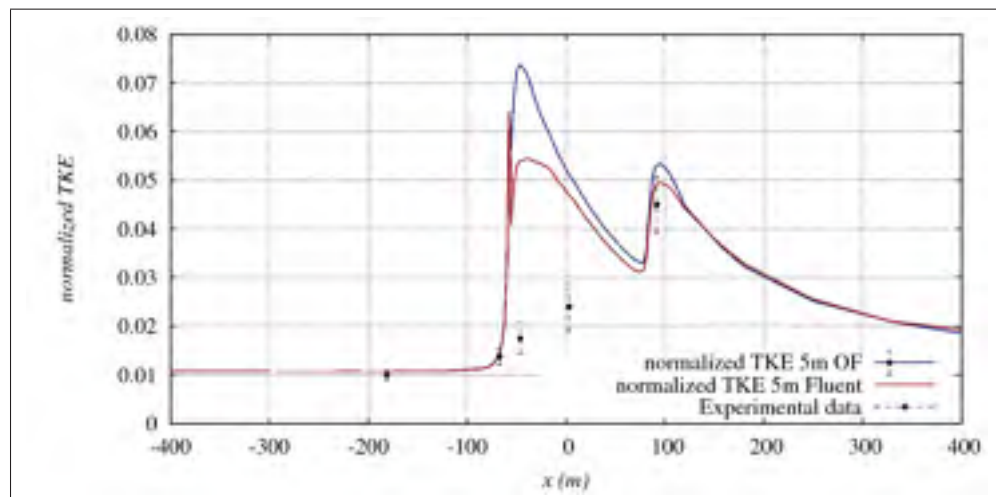


Figure 2.5 TKE at 5 meters high along line B

The figures 2.6 and 2.7 represent the speed-up factor obtained through simulations along the line B at 2 m and 5 m above the ground level respectively.

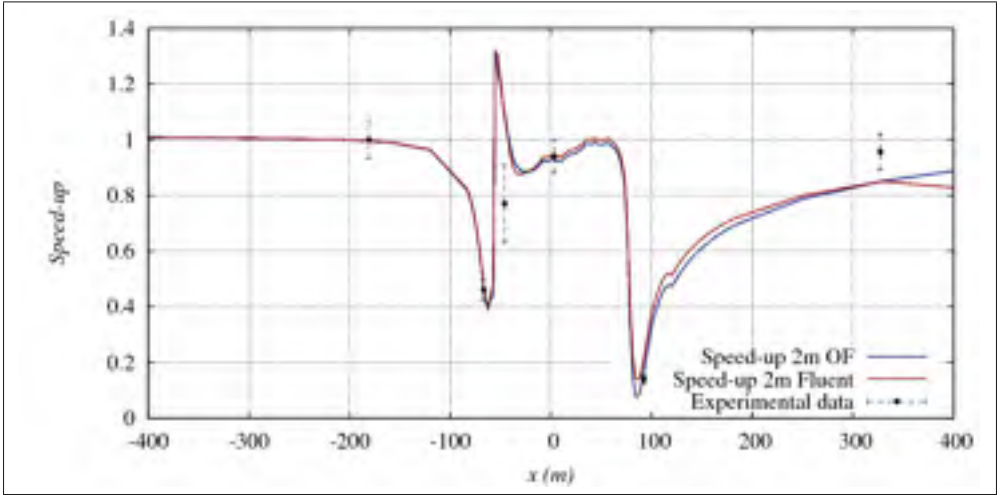


Figure 2.6 Speed-up at 2 meters high along line B

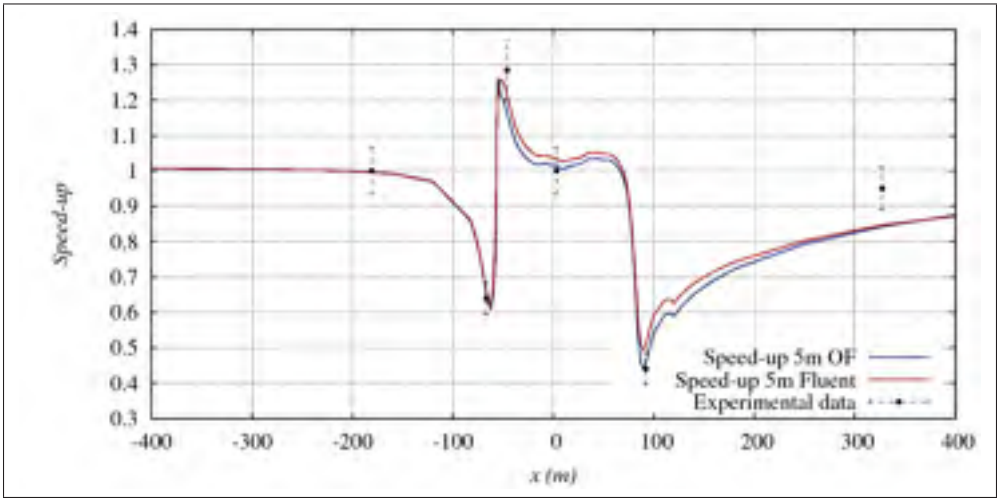


Figure 2.7 Speed-up at 5 meters high along line B

2.4.2 Errors and discussion

To compare the behaviour of CFDWind 1.0 applying it within both softwares, the average relative error (eq. 2.1) in percentage is calculated for speed-up factor and normalized TKE.

$$\%error = \frac{1}{N} \sum \left| \frac{F_{predicted} - F_{measured}}{F_{predicted}} \right| \quad (2.1)$$

where :

- $F_{predicted}$ are simulation results
- $F_{measured}$ are data
- N are the number of data points

As it can be observed in tables 2.2 and 2.3, both softwares present similar accuracy for speed-up. The model presents some problems to predict TKE and overpredict it, specially in the upstream cliff zone where a quite different prediction is done through Fluent and OpenFOAM. In this zone, the velocity gradients are higher and a mesh refinement could be useful. Nevertheless, the most plausible cause of this difference between the two codes is probably due to the different discretization schemes.

Table 2.2 Speed-up percentage error

| Software | height = 2m | height = 5m |
|----------|-------------|-------------|
| OpenFOAM | 10.27% | 5.38% |
| Fluent | 15.57% | 6.297% |

Table 2.3 Normalized TKE percentage error

| Software | height = 2m | height = 5m |
|----------|-------------|-------------|
| OpenFOAM | 27.42% | 33.10% |
| Fluent | 35.53% | 30.29% |

To summarize the verification of the use of CFDWind1.0 through OpenFOAM, it has to be said that the combination show high acceptable results in terms of speed-up but show more difficulty

to capture the behavior of the normalized turbulent kinetic energy. However, the target of this part of the work was not to analyze the physical modeling of CFDWind1.0, but to ensure that CFDWind1.0 through OpenFOAM has the same behaviour as the previous validation of CFDWind1.0 through Fluent. According to figures 2.4 to 2.7, this point is verified.

CHAPTER 3

MESH SENSITIVITY ANALYSIS OF CFD WIND FLOW MODEL FOR COMPLEX TERRAIN

3.1 Definition and choice of the Sensitivity Analysis Method

Models are used to predict or compare the future performance of a new system, a modified system, or an existing system under new conditions (Carson (2002)). On one hand, in the current chapter, the wind flow model CFDWind 1.0 is simulated over new conditions (complex terrain meshed with WindMesh). On the other hand, the wake model CFDWake 1.0 is used over a modelisation of offshore wind farm. Before applying model, there are two different steps to judge how good it is with respect to the system indeed modeled: Verification and Validation. Verification consists of demonstrating that the code is correct; it is capable of achieving correct mathematical solutions to the governing continuum equations in the limit of $\delta \rightarrow 0$ (Roache (2008)). Validation is the process of determining the degree to which a model (and tis associated data) is an accurate representation of the real world from the perspective of the intended uses of the model (Roache (2008)).

In line with the Joint Research Centre of the European Comission, an ideal sensitivity analysis should include a multidimensional averaging, taking into account the effect of a factor while others are varying as well. However most of analysis met in the literature are local or nominal range method (see Kuo (2005)). As Frey *et al.* (2002) presented, local sensitivity analysis is applicable to deterministic models, where predictions should be done without random criteria. This is the case of this study. The choice of the sensitivity analysis had been done following Mokhtari *et al.* (2005) guideline of the figure 3.1.

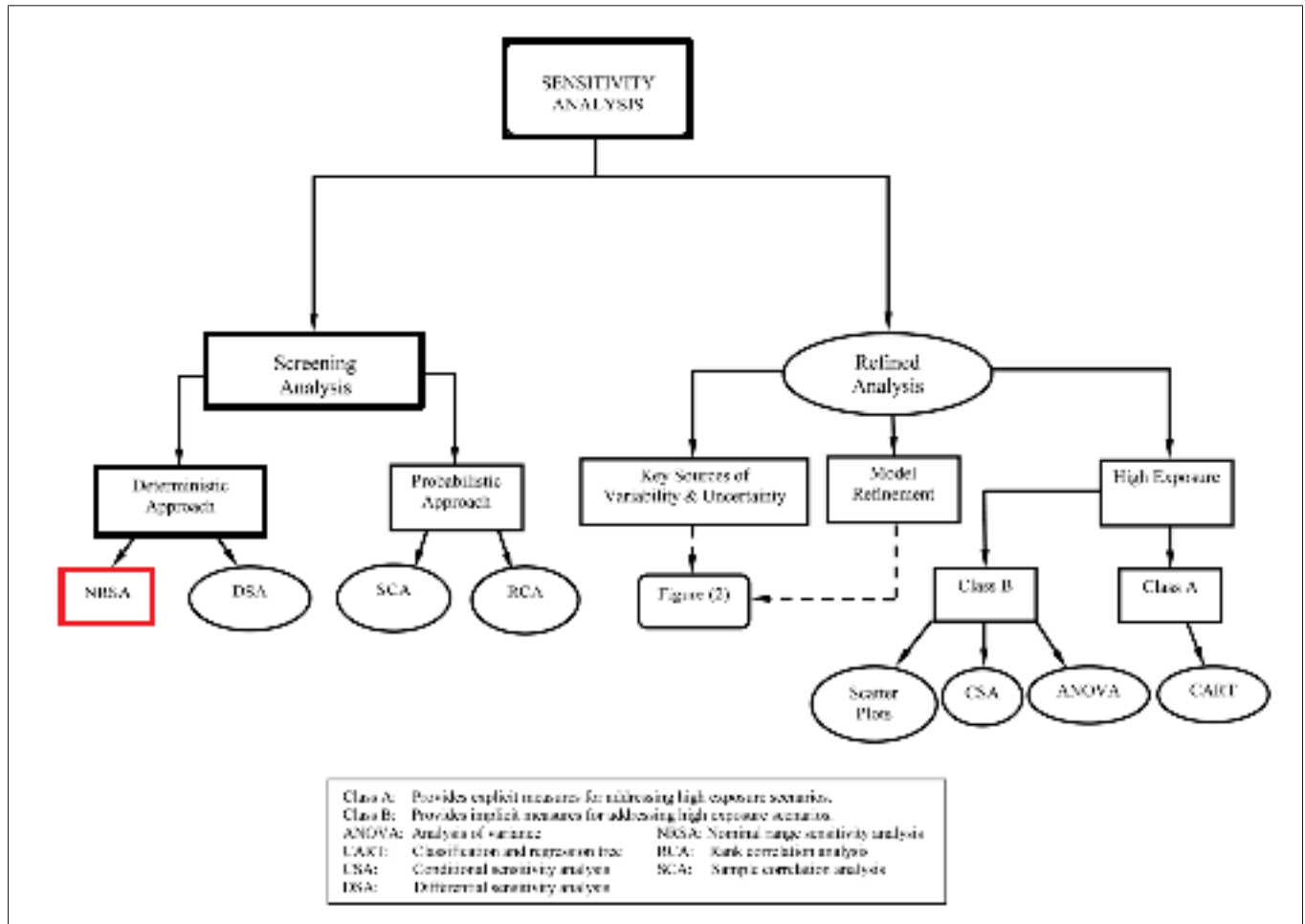


Figure 3.1 Decision framework for selecting an appropriate sensitivity analysis method

The criteria to choose the appropriate sensitivity analysis is the following. Since the study is not focussed on CFDWind1.0 deling but on geometrical modeling, the target is to analyze OpenFOAM and WindMesh. Both tools are relatively recent and no previous sensitivity analysis have been done over them. So, the refined analysis can not be done yet. Screening analysis is chosed. Our model is deterministic since the simulations with same inputs must show same results. The option proposed are Nominal Range Sensitivity Analysis (NRSA) and Differential Sensitivity Analysis (DSA). Patil and Frey (2004) said that DSA is used to evaluate the effects

on the output of very small perturbations in nominal values of inputs. Since the objective in this work is to obtain quantitative values of inputs and discrimination of important inputs, the sensitivity analysis chosen is NRSA. Frey *et al.* (2002) describe NRSA as an *"evaluation of the effect on model outputs exerted by individually varying only one of the models inputs across its entire range of plausible values while holding all other inputs at their base-case values"*. This is exactly the kind of analysis wanted and the one it is possible to do due to the computational and time limitations, and the impossibility of doing more than 3000 simulations.

The major objective of using a CFD software is to simulate in a accurate way the real behavior of the fluid. The behavior of the simulated fluid is directly related to the wind flow modelling, turbulence, etc. and also with the correct representation of the environment. Especially for very complex terrains, a capital issue is to create a mesh depicting properly the terrain and the conditions under which the wind arrive to the zone of study. Since the wind flow model has already shown good results in terms of wind speed (see the previous chapter), the aim of this part of the project is to guarantee the mesh independence on the layout. In the previous chapter, the mesh used for the verification with OpenFOAM had to be the same as the one used for Fluent. Therefore, no grid independence was done, even though the geometrical parameters used were similar to the ones proposed for the base case of this first analysis. To achieve grid independence in the present study, a NRSA is done for the geometric inputs on the grid generator. WindMesh is the meshing tool developed at Barcelona Supercomputing Center. Some details concerning WindMesh are detailed in Appendix II.

3.2 Test case

Due to privacy policy of the wind farm developer, several details are omitted in this work. The Wind Farm selected for this work is located in Spain over a very complex terrain being the surface roughness constant, $z_o = 0.03m$. There are 37 wind turbines with a hub height of 55 m placed along two main rows oriented to SSW wind directions (fig. 3.2). In this figure, there are no UTM coordinates due to privacy policy. The main energetic wind direction is SSW (fig. 3.3). Therefore the simulations will be done into this sector. This fact has

some implications concerning the boundary conditions because WindMesh1.0 is not able to rotate and the computational domain has to be built using the axis North-South and East-West. West and South boundaries are considered as inlet boundaries. North and East boundaries are considered as outlet boundaries.

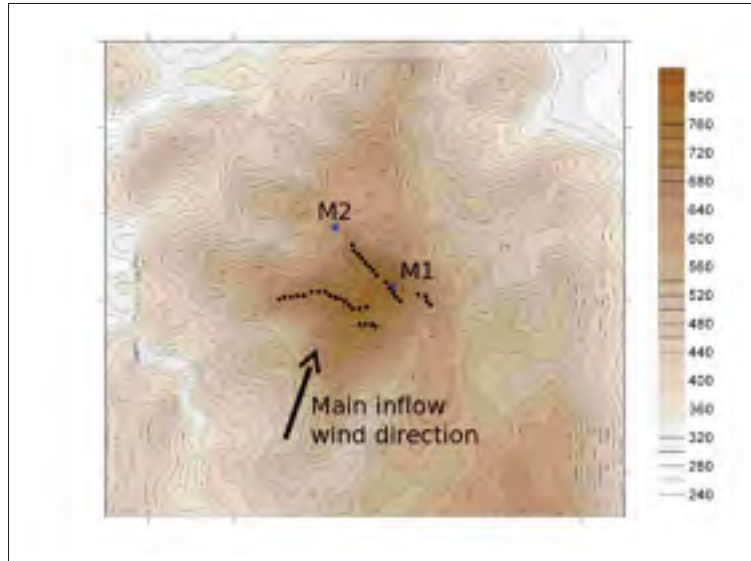


Figure 3.2 Complex terrain wind farm orography and wind turbine positions

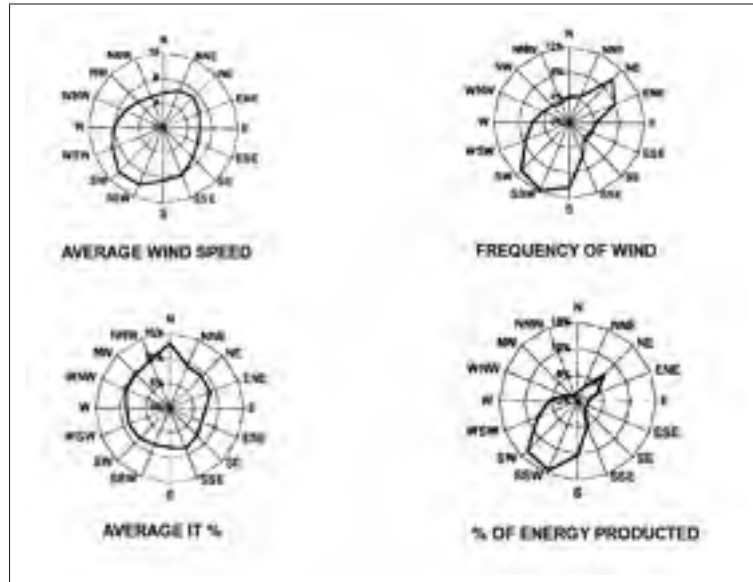


Figure 3.3 Complex terrain wind farm wind roses

3.3 Sensitivity Analysis

3.3.1 Base case

The parameters selected for the Base Case simulation are chosen according to different experts judgement found in the wide literature of CFD wind flow simulations (see Franke *et al.* (2007), Cabezón *et al.* (2011b)). To begin with, Stull (2009) shows that the turbulent phenomena taking place in microscale has an order of magnitude around 20 meters ($\mathbf{Dx} = \mathbf{20\ m}$) in an horizontal spatial scale. As Cabezón *et al.* (2011b) have indicated, the minimum number of nodes below the hub height has to be 10, in order to capture the mean velocity gradients near the ground. The choice of the top height has been based on the wind engineering reference guideline of $Z_{top} = 5H$ (with $H = 500m$ the height between the lowest and the highest point of our terrain (fig. 3.4), the number of verticals cells of the domain has been fixed to $\mathbf{N_z} = \mathbf{30}$ and the first cell height to $Z_1 = 1m$ for the base case.

On the other hand the domain extension has to be considered. As the simulation of the flow on the wind farm zone implies a very high computational cost insomuch as it is the finest zone of the mesh, the extension of that area is slightly higher than the distance between the two turbines away from each other, $L_{WF} = 3600m = 1WF$ (with a WF measure of length that will widely

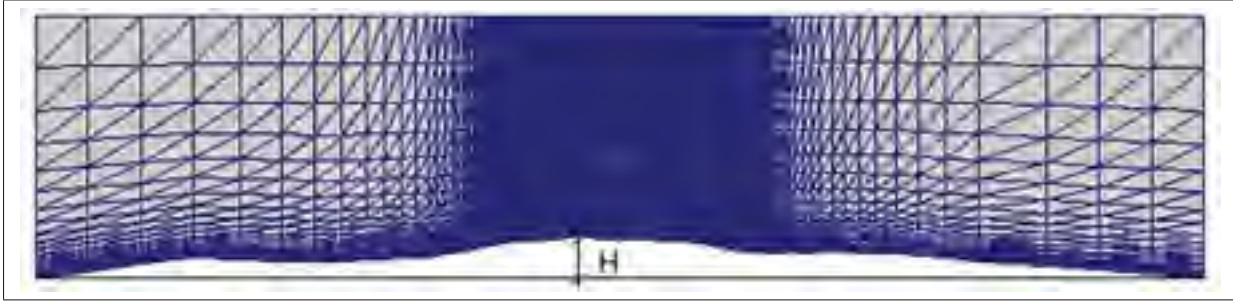


Figure 3.4 Plane along the SSW direction over wind farm

used in this memoir). For this reason, the extension of the Transition Zone is $L_{TZ} = 1WF$ in the four main directions. The buffer area is considered as $L_{BF} = 2km$ long although it could be enlarge considerably due to its low computational cost. The three different zones are presented on figure 3.5 Appendix II. Finally, the ratio between the horizontal length of the cells in the wind farm zone and the buffer zone is fixed to $\lambda = 30$. This ratio allow to know the importance of the horizontal discretization in the buffer zone.

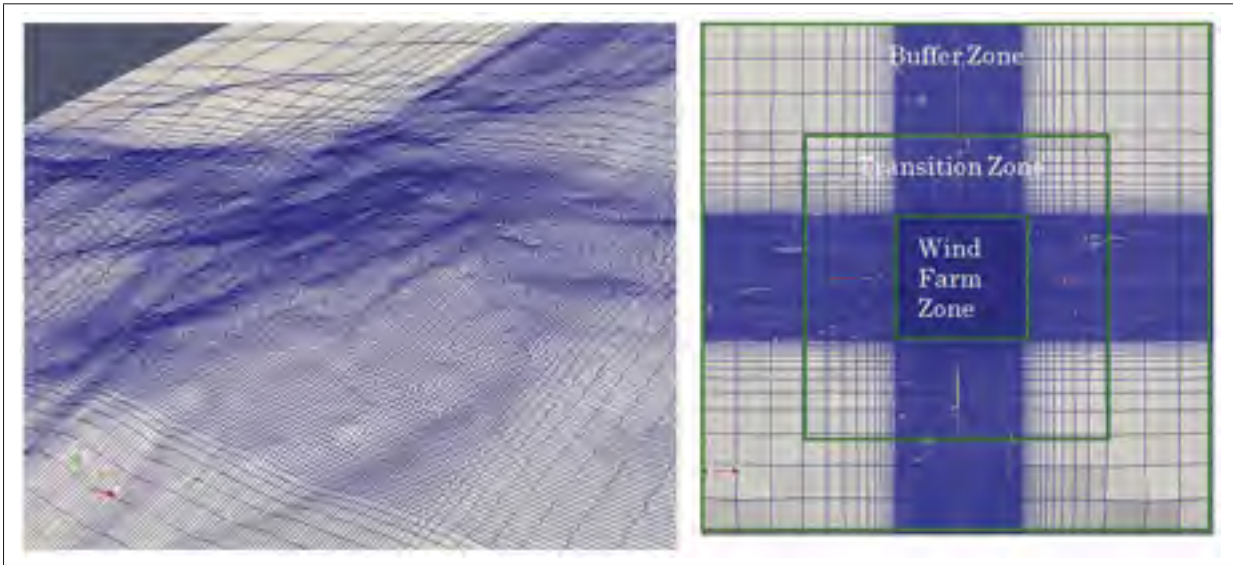


Figure 3.5 Details on the three zones of the computational domain and their resolution

3.3.2 Other cases

In table 3.1, all the cases of the sensitivity analysis are presented.

Table 3.1 Table for Sensitivity Analysis of Wind Flow Model over complex terrain

| ID Case | Name Case | Dx [m] | N_z | $Z_{top}[m]$ | $Z_1[m]$ | $L_{WF}[WF]$ | $L_{TZ}[WF]$ | $L_{BF}[km]$ | λ |
|----------|--|-----------|-----------|--------------|------------|---------------|----------------|--------------|-----------|
| 0 | Base Case | 20 | 30 | 5H | 1 | WF | WF | 2 | 30 |
| 1A | Horizontal grid resolution | 12 | 30 | 5H | 1 | WF | WF | 2 | 30 |
| 1B | | 30 | 30 | 5H | 1 | WF | WF | 2 | 30 |
| 1C | | 35 | 30 | 5H | 1 | WF | WF | 2 | 30 |
| 1D | | 60 | 30 | 5H | 1 | WF | WF | 2 | 30 |
| 2A | Number of vertical cells | 20 | 20 | 5H | 1 | WF | WF | 2 | 30 |
| 2B | | 20 | 40 | 5H | 1 | WF | WF | 2 | 30 |
| 2C | | 20 | 10 | 5H | 1 | WF | WF | 2 | 30 |
| 3A | Domain Height | 20 | 30 | 2.5H | 1 | WF | WF | 2 | 30 |
| 3B | | 20 | 30 | 10H | 1 | WF | WF | 2 | 30 |
| 3C | | 20 | 30 | 7.5H | 1 | WF | WF | 2 | 30 |
| 3D | | 20 | 30 | 12H | 1 | WF | WF | 2 | 30 |
| 3E | | 20 | 30 | 15H | 1 | WF | WF | 2 | 30 |
| 4A | Height of the first cell | 20 | 30 | 5H | 0.5 | WF | WF | 2 | 30 |
| 4B | | 20 | 30 | 5H | 2 | WF | WF | 2 | 30 |
| 4C | | 20 | 30 | 5H | 0.6 | WF | WF | 2 | 30 |
| 5A | Length of Wind Farm Area | 20 | 30 | 5H | 1 | 0.5 WF | WF | 2 | 30 |
| 5B | | 20 | 30 | 5H | 1 | 2 WF | WF | 2 | 30 |
| 6B | Length of Transition Area | 20 | 30 | 5H | 1 | WF | 1.5 WF | 2 | 30 |
| 6C | | 20 | 30 | 5H | 1 | WF | 1.67 WF | 2 | 30 |
| 6D | | 20 | 30 | 5H | 1 | WF | 2 WF | 2 | 30 |
| 7A | Length of Buffer Area | 20 | 30 | 5H | 1 | WF | WF | 1.2 | 30 |
| 7B | | 20 | 30 | 5H | 1 | WF | WF | 4 | 30 |
| 7C | | 20 | 30 | 5H | 1 | WF | WF | 8 | 30 |
| 7D | | 20 | 30 | 5H | 1 | WF | WF | 16 | 30 |
| 7E | | 20 | 30 | 5H | 1 | WF | WF | 24 | 30 |
| 8A | Ratio of first to last cell size (λ) | 20 | 30 | 5H | 1 | WF | WF | 2 | 20 |
| 8B | | 20 | 30 | 5H | 1 | WF | WF | 2 | 40 |

3.4 Sensitivity results

3.4.1 Criteria

It has to be reminded that optimizing is not just to refine the grid domain but to reduce the computational time of simulation. The parameters have been chosen by considering both aspects. In this work, the grid convergence in wind speed velocity will be considered for an average difference of 1% (see eq. 3.1) between two consecutive cases in the wind turbine positions. As the range of the wind speed velocities is about 10m/s, the error will be of the order of a tenth of a m/s. Once this difference is achieved, the coarser value of the input parameter will be chosen as optimum. In this manner, as an example, if the sensitivity analysis is built on the height of the domain and the difference is lower than 1% between the cases 3B and 3C, then a value of 7.5H as height of the domain will be recommend for CFDWind1.0 and WindMesh users over complex terrain.

$$\frac{\Delta V_{fc}}{V_{coarse}} = \frac{V_{fine} - V_{coarse}}{V_{coarse}} \leq 1\% \quad (3.1)$$

The error on TKE is also presented in the results due to its relevance in wind engineering studies. The high errors on TKE will be discussed. Nevertheless, the error in wind speed velocity is the only one taken into account to choose the optimal parameter. In terms of simulation convergence, the residuals have to achieve 10^{-5} for pressure and 10^{-7} for the rest of the fields. The number of iterations depends on every single case, going from 1000 to 12000 iterations.

3.4.2 Average relative error

In table 4.2, the average relative error in the wind turbine positions, on Speed-up and TKE, between two consecutive cases are presented.

Table 3.2 Results of Sensitivity Analysis for Wind Flow model

| | ID case | Input Parameter | % Wind speed error | % TKE error |
|---------------------------|-----------|-----------------|--------------------|-------------|
| Horizontal Resolution | 1A | 12 m | 0.0289 | 0.1023 |
| | 1C | 15 m | 0.2943 | 1.7901 |
| | Base Case | 20 m | 0.6928 | 0.3216 |
| | 1B | 30 m | 7.0076 | 0.6562 |
| | 1D | 60 m | - | - |
| Vertical Levels | 2C | 10 levels | 1.5531 | 12.5465 |
| | 2A | 20 levels | 0.3991 | 1.1226 |
| | Base Case | 30 levels | 0.0895 | 0.0932 |
| | 2B | 40 levels | - | - |
| Domain Height | 3A | 2.5 H | 26.1089 | 30.1785 |
| | Base Case | 5 H | 6.6683 | 2.9998 |
| | 3C | 7.5H | 1.8109 | 0.7996 |
| | 3B | 10 H | 1.231 | 1.4161 |
| | 3D | 12 H | 0.0888 | 1.3289 |
| | 3E | 15 H | - | - |
| First Cell Height | 4A | 0.5 m | 1.5531 | 0.1622 |
| | 4C | 0.6 m | 0.3991 | 0.0961 |
| | Base Case | 1 m | 0.0895 | 0.3823 |
| | 4B | 2 m | - | - |
| Length of Wind Farm Zone | 5A | 0.5 WF | 2.7412 | 10.5338 |
| | Base case | 1 WF | 0.0174 | 6.317 |
| | 5B | 2 WF | - | - |
| Length of Transition Zone | Base Case | 1 WF | 0.452 | 0.7548 |
| | 6B | 1.5 WF | 0.1756 | 0.5264 |
| | 6C | 1.67 WF | 0.1616 | 0.1253 |
| | 6D | 2 WF | - | - |
| Length of Buffer Zone | 7A | 1.2 km | 3.4604 | 1.7767 |
| | Base case | 2 km | 3.6869 | 4.0492 |
| | 7B | 4 km | 1.5013 | 3.1763 |
| | 7C | 8 km | 1.1875 | 2.9896 |
| | 7D | 16 km | 0.6118 | 0.9367 |
| | 7E | 24 km | - | - |
| λ | 8A | 20 λ | 0.613 | 4.926 |
| | Base case | 30 λ | 1.6064 | 2.2196 |
| | 8B | 40 λ | - | - |

3.4.3 Discussion on the selection of input parameters

The discussion of the selection will be based on bibliography and experience in CFD simulations.

a. Horizontal grid resolution

As Stull (2009) expose in his book, the phenomena taking place in our scale of study and having a non-negligible effect on wind engineering field have as maximum an horizontal spatial scale of 20-30m. CFDWind1.0 neglects the thermal effects, so it can be ensure that the mechanical turbulence due to the orography will mark the difference of obtained results. Even if the difference between 30m and 20m is under the chosen criteria of 1%, the horizontal grid resolution advisable is 20 m to be able to capture the recirculation of the wind beacuse of the orography effect even though the error of TKE is higher between 20 and 15 m cases.

b. Number of vertical cells

The number of vertical cells is important related with the number of nodes of the grid below the hub height. Depending on it, the solver is capable of characterizing accurately the vertical gradient of the different variables. As we can observe in fig. 3.6 and fig. 3.7, a grid with 10 nodes in the vertical direction is quite far to reproduce faithfully the vertical profiles. The case 2A (20 nodes) present accurate results, nevertheless, 25 verticals levels will be recommended. The geometric distribution in the vertical direction implies that under the hub height there are 11 nodes. It should be clarified that Franke *et al.* (2007) recommend an cell-to-cell expasion ratio below 1.5, and normally taking 1.2 as the maximum value. Nevertheless the vertical expansion ratio is 1.30 in the case of 20 vertical levels, so maximum value of Franke *et al.* (2007) seems highly conservative for studies in complex terrain. In the case of 10 vertical levels the expansion ratio is 2.15, clearly out of the recommended limits.

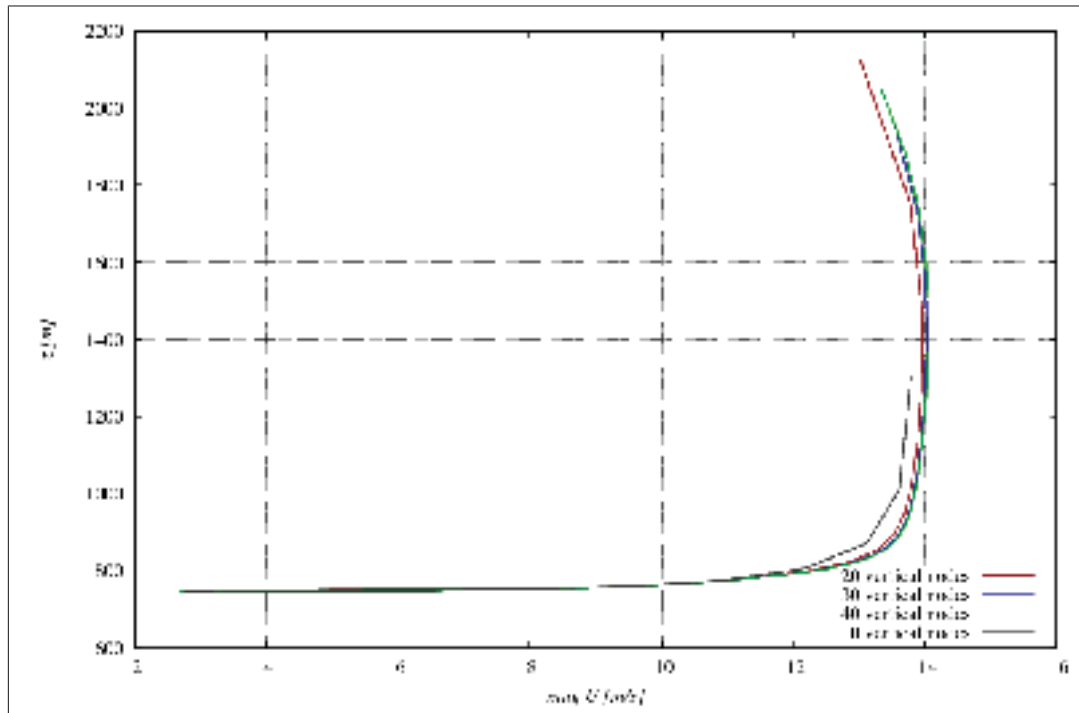


Figure 3.6 Wind speed profile at the wind farm center depending on vertical levels

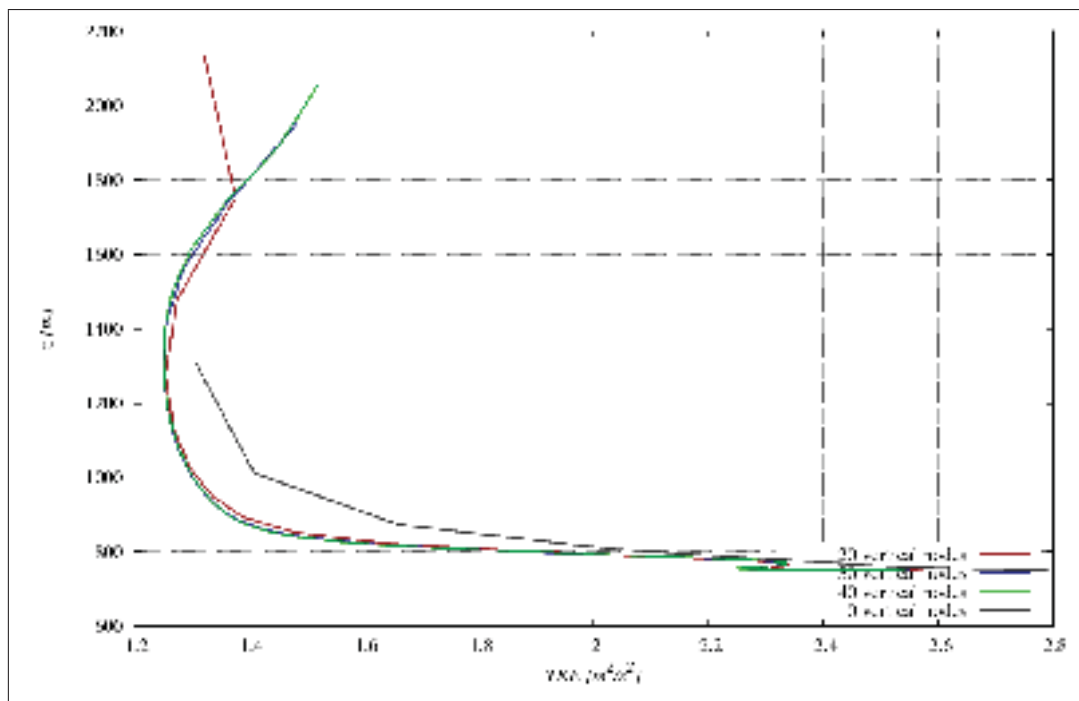


Figure 3.7 TKE profile at the wind farm center depending on vertical levels

c. Height of the computational domain

Concerning domain height, it is possible to find cases where it varies from $5H$ (Franke *et al.* (2007)) to $40H$ (Martinez (2011)). Despite using $5H$ the default value, the wind engineering guideline recommend this domain height for urban studies. In a case with complex terrain, the blockage area is higher than that produced by a single building. In fact, the blockage effect can be appreciated by an important acceleration of the wind flow speed for those cases where height is $2.5H$ and $5H$ (see fig 3.8). To satisfy our criteria of selection, a height of $12H$ will be recommended.

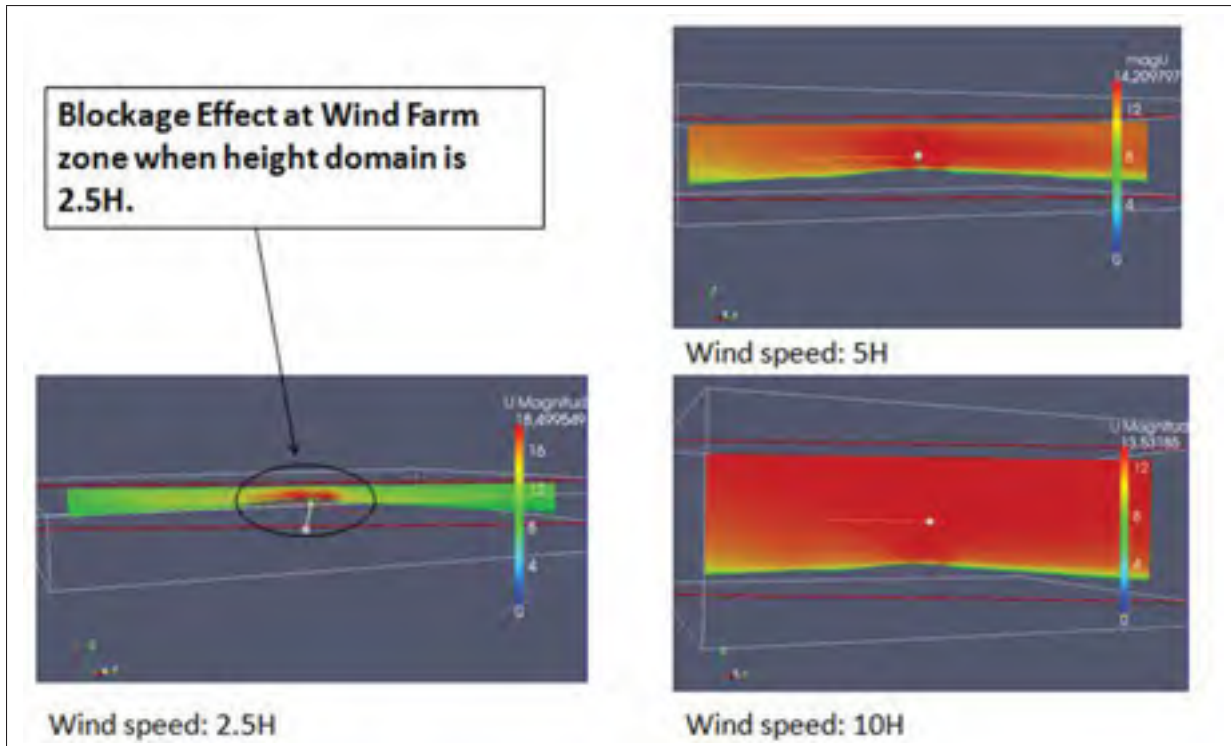


Figure 3.8 Wind flow along main energetic directions for three different height of the domain

d. Height of the first cell

In relation to the height of the first cell, it does not seem to have a major importance for studies at tens of meters above the ground. An appropriate criteria is more related to the number of nodes in the first hundred meters. In the case where the Blocken *et al.*

(2007) recommendation is not considered (eq. 1.26), the results do not vary significantly. The parameter is fixed to 1 m to simplify. The first cell height is more important in the recirculation zones (downstream) (see Palma *et al.* (2008)). As the wind farm is not located in recirculation zones, this parameters becomes less important.

e. Lambda

By varying the paramaters called λ , we are changing the horizontal length of the cells located in the buffer zone. Observing the profiles of the wind speed and the TKE (fig. 3.9) entering to the transition zone from the buffer zone in the wind flow direction, it is possible to conclude that the discretization of the buffer zone has no direct effects on the physical variables. However, an increase of the length of the Buffer Zone cells involves changes in horizontal expansion of the transition zone. Transition zone is formed by cells expanded linearly from the Wind Farm Zone to the Buffer Zone. For each one of the three cases, the horizontal expansion ratio and the number of cells are different. In the Base case and the case 8B, the discretization of the transition zone does not capture the increasing gradient of the TKE (see fig. 3.10). The ratios of the horizontal expansion for the cases of 20, 30 and 40 λ are respectively 1.117, 1.196, 1.279 so it appears more sensitive than the vertical ratio of expansion. As λ is not a critical parameter in terms of computational time, the ratio proposed would be the finest: $\lambda = \frac{L_{BZ}}{L_{WF}} = 20$.

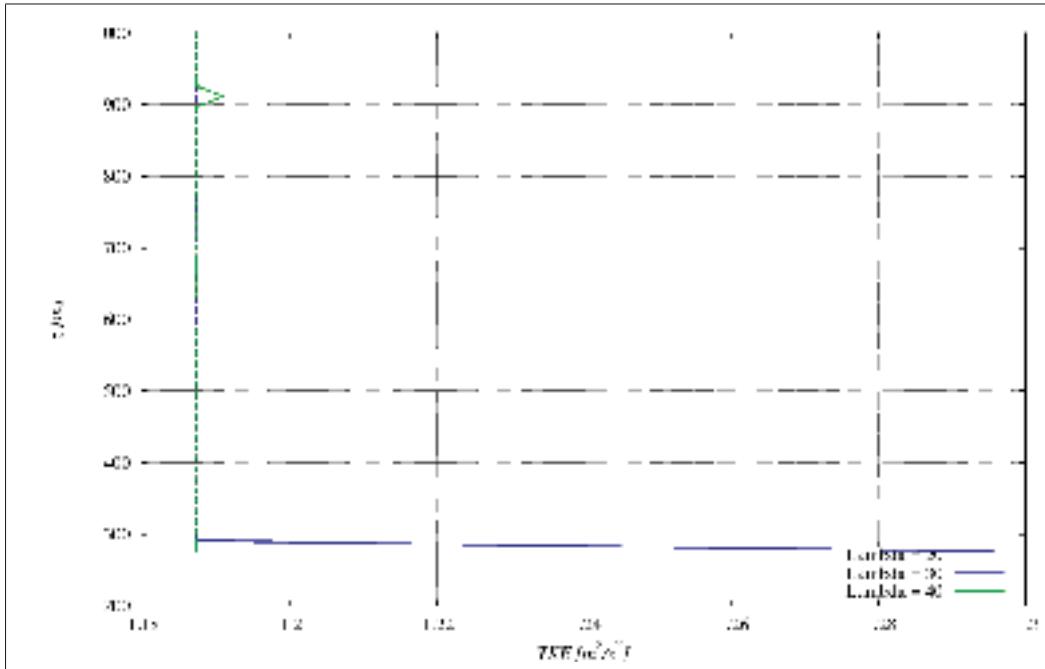


Figure 3.9 TKE profiles at the entrance of the buffer zone depending on λ ratio

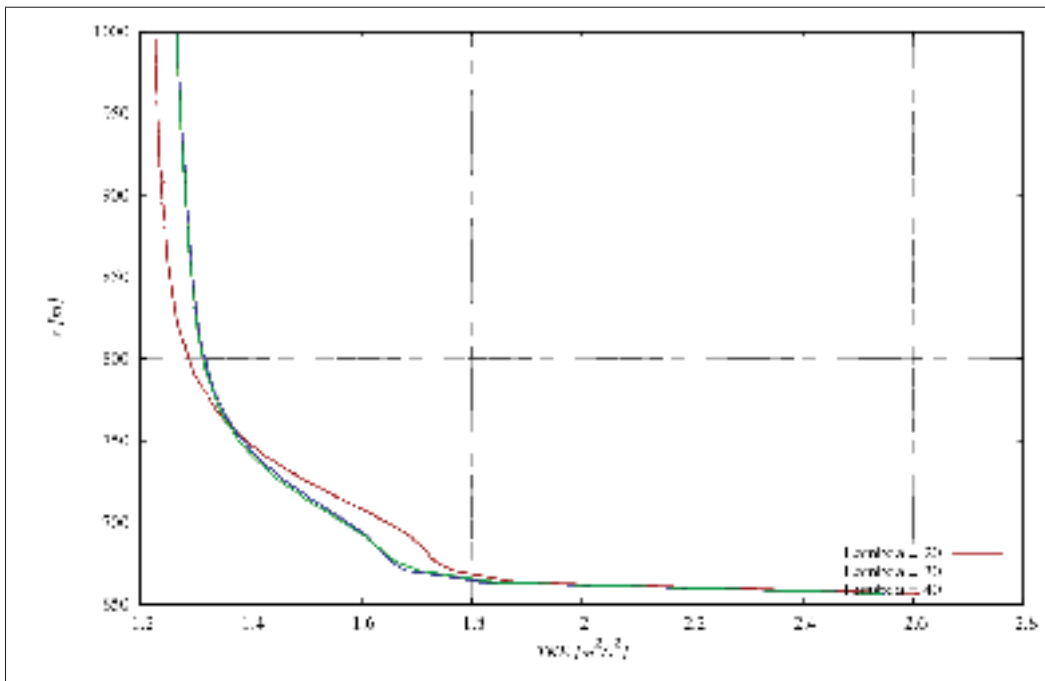


Figure 3.10 TKE profiles at the entrance of the transition zone depending on λ ratio

f. Transition Zone

Extending the transition zone implies that buffer zone is located further of the wind farm zone. Then, even being a flat zone with a small slope, its slope can be different. This is the origin of the different wind speed profiles at the entrance of the transition zone (fig. 3.11). Approaching to the wind farm zone, the wind speed profiles become increasingly similar (fig. 3.12) because the orography of the wall is the same for all the cases near the wind farm zone. By observing the relative errors, we can conclude that the differences for velocity and TKE are negligible so the chosen value is an extension of 1 WF.

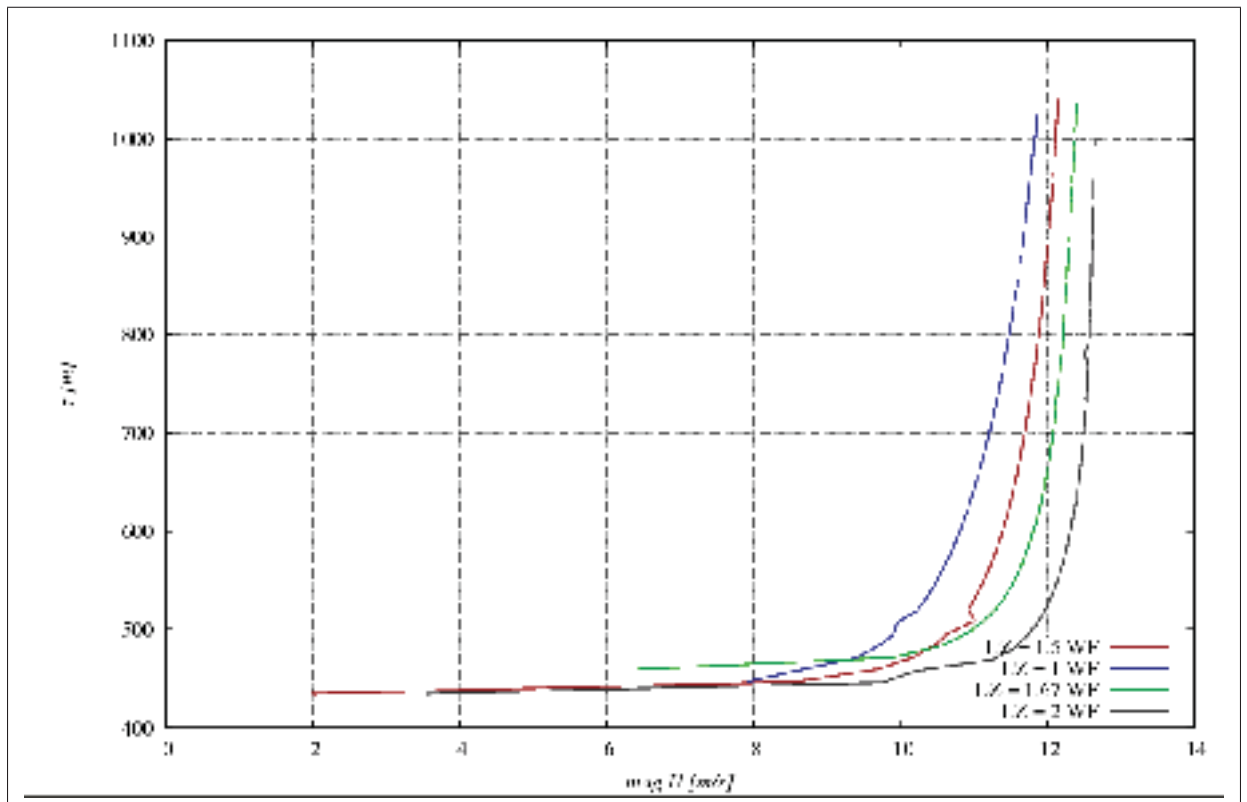


Figure 3.11 Inlet wind speed profiles at the entrance of the transition zone depending on transition zone length

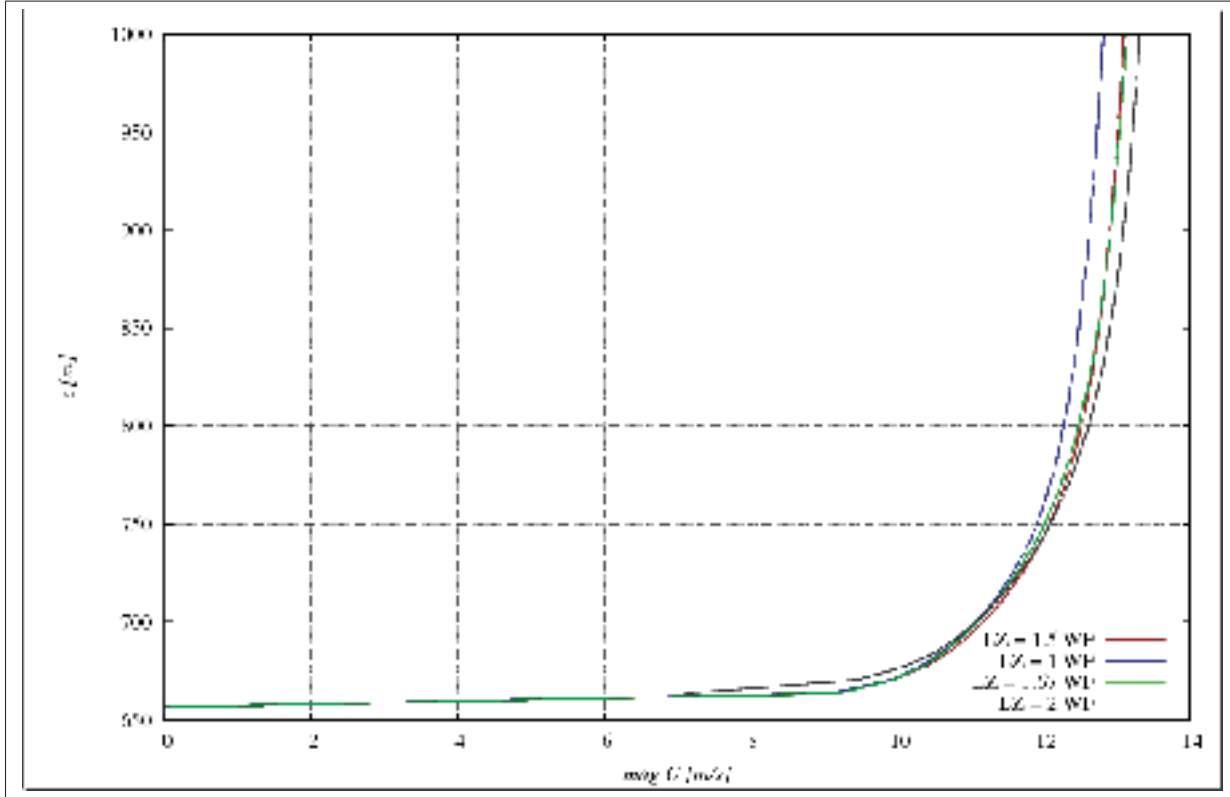


Figure 3.12 Inlet wind speed profiles at the entrance of the wind farm zone depending on transition zone length

g. Buffer Zone

z_{Ground} is one of the outputs given by WindMesh. It is the lowest height of the outer contour of the Transition Zone. WindMesh imposes that the entire contour of the Buffer Zone is located at the height of z_{Ground} . In this manner, the outer contour of the buffer zone will achieve the outer contour of the transition zone by slopes of straight lines. Accordingly, the more widespread is the buffer zone, the more smooth will be its slope. Ideally, the buffer zone should be completely flat, so the more widespread is, the more reliable will be the results. Following our recommendation criteria for choosing meshing parameters, 16 km of extension would be the minimum extension to consider the differ-

ence in the results as negligible. In the newest version of WindMesh, the buffer area is divided into two different zones. The outer zone is completely flat and the inner zone behaves as the ones used in our work. Unfortunately, at the beginning of this work it had not been developed yet. Finally, the optimal extension of each zone of the domain should be analysed.

h. Wind Farm Zone

As expected, if some of the wind turbine positions are located outside the wind farm zone the difference in terms of wind speed and TKE are very important. The extension of Wind Farm Zone is probably the most critical parameter of our sensitivity analysis because it is a factor that increase the total number of cells exponentially because it affects both horizontal directions. An extension of 1 WF, implies a domain containing 1.6 millions cells while 2 WF of extension implies 4.5 millions of cells. Comparing the output of the base case (1 WF) and the case 5B (2 WF) it is possible to appreciate that eventhough the wind speed doesn't seem very sensitive to the variation of the wind farm extension, TKE does as it can be observed in figure 3.13. This phenomena is about the solver and the discretization because the wind turbine locations with biggest difference are located near the boundaries of the wind farm zone. Near the boundaries, the calculation of the TKE still has an influence of the coarser horizontal resolution of the transition zone.

As the Wind Farm resolution is the most critical parameter in terms of computational time, an extra case is run to ensure the influence of adding discretization in the upstream direction. Both cases are done under the recommended parameters and changing the extension of the wind farm zone. On the one hand, a total extension of 1 WF in both horizontal directions (N-S, W-E). On the other hand, an addition of 0.25 WF extension in the upstream directions (south and west). No extension is considered necessary on the downstream because in this study we are not interested in wakes. Extending the Wind Farm Zone to the upstream direction and comparing the results with the case 5B (2WF), the difference in TKE falls from 6.317% to 1.653%. In velocity, the differences are

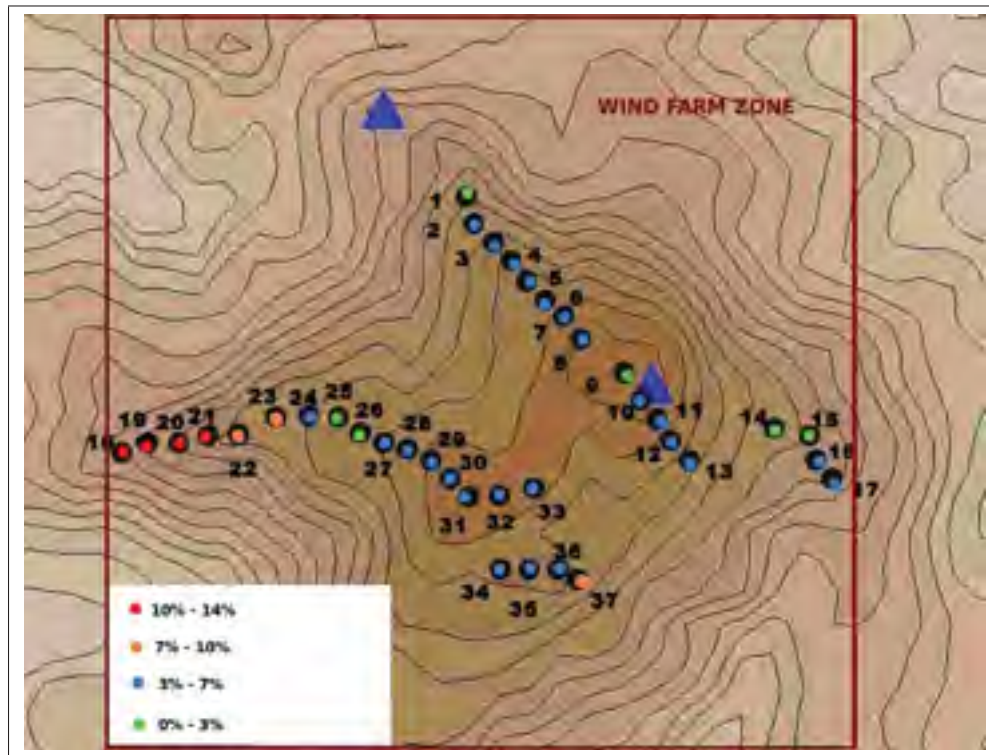


Figure 3.13 Relative error on TKE comparing Base Case and case 5B

lower than 0,15%. As TKE is a secondary factor in front of wind speed when it comes wind resource study, and the extension of the wind farm zone is critical in terms of computational time, the addition of 0.25 WF in the upstream direction will be advisable when high computational power is available.

The table 3.3 is an overview of the converged and recommended meshing parameters.

CFDWind 1.0 over complex terrain using WindMesh has been verified, the whole model has to be validated by comparing the simulation results of the ideal case to data measurements.

3.5 Validation results

Once the optimal values are determined, a new simulation is run using the and the results are compared with real data. The comparison is done through a methodology detailed below:

Table 3.3 Guideline of geometric parameters for CFD wind simulations over complex terrain

| Geometric parameter | Recommended |
|-------------------------------|---|
| Δ_x | 20-30 m |
| N_z | 25 levels |
| Domain Height | 12 H |
| z_1 | 1 m |
| L_{WF} | 1 WF (+ an advisable extension of 0.25WF in the upstream direction) |
| L_{TZ} | 1 WF |
| L_{BZ} | 16 km |
| ratio $\frac{L_{BZ}}{L_{WF}}$ | 20 |

- a. Just the wind turbine positions located in freestream are taking into account (wind turbines: 18-37) because for the incoming wind of (202,5° sector), the existing wakes are not modelled on the simulations.
- b. Only experimental wind speed above 6 m/s are considered. Wind speed below 6 m/s is considered as negligible in terms of production by the company.
- c. The horizontal component of the wind speed at the hub height have been post-processed from the model. The output of OpenFOAM in terms of wind speed velocity is (u, v, w) . To build the speed-up ratios, $\sqrt{u^2 + v^2}$ is considered and the vertical component is neglected.
- d. The comparison is done in terms of speed-up ratios to avoid the presence of real and absolute data in this work. This is a request of the company that operates the onshore wind farm. In addition, the wind profile used in the simulation is probably different from the one blowing at the onshore wind farm, so a comparison of absolute velocity would make no sense. In the contrary, by comparing speed-up ratios, the relative wind speed between different turbines are compared.
- e. The reference velocity is the data of the wind turbine number 34 (In the figure 3.14 it's the number 33). This turbine is the chosen one because it is the first turbine contacting a wind coming from SSW (see figure 3.13

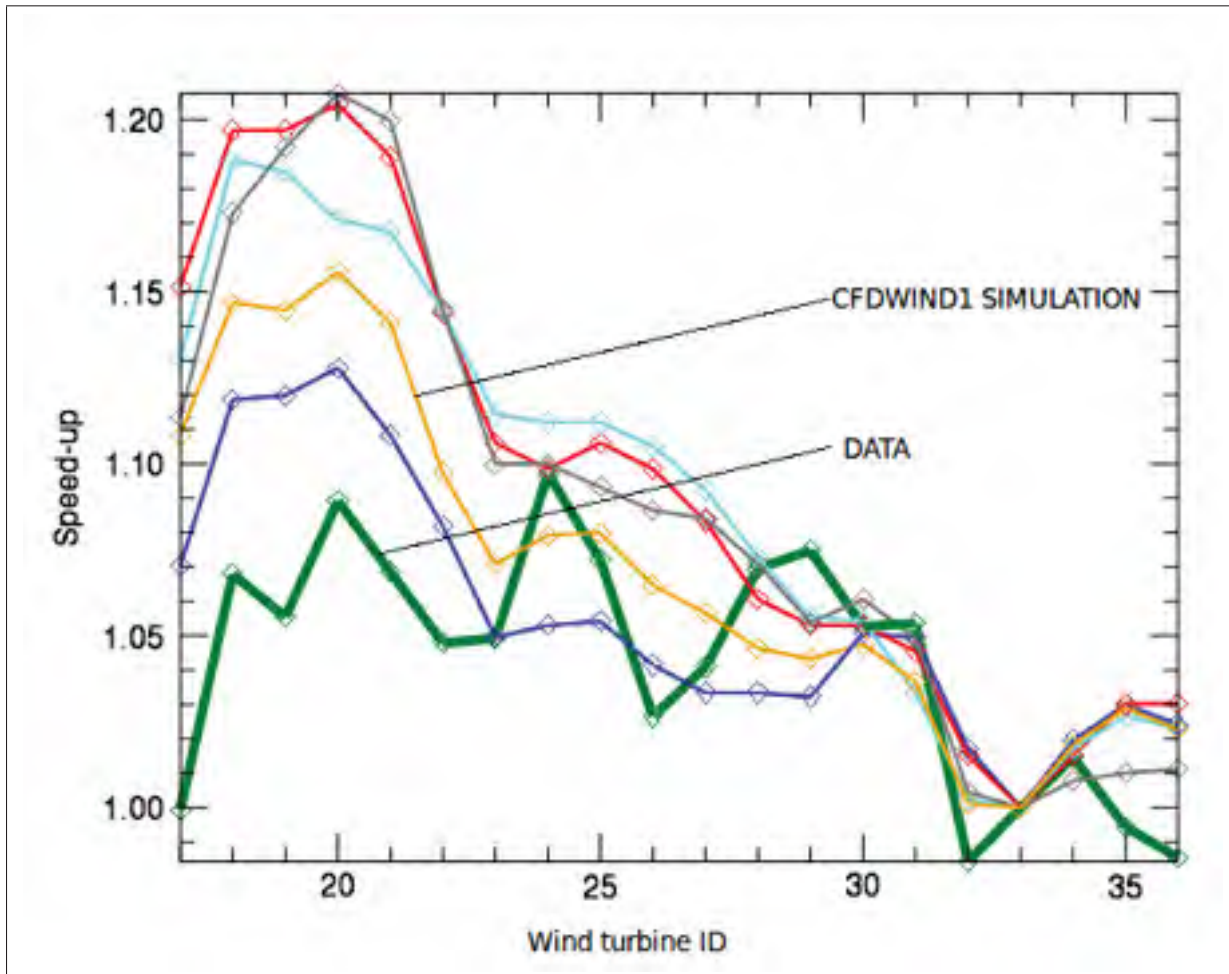


Figure 3.14 Comparing data with different modelisation results

In the figure 3.14, the results on wind speed ratio using CFDWind1.0 through OpenFOAM are compared to real data among other commercial softwares (without specification) as WASP, MeteoDyn, WindSim or Alya (developed at BSC). All the softwares show the same trend in terms of wind speed ratio. They present good accuracy from the wind turbine 24 to the wind turbine 36. Nevertheless, all of them shown an important over-prediction in the western zone of the wind farm (ID 17 to 23). Such prediction error could have different explanations. Observe that the positions are in the high part of a sloped zone. Softwares could have problems

to mesh correctly the slope or numerical methods could forecast an acceleration of the wind that really has no place. The relative error on predictions between data (green line in figure 3.14) and CFDWind1.0 is **2,23%**. As the error is lower than the one obtained applying commercial models, the geometrical parameters recommended can be considered as an accurate guideline for further studies using CFDWind 1.0 over complex terrain of similar dimensions and characteristics as the one studied in this sensitivity analysis.

CHAPTER 4

MESH SENSITIVITY ANALYSIS OF CFD WAKE MODEL OVER OFFSHORE WIND FARM

4.1 Offshore wind farms: Advantages and disadvantages

Although at the beginnings of the 17th century, Don Quijote already faced some windmill, the wind has started to be a powerful source of energy towards the eighties. Since then, the development of wind turbines has grown uniformly. Nowadays, offshore wind energy is becoming more important and research is moving to new problems such as: wakes created by big wind turbines.

Offshore wind farms present several advantages compared with onshore wind farms. As roughness is significantly lower in the sea, sea wind speed is higher and the exploitable wind resource increase significantly. Due to this higher wind resource, the installed turbines can have a larger diameter and generate an average of almost 4 times more wind power than onshore windfarms. In addition, water covers more than two-thirds of Earth surfaces without topography problems, so the possibilities of offshore wind farm installation are practically unlimited.

Nevertheless, some inconvenients have to be taken into account. As previously detailed, the low roughness length at the seas and the stable atmosphere typical of offshore climates leads to low ambient turbulence values, that makes difficult to re-establish the wind flow after passing through wind turbines. That implies bigger wakes. Hence, two consecutive turbines of a same row of in the wind flow direction have to be further one from each others.

R&D departments are working on the development of floating platforms for wind turbines. These structures will allow more possibilities of installation in offshore, but currently, they are too expensive in execution and maintenance to justify them. Nowadays, most of the offshore wind farms are located near the coast and the turbines are embedded in the seabed. This operation considerably raises the cost of installing offshore turbines.

4.2 Horns Rev Wind Farm

Located 14 km away from Blavands Hulk, at the south western coast of Denmark, Horns Rev is probably the best known and photographed offshore wind farm in the world. Up to 80 Vestas V80 turbines with a hub height of 70 m and 80 ms of diameter are placed in a grid pattern of 8 rows (east-west) and 10 columns (north-south). Each turbine has an installed nominal power of 1.8 MW and the total wind farm output is about 150 MW (Elsamprojekt (2000)).

As the main wind direction is 270° , the behaviour of the 6 inner rows can be considered similar, therefore just 3 rows will be simulated (see fig. 4.1 and 4.2).



Figure 4.1 Horns Rev Wind Farm layout

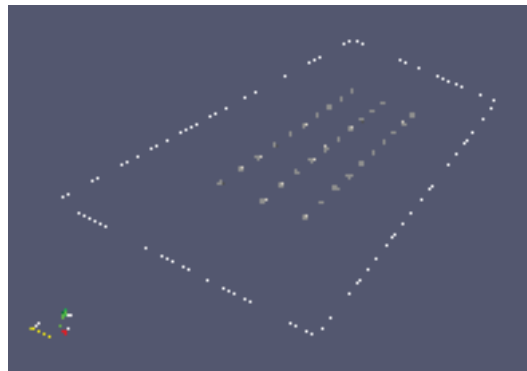


Figure 4.2 Representation of the Horns Rev Offshore Wind Farm with Paraview

4.3 Computational Domain

Offshore wind farms are easier to simulate since water is considered as a flat terrain with low surface roughness (z_0 lower than 0.001m) . The application used to create the mesh is blockMeshDict (OpenCFD (2009)) contained in OpenFOAM's package. The domain is 10 km long (in the wind flow inlet direction (west-east)) and 3.2 km wide (north-south). Since the wind farm currently studied has different characteristics regarding the already studied, the height of the computational domain is again a geometrical parameter to analyze. The first wind turbine is located at 2 km downstream of the inlet boundary and the last one at 3 km upstream of the outlet boundary. Horizontal resolution is constant where as the vertical direction is the graded within different expansion ratios.

4.4 Limitations of the numerical model and *simpleWindFoam* solver

The turbulence and the wind flow models applied in this second part of the project are the ones used in the first sensitivity analysis. For this study, k- ϵ turbulent model modified according to Panofsky *et al.* (1977) and CFDWind1.0 wind flow model are used. Due to the amount of simulations during the whole project, the offshore grid dependence analysis is also done through RANS model, while Wolton (2008) has shown the improvements achieved by modelling in LES. The obtained results could be extended as recommended geometric parameters for future works using OpenFOAM and actuatorDisk (OpenCFD (2009)) application with a LES turbulent model.

There are two differences related to boundary conditions in regard to the first sensitivity analysis: the roughness length and the lateral patches. First, being an offshore wind farm, this parameter is reduced from 0.03 m in the case of the onshore wind farm to 0.000085 m (Elsam-projekt (2000)) for the considered flow case ($U_{ref} = 8$ m/s, $H_{ref} = 40$ m, wind direction: 270° , $TI = 12.24\%$). Second, this time, the wind inflow direction is 270 and enters perpendicularly to the inlet patch of the domain. As the flow direction is the same as the X-axis of the domain, northern and southern patches are considered as *symmetryPlane*.

As observed before, the major change regarding the first sensitivity analysis is the solver `simpleWindFoam` (OpenCFD (2009)) and its application `actuatorDisk`. The main feature of interest is the possibility of simulating the wind turbines as rotor disks by separating those cells laying inside the rotor disk and introducing a momentum source term to these cells. Thirty actuator disks are created. There is a nuance between the actuator disk concept and the `actuatorDisk` application from OpenFOAM, the thickness of the disk. Since, in OpenFOAM, the actuator disk is represented by cells instead of planes, the disks obtained have a non-zero thickness.

4.4.1 Actuator Disk Model

From the momentum theory (see Manwell *et al.* (2009)), the force extracted (eq. 4.1) from the incoming wind by the actuator disk (wind turbine) depends on the rotor area A , the upflow wind speed (V_o taken at 160 m (2D) from each actuator disk), the thrust coefficient C_t (fig. 4.3 represent the theoric curve of the thrust coefficient according to Vestas) and the air density ρ is:

$$T = \frac{1}{2} \rho V_o^2 A C_t \quad (4.1)$$

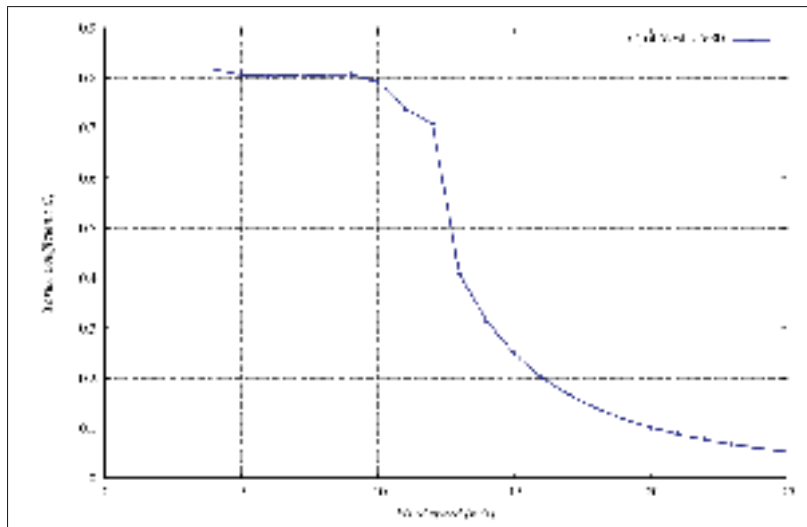


Figure 4.3 Thrust coefficient curve of the wind turbine modelled: Vestas V80

The actuator disk is decompose into i cells and the force extracted T is applied proportionally to its volume into the i cells. To choose the cells that represent the actuator disk, OpenFOAM use the utility `cellSetDict` (OpenCFD (2009)) (fig. 4.4).

```
// Name of set to operate on
name actuationDisk1;

// One of clear/new/invert/add/delete/subset/list
action new;

// Actions to apply to cellSet. These are all the topoSetSource's ending
// in ..ToCell (see the meshTools library).
topoSetSources
{
    // Cells with centre within cylinder
    cylinderToCell
    {
        p1      (150 0 36.23232143); // start point on cylinder axis
        p2      (152.5987832 0 36.23232143); // end point on cylinder axis
        radius   15;
    }
}
```

Figure 4.4 Example of *cellSetDict* file

It allows to create zones inside the domain in order to apply a special characteristic (the source term). The geometric shape defining the cells composing the actuator disk are cylinders with a 80 m diameter. The cells are chosen if they lay entirely within the cylinder. As known data, the user must enter a couple of points (extreme points of the cylinder axis) and the radius of the cylinder (radius of the turbine). The actuator disk will have the thickness of a single cell to be closer to the theory of the actuator disk model. In the case of the figure 4.4, the cylinder built has a wide of 2.5987 m ($p2_x - p1_x$) and a radius of 15 m.

4.4.2 Iterative algorithm of *simpleWindFoam*

Before showing the algorithm, it must be mentioned that this solver is prepared to work for a wide range of velocity bins. Nevertheless, as we are just interested on the geometric parameters, we will execute this solver in a single velocity bin. Thus, once the 30 cell zones (30

turbines) are created within the computational domain, the solver *simpleWindFoam* execute an iterative algorithm of five steps:

- a. Reading of the wind speed V_o of each cell located in the upstream direction at 160 m (2D) of each actuator disk. In the first place, V_o is obtained by applying the log-law at the hub height.
- b. Reading of thrust coefficient (fig. 4.3) provided by Vestas and according to the upstream V_o .
- c. Calculation of the source term (see eq. 4.1).
- d. Weighted distribution of the source term into the cells composing each actuator disk according to its size in front of the whole actuator disk.
- e. Start of simulation applying the source term.

4.5 Sensitivity Analysis

4.5.1 Base case

Analogously, the selected parameters for the Base Case simulation are chosen taking into account already existing literature, and the previous wind flow sensitivity analysis.

The **horizontal grid resolution** (Δ) is fixed at **0.2D** (being D the diameter of the actuator disk). This resolution is coarser than the one proposed by Cabezón *et al.* (2011b) because the present case of study is concerned with a much larger physical domain and therefore, the resolution proposed in the aforementioned article would implied a computational cost sixteen times higher.

Concerning the **vertical expansion ratio**, it is interesting to do a balance between high resolution in the lowest part of the domain and a non-deformed construction of the actuator disk (See

the case of $ratio = 350$ in the figure 4.7). The initial expansion ratio is fixed at **200**, having 9 cells under hub height.

In the first sensitivity analysis of this work it has been shown that 12 times the height of the obstacles of the domain is enough to avoid significant blockage effect. For the current analysis, flat terrain has to be considered so in principle, the domain should not be so high. The **height of the domain** chosen for the base case is 10 times the rotor diameter, so **800 m**. The **number of cells in the vertical direction is 20**. Finally, having an overview of the literature, the **upstream distance** where wind speed can be considered as freestream for isolated turbines is generally considered as **2D** (Yellow cell in the figure 4.5 at least (Cabezón *et al.* (2011b))).

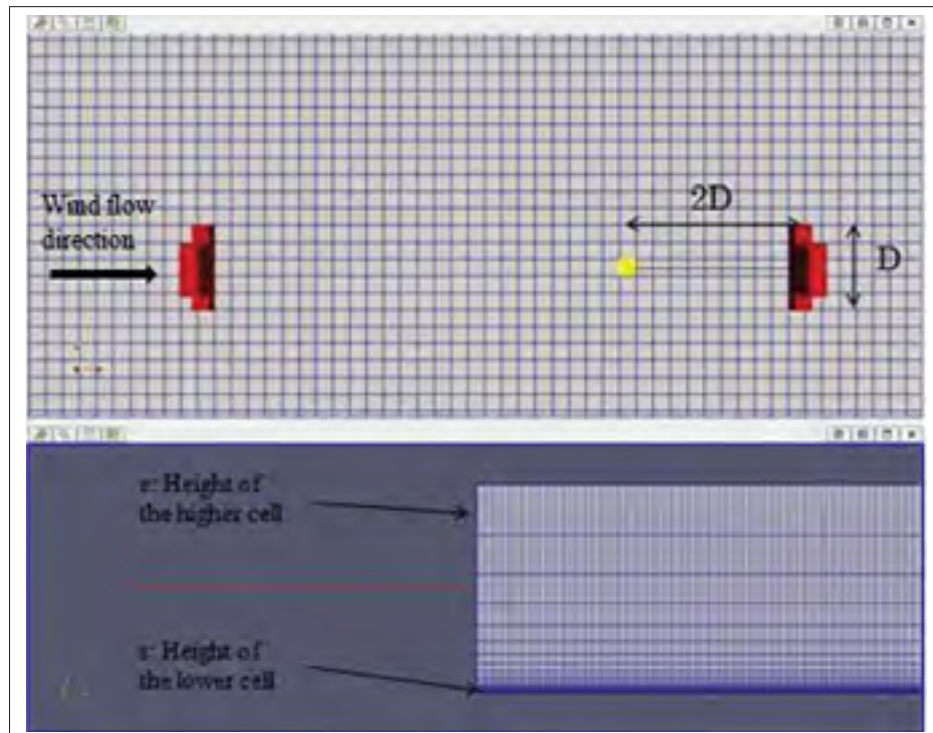


Figure 4.5 View of the computational domain from the top (above) and from south patch (beyond)

4.5.2 Other cases

In table 4.1, all the cases of the second sensitivity analysis are presented.

Table 4.1 Table for Sensitivity Analysis of Wake Model over offshore wind farm

| ID Case | Name Case | Δ [D] | Vertical Ratio | Domain height [D] | V_o | Vertical levels |
|---------|------------------------------|--------------|----------------|---------------------|----------|-----------------|
| 0 | Base Case | 0.2 | 200 | 10 (800 m) | 2 | 20 |
| 1A | Horizontal Resolution | 0.1 | 200 | 10 (800 m) | 2 | 20 |
| 1B | | 0.4 | 200 | 10 (800 m) | 2 | 20 |
| 2A | Vertical Ratio | 0.2 | 20 | 10 (800 m) | 2 | 20 |
| 2B | | 0.2 | 100 | 10 (800 m) | 2 | 20 |
| 2C | | 0.2 | 350 | 10 (800 m) | 2 | 20 |
| 3A | Domain Height | 0.2 | 200 | 7 D (560 m) | 2 | 20 |
| 3B | | 0.2 | 200 | 12 D (960 m) | 2 | 20 |
| 4A | Up Stream distance for V_o | 0.2 | 200 | 10 (800 m) | 1 | 20 |
| 4B | | 0.2 | 200 | 10 (800 m) | 3 | 20 |
| 5A | Vertical levels | 0.2 | 200 | 10 (800 m) | 2 | 10 |
| 5B | | 0.2 | 200 | 10 (800 m) | 2 | 40 |

4.6 Sensitivity results

Regarding as this second sensitivity analysis, the criteria for choosing the recommended parameters are the same than for the previous case. If two cases show a difference lower than 1% in wind speed the coarser value of the parameter is considered as optimal.

Table 4.2 Results of Sensitivity Analysis for Wake Flow model

| | ID case | Input Parameter | % Wind speed error | % TKE error |
|-----------------------|-----------|-----------------|--------------------|-------------|
| Horizontal resolution | 1A | 0.1 D | 0.2030 | 1.3129 |
| | Base Case | 0.2 D | 0.3632 | 5.6656 |
| | 1B | 0.4 D | - | - |
| Vertical Ratio | 2A | 20 | 0.3871 | 5.9788 |
| | 2B | 100 | 0.304 | 2.0537 |
| | Base Case | 200 | 0.845 | 3.0718 |
| | 2C | 350 | - | - |
| Domain Height | 3A | 7 D | 1.4678 | 2.8849 |
| | Base Case | 10 D | 0.2294 | 3.1455 |
| | 3B | 12 D | - | - |
| Up Stream Velocity | 4A | 1 D | 0.049 | 0.1113 |
| | Base case | 2 D | 0.579 | 2.7298 |
| | 4B | 3 D | - | - |
| Vertical levels | 5A | 10 | 1.7807 | 22.348 |
| | Base Case | 20 | 0.1034 | 1.5793 |
| | 5B | 40 | - | - |

4.6.1 Discussion on the selection of input parameters

a. Horizontal Resolution

In the sensitivity analysis for complex terrain, it has already been observed that the relative differences are higher for TKE than for wind speed. As in that case, for the horizontal resolution sensitivity analysis, the wind speed predictions present a negligible difference although TKE is highly sensitive to the horizontal resolution (fig. 4.6). The recommended value is 0.2 D. An additional inhouse study, has shown that the simulation results are more sensitive to a variation of the resolution in the cross direction than in the flow direction. A variation of resolution on the cross section varies the shape of the actuator disk and the wake flow while a variation in resolution in the flow direction only varies the thickness of the actuator disk and it as significative speking in terms of far wake. Such study expose the high gradients velocity in TKE in the wind flow cross sectional plane (see Versteeg and Malalasekera (2007)).

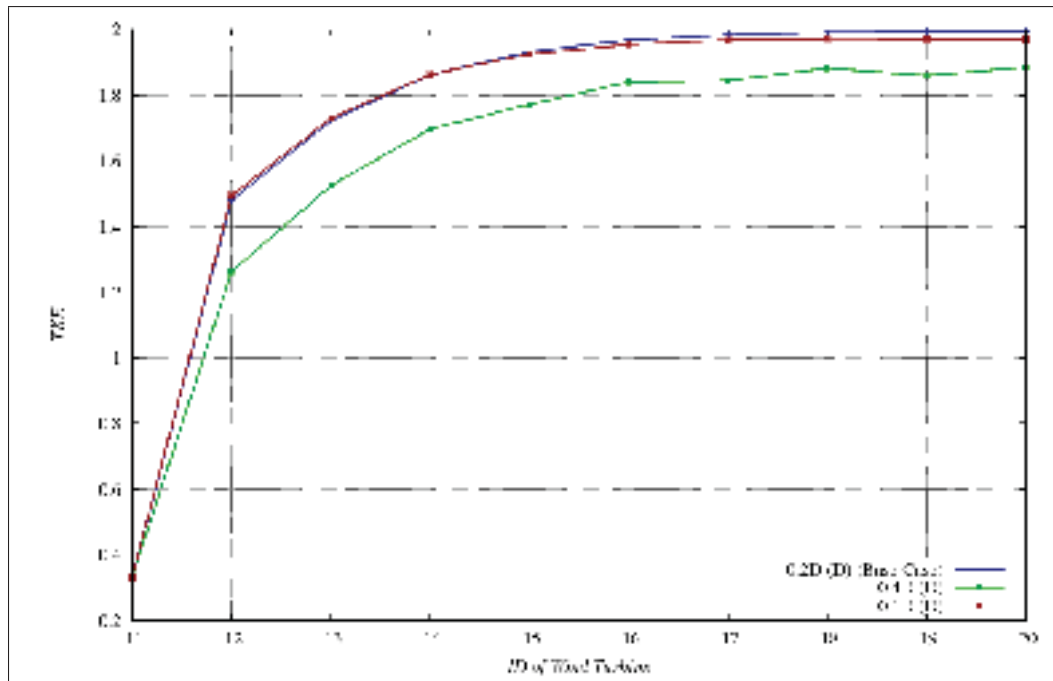


Figure 4.6 TKE for the internal row positions depending on mesh horizontal resolution

b. **Total Vertical Expansion Ratio**

When the vertical expansion ratio is chosen, the user has to be very careful about two different aspects. On the one hand, the ratio has to be high enough to capture the vertical gradients in the first two hundred meters. On the other hand, and taking into account how the application *actuatorDisk* creates the turbines, its shape can be extremely poor as for a vertical ratio of 350 (see fig. 4.7). According to the results, a vertical expansion ratio of 100 seems to make a good balance between both aspects.

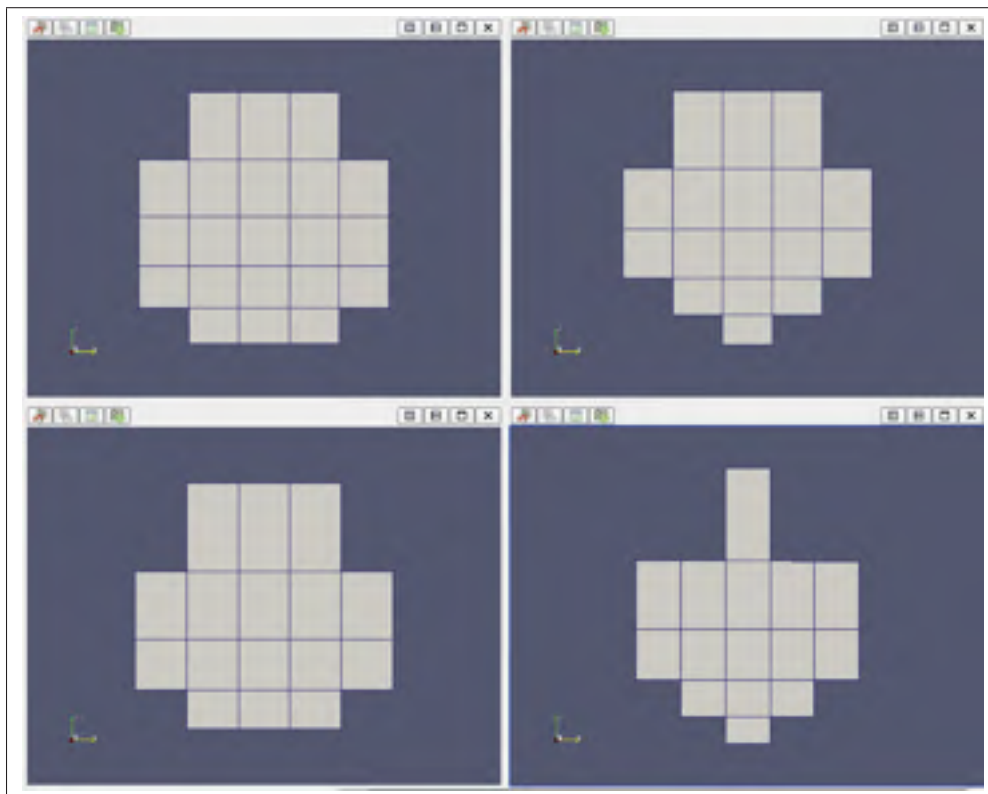


Figure 4.7 Shape of the actuator disk by vertical ratio: 20, 100, 200, 350 (from left to right and from top to bottom)

c. Domain Height

When the sensibility analysis is done for the height of the domain, the number of cells in the actuator disk should be as similar as possible for each single case. Contrary to the horizontal resolution study, the philosophy is to analyze just the blockage effect. Therefore, the vertical ratio and the number of vertical cells should be slightly modified in order to fix the same number of cells in the rotor disks. *MeshSpace* application is used to vary the height of the domain by maintaining the vertical distribution of cells in the first few hundred meters. *MeshSpace* is a calculator for grading the mesh in the blockMesh format. It can be downloaded at www.cfd-online.com. This tool solves the system of equations 4.2, where, L, n, k, r, d_s and d_e are respectively the height of the domain, number of cells in the vertical direction, cell-to-cell expansion ratio, total expansion ratio, bottom cell size and top cell size. The user must introduce a value for three of these parameters (one of them has to be L) and *MeshSpace* calculates the rest of them. *MeshSpace* does not always respect the exact values introduced by the user but use them as an approximation.

$$\left\{ \begin{array}{l} L = \sum_{i=0}^{n-1} d_s k^i \\ \frac{d_e}{d_s} = r \\ r = k^{n-1} \end{array} \right. \quad (4.2)$$

To generate a similar mesh structure in the first few hundred meters, the parameters to fix are, the height of the domain L, the first cell size d_s and the cell-to-cell expansion ratio k. As it can be observed by the red lines in the figure 4.8, the vertical expansion is mostly similar for the cases of 7D and 12D than for 10D.

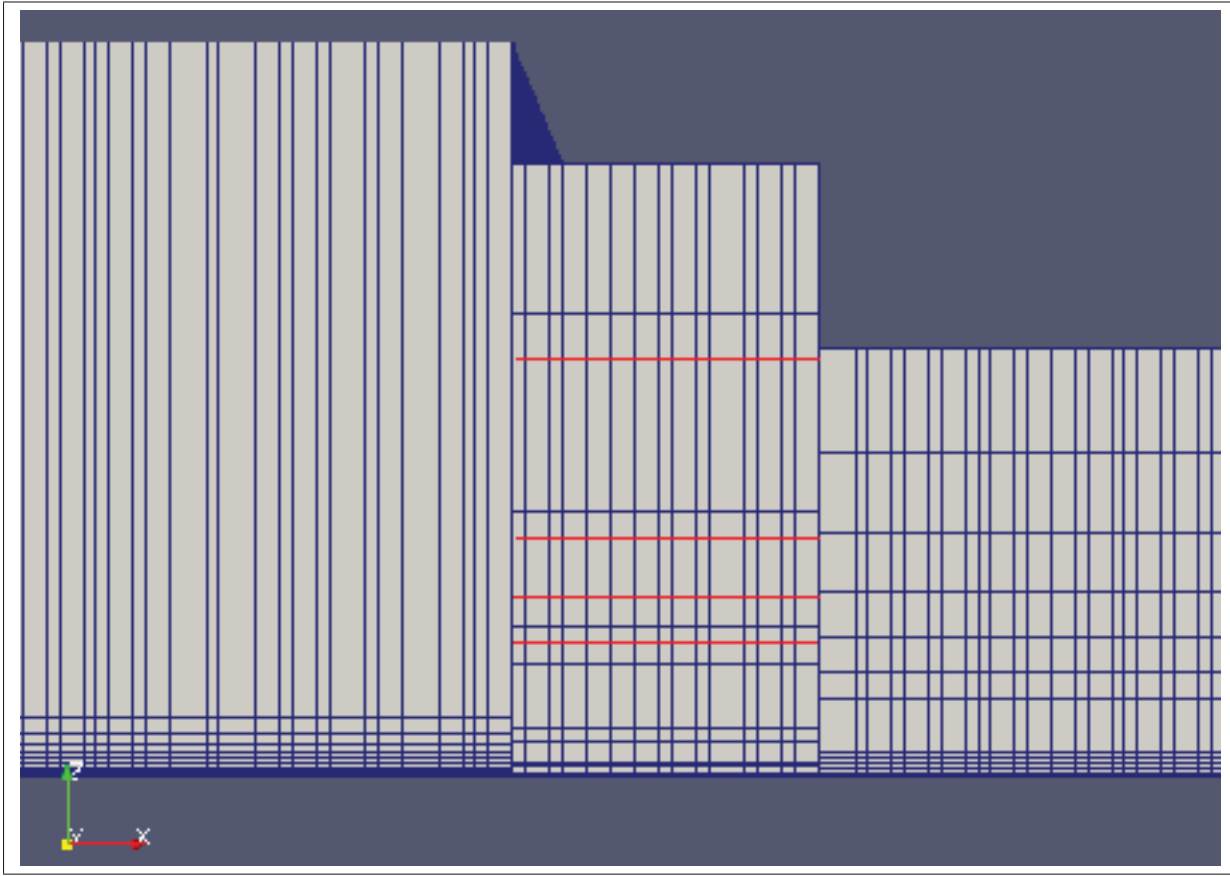


Figure 4.8 Vertical expansion for a domain height of $L=12D$ (left), $10D$ (center) and $7D$ (right)

Nevertheless, in terms of wind speed, the unequal vertical expansion has no effect and the results show a blockage effect when the domain height is $7D$. The blockage effect accelerates artificially the flow. This acceleration is no longer observed when the domain height is higher than $10D$ (fig. 4.9). So, the recommended height for the domain is ten times the turbine diameter ($10D$).

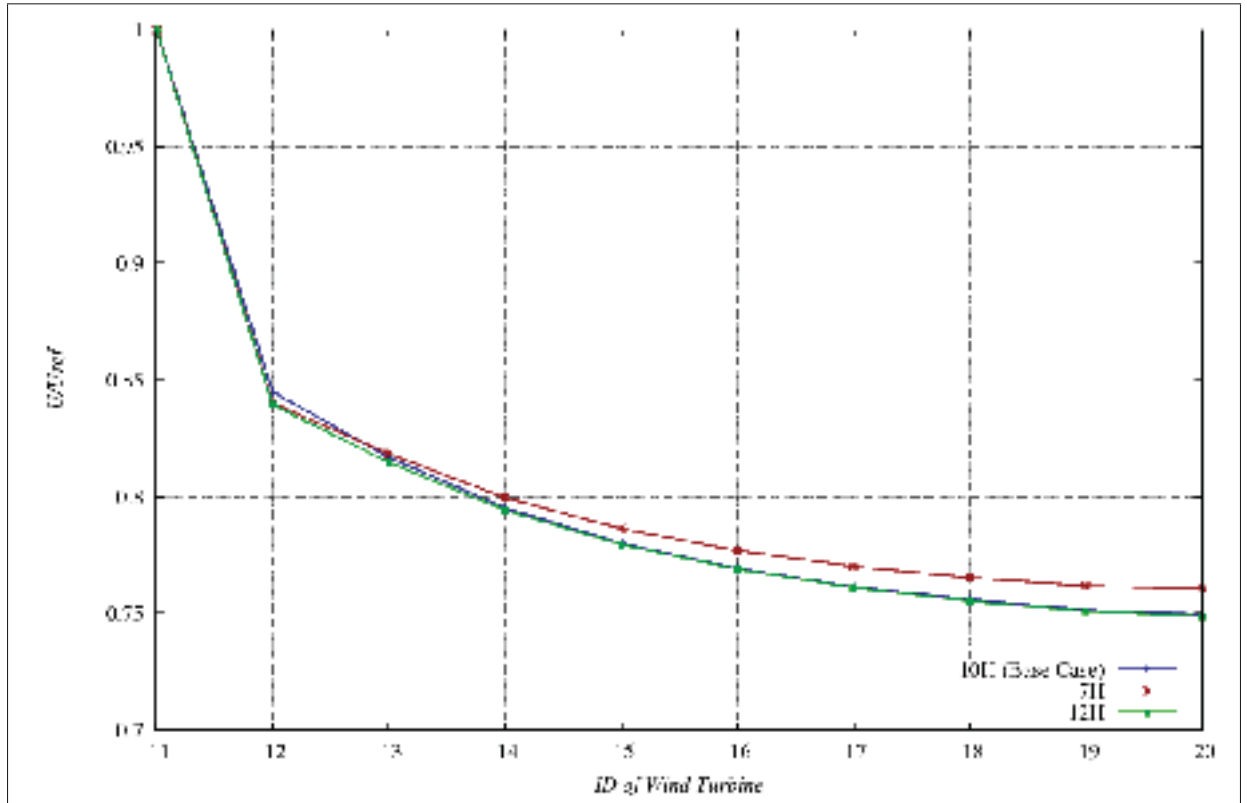


Figure 4.9 Wind speed ratios for the internal row positions depending on domain's height

d. **Up Stream Distance for Velocity**

The distance at which V_o is taken to apply the source term depends on the separation of two consecutive turbines. By checking the figure 4.10, in free stream (first point), 2 D is far enough from the actuator disk to avoid the effect of its presence. Nevertheless, since we deal with turbines located in the wake region, the wake of the previous turbine causes more wind speed deficit than the presence of the downstream turbine. In similar cases, V_o must be prescribed at 2 D in the upstream direction of the turbine where the wind speed is less affected by the surroundings.

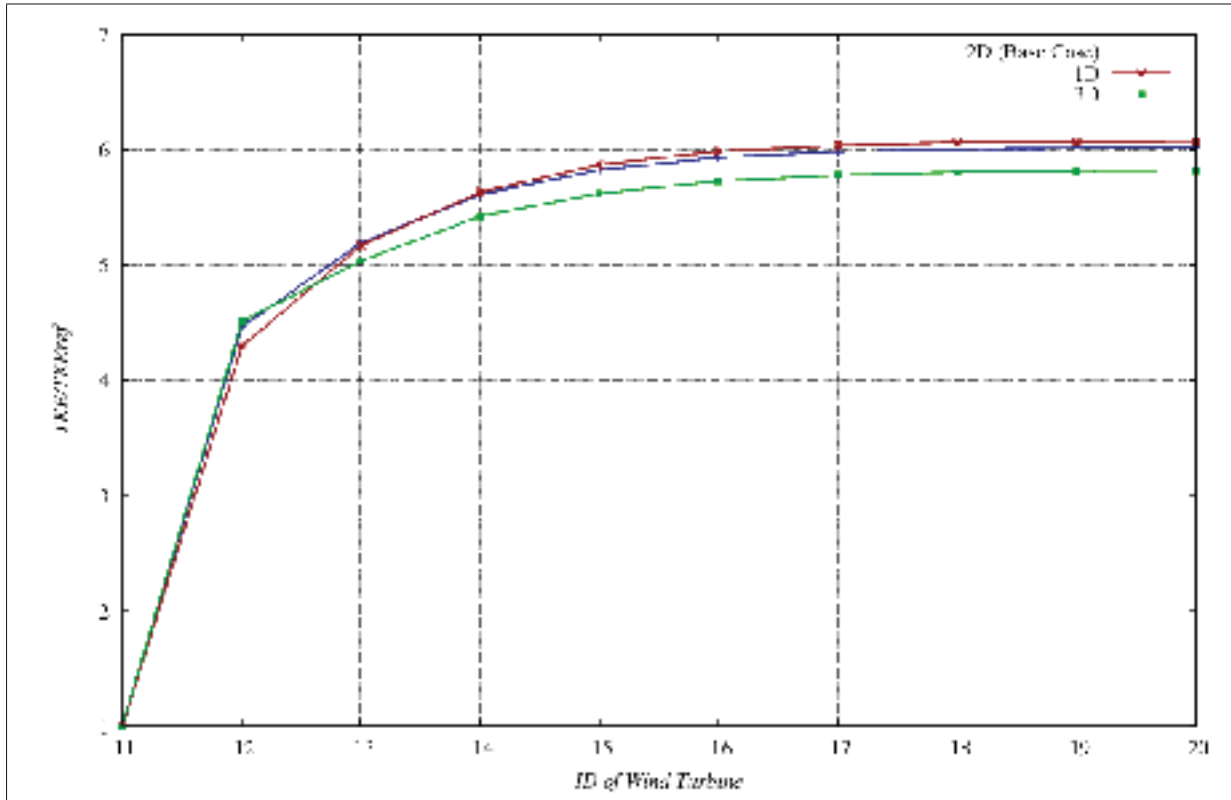


Figure 4.10 TKE for the internal row positions depending on the V_o applied to the source term

e. **Vertical levels**

The last parameter under study is the number of vertical levels of the computational domain. As it has been discussed previously, an increase of vertical levels implies a linear increase in computational cost. Nevertheless, it is important to have a minimum number of cells to capture in an accurate way the gradients of the fields of study. In flat terrain, and regardless of thermal effects, gradients at hub height are generally lower than in complex terrain, so, 20 verticals levels are enough to converge the results, in comparison to the 25 recommended in the preceding mesh sensitivity analysis of the third chapter. The relative error between 20 and 40 levels, in terms of wind speed is approximately 0.1%.

Table 4.3 shows an overview of the converged parameters taking as convergence criteria a difference lower than 1% in terms of wind speed between two consecutive cases (same criteria as for the first sensitivity analysis).

Table 4.3 Guideline of geometric parameters for CFD wake simulations over an offshore wind farm

| Geometric parameter | Recommended |
|--------------------------------|-------------|
| Horizontal resolution | 0.2D |
| Total vertical expansion ratio | 100 |
| Domain Height | 10 D |
| Up stream velocity | 2D |
| Vertical levels | 20 |

After having verified CFDWake 1.0 over flat terrain and using *blockMeshDict* application, it is time to compare the simulation results of the ideal case (with recommended parameters) to data measurements.

4.7 Validation results

Data at our disposal for validating the model correspond to one single velocity bin: $8m/s$ at hub height. Based on that, the simulations have been done with: $H_{ref} = 70m$ and $U_{ref} = 8m/s$. Using the power curve provided by the manufacturer, the power provided for each actuator disk can be reached. Finally, taken as reference the power obtained at freestream, the power ratios are calculated normalized to the power of the wind turbine located in freestream.

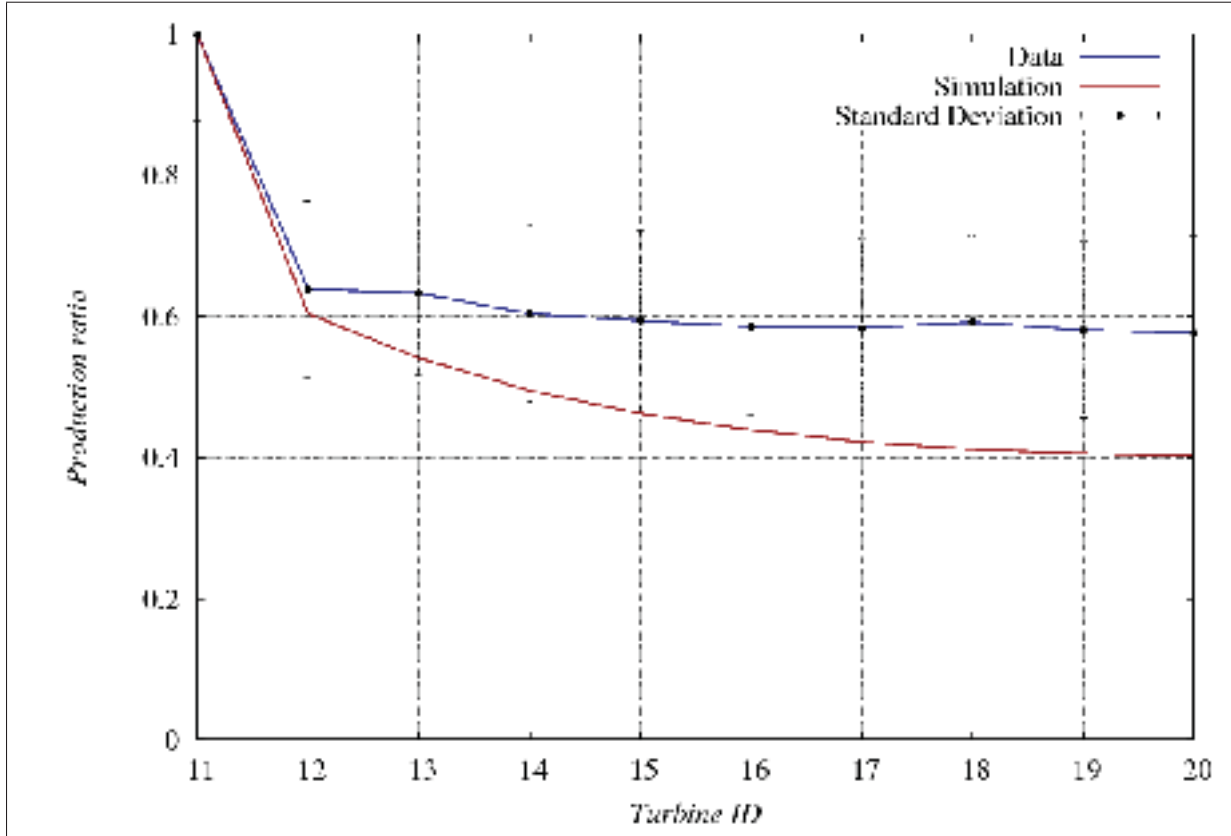


Figure 4.11 Comparison: Power ratio for center row. Data VS Simulation

This time, the average relative error is **30.35%**. As it can be observed in the figure 4.11, after achieving grid convergence, CFDWake1.0 model follow the general trend shown by the actuator disk model. An underestimation in terms of wind speed in the far wake of every actuator disk. Then, the recommended geometrical parameters could only be used as a starting point for a new grid convergence analysis using a different technic for turbulence model. The current model can not be considered as validated. Some future works and improvements are proposed in the conclusion.

CONCLUSION

With the aim of ever improving the understanding of physical phenomena and to better represent the behaviour of fluids, Computational Fluids Dynamics (CFD) has become the main tool in wind engineering during the last decades. While CFD has already shown great accuracy, the computational cost has always been the foremost obstacle to get over. The main goal of the memoir was to ensure good accuracy in results saving computational cost and time by optimizing the computational grid parameters, defining its geometry and ensuring the mesh independence in two specific cases of study: Using CFDWind1.0 over complex terrain and CFDWake1.0 over offshore terrain.

To achieve that goal, two mesh sensitivity analyse have been carried out. On the one hand, a study of freestream windflow for complex terrain. On the other hand, a wake model study over the Horns Rev offshore wind farm. CFDWind 1.0, the validated wind flow model developed at the National Renewable Energy Center of Spain (CENER) was used in both cases. CFDWind 1.0 model is based on the RANS solution of the Monin-Obukhov theory and the Richards and Hoxey (1993) computational approach. Thermal effects and Coriolis forces are neglected. In the first case, the grid was generated with WindMesh meshing tool developed at Barcelona Supercomputing Center. In the second one, two OpenFOAM's applications were used: *blockMeshDict* to generate the mesh and the *actuatorDisk* library to simulate wind turbines and to create wake effects.

In both cases the methodology was the same. First, geometrical parameters recommended in literature are chosen to build a basic case. Then, every parameter is modified keeping constant the remaining ones. A geometric value was considered optimum when the difference in terms of speed-up is lower than 1% over key positions previously selected between two consecutive cases. Results on turbulence kinetic energy are also taking into account. Once optimal parameters were chosen (table 4.4 for complex terrain and table 4.5 for offshore wind farm), the optimal mesh was built and the case was run until convergence of each physical variable is reached. The convergence criteria chosen was a difference lower than 1% in terms of wind

speed between two consecutive cases. Finally, simulation results were compared to field measurements.

Table 4.4 Guideline of geometric parameters for CFD wind simulations over complex terrain

| Geometric parameter | Recommended |
|-------------------------------|---|
| Δ_x | 20-30 m |
| N_z | 25 levels |
| Domain Height | 12 H |
| z_1 | 1 m |
| L_{WF} | 1 WF (+ an advisable extension of 0.25WF in the upstream direction) |
| L_{TZ} | 1 WF |
| L_{BZ} | 16 km |
| ratio $\frac{L_{BZ}}{L_{WF}}$ | 20 |

Table 4.5 Guideline of geometric parameters for CFD wake simulations over an offshore wind farm

| Geometric parameter | Recommended |
|--------------------------------|-------------|
| Horizontal resolution | 0.2D |
| Total vertical expansion ratio | 100 |
| Domain Height | 10 D |
| Up stream velocity | 2D |
| Vertical levels | 20 |

The speed-up results obtained on the complex terrain case have shown good accuracy to measurements. The average error was 2.23%. As other models, CFDWind 1.0 over the optimal mesh showed problems to fully represent the fluid behaviour over positions at steep slope areas in the upstream direction (see figs. 3.13 and 3.14). In these positions (18 to 26) all the models overestimated wind speed. It could be a hard task to discretize steep specific areas with cells of tens of meters. Nevertheless, the prediction error in these positions is still low. The simulation results on the considered positions with smoother slope in the upstream direction shown errors lower than 2% between simulation results and real data.

On the contrary, the mesh sensitivity analysis on CFDWake 1.0 wake model over flat terrain showed great difficulties to capture the wake effects within an offshore wind farm. In this sec-

ond study, the relative error between simulations and measurement data increase until 30.35%. The wake model present an important underestimation of wind speed (and hence, of wind power) with respect to measurement. It is clear that the computational limitations in this project have to see with the relative error. Although some of the parametric recommendations are a good starting point for future works, the upstream wind speed and estimation of the turbulence modelling can be highly optimized. Three ways of improvement in future work are proposed.

First of all, to represent the wake in an accurate way, it is important to apply the right source term to the actuator disk. As observed previously, the source term depends on the upstream wind speed (V_o or U_∞). In turn, V_o depends on where it has been assessed. To not depend on this parameter, Politis *et al.* (2011) present an iterative method providing through thrust coefficient and the axial induction factor an V_o not linked to the determination of a certain distance upstream of the actuator disk.

Another major domain of improvement is related to higher order turbulence models such as RSM (being studied at CENER) or LES. LES models are able to handle unsteady, anisotropic, turbulent flows dominated by large-scale structures and turbulent mixing. Jimenez *et al.* (2007) and Rethore (2009) have already shown the accuracy of LES in wake prediction in comparison to RANS modelisation. Nevertheless, nowadays, most of LES models are applied when there is just one turbine to model. In cases of offshore wind farms the computational cost is still an impassable drawback.

The last way to improve results proposed for further work is the Reynolds Stress Model (RSM). This approach, also called differential second-order closure model does not rely on the Boussinesq hypothesis, so it makes it suitable for anisotropic flows. As its name clarify, through this method, all the components of the Reynolds Stress Tensor are computed and the eddy viscosity approach is discarded. Six additional partial differential equations appear, then, the computational cost increases too. As for LES case, Cabezón *et al.* (2011b) have obtained results with good accuracy when applied to a single wind turbine, but with the current computers, the computational effort to simulate an entire wind farm is still too high. Therefore, in addition to the

improvement in terms of turbulence model, we must advance in terms of computational calculation to be able to represent the wakes over entire wind farms in an accurate way and within a reasonable time according to the industry.

APPENDIX I

FOLDERS STRUCTURE FOR AN ABL SIMULATION USING *SIMPLEFOAM* SOLVER

In this annex will be treated the points having more importance for an average execution of OpenFOAM. All the details are widely developed in OpenCFD (2009). The basic file structure of a *case* is divided in three main folders: *0*, *constant* and *system*. In addition, the *case* has to be contained in a *run*. *run* is located at the same height as *applications*, *turbulence models*, *lib* and *applications*, containing the different utilities offered by OpenFOAM that will be used.

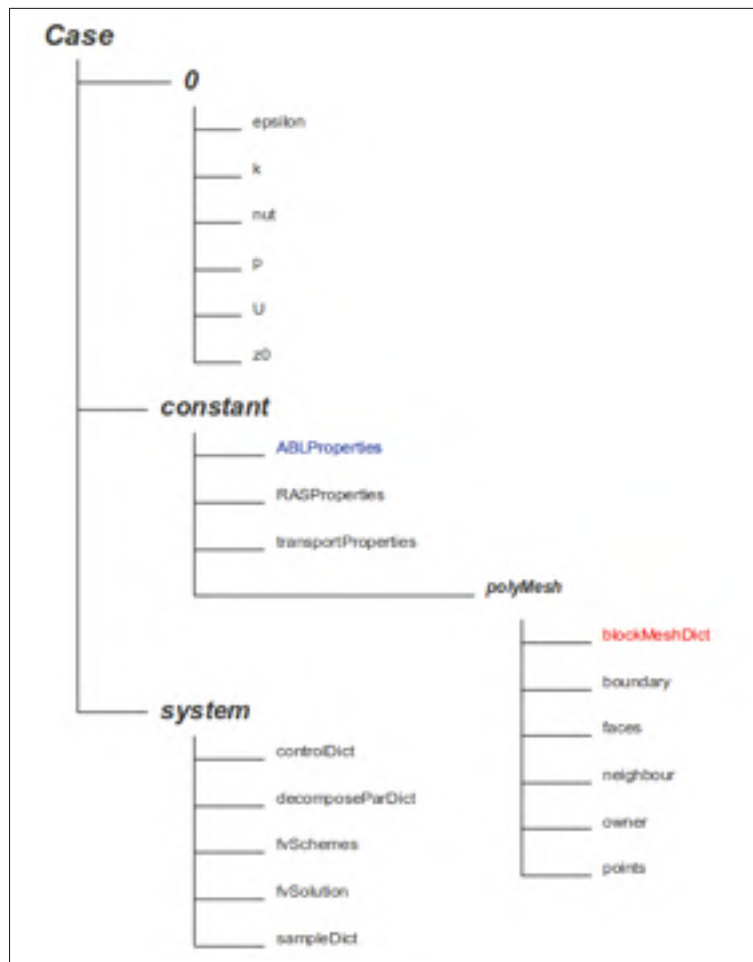


Figure I.1: File structure of an OpenFOAM case

1 0 folder

Contains the files where boundary conditions are set. There is one file for each different field (*epsilon*, *k*, *nut*, *p*, *U* and *z0*) and in each file, the profiles or values of the variables are set patch by patch. *k* and *epsilon* are added according to the utilization of *simpleFoam* solver and $k - \epsilon$ turbulent model. An identical folder (also called *Time directory* in the OpenFOAM's guide) will be created for each *writeInterval* time (see OpenCFD (2009)) containing the results of each field at each time. When running in parallel, before obtaining the folder of the *writeInterval* step, if the user want to know the results at time step 4000, he must may execute the command: **reconstructPar -time 4000**

2 constant folder

Contains the physical properties of the fluid (i.e. air viscosity), the model's constant and an entire definition of the discretized mesh in the folder *polyMesh*. Usually, the mesh is built by executing *blockMesh* command in the *case* folder. Nevertheless, in the wind flow model study, the file *blockMeshDict* does not exist since the mesh is created within WindMesh software. The files *boundary*, *faces*, *neighbour*, *owner* and *points* are outputs of WindMesh execution. Through *boundary* can be set the characteristics of each domain patch, among: *patch*, *wall*, *symmetryPlane*, *empty*, *wedge* or *cyclic*.

Observe *ABLProperties*. This file does not exist in OpenFOAM1.7. It allow to initialize the physical values inside the computational domain and on the patches. So convergence is favored.

3 system folder

Contains the files whereby the simulation is controled:

- *controlDict* control the execution time by choosing *startTime*, *endTime*
- *decomposeParDict* determines how the computational domain is divider in case of parallel running. The user can set two different aspects of the parallelization. The number of processors used and the method of decompososition of the domain (i.e. *hierarchical*, *simple*, *manual*,

metis)

- *fvSchemes* determine which numerical schemes are set and the different terms (divergence, converge, laplacians, etc...) are solved. On this work, only first and second order upwind discretization schemes will be used.

- *fvSolution* permits to set how accurate our results must be by fixing convergence tolerance, relaxation factors. In this file, user must choose the algorithm through which equations for velocity and pressure are solved.

- *sampleDict* is the only one of the *folder* used during post-processor, when simulation is over. Through *sampleDict* the user can set his interest fields and points or lines of study. By typing the command **sample -time 4000**, the user could know the exact values of his fields of interest in his points or lines of interest in the timestep 4000. A new *sets* folder will be create containing another folder called *4000*. The results are dump inside it.

APPENDIX II

WINDMESH

WindMesh is an inhouse code for meshing developed at Barcelona Supercomputing Center (BSC) and used by CENER to model wind farms for CFD simulations. This software need a map file and an inp file as inputs. After reading the map file, *WindMesh* execute a Delaunay triangulation to create the ground patch of the domain. Then, a vertical extrusion of the points composing the surface created is done up to the absolute top height (Z_{top}). Currently, an improvement including orthogonality of the mesh lines and elliptic smoothing is being tested at BSC. The grid is divided in three different zones: **Wind Farm Zone**, **Transition Zone** and **Buffer Zone** (II.1.) which have their own horizontal resolution. The geometric parameters that will define the mesh have to be introduced in II.2.

0.1 WindMesh input parameters

Before defining all the WindMesh parameters, it has to be pointed that the Wind Farm Zone (*FARM ZONE*) and the Transition Zone have to be contained inside the surface covered by the map file, where as Buffer Zone hasn't.

xmin, FARM ZONE: Lowest UTM coordinate in the East-West direction

xmax, FARM ZONE: Highest UTM coordinate in the North-South direction

ymin, FARM ZONE: Lowest UTM coordinate in the East-West direction

ymax, FARM ZONE: Highest UTM coordinate in the North-South direction

cell_size_x: Length of FARM ZONE cells in meters in the x direction

cell_size_y: Length of FARM ZONE cells in meters in the y direction

size_left(m), TRANSITION ZONE: western extension of the transition zone

size_right(m), TRANSITION ZONE: eastern extension of the transition zone

size_bottom(m), TRANSITION ZONE: southern extension of the transition zone

size_top(m), TRANSITION ZONE: northern extension of the transition zone

size_left(m), BUFFER ZONE: western extension of the buffer zone

size_right(m), **BUFFER ZONE**: eastern extension of the buffer zone

size_bottom(m), **BUFFER ZONE**: southern extension of the buffer zone

size_top(m), **BUFFER ZONE**: northern extension of the buffer zone

cell_size_x: Length of buffer zone cells in meters in the x direction

cell_size_y: Length of buffer zone cells in meters in the y direction

ztop: Height of the domain in meters (above the lowest point of the surface)

cell_distribution: Type of vertical distribution cell

first_cell_height: Height of the first cell

number_of_cells: Number of vertical levels

default_value, **ROUGHNESS**: Roughness length over the terrain (z_0)

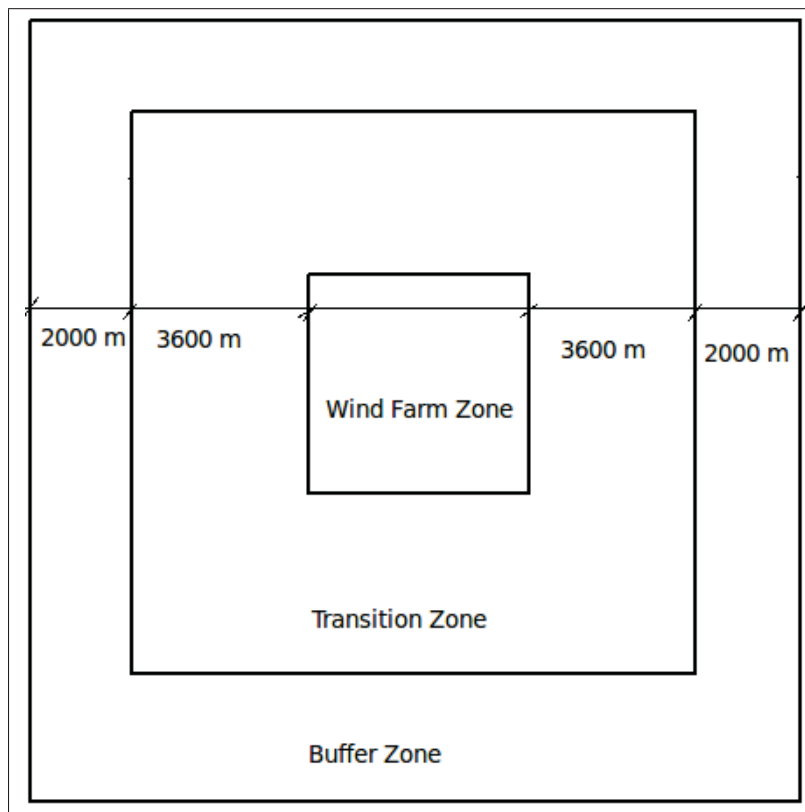


Figure II.1: Scheme of surface's zones

```

MESH
  FARM_ZONE
    xmin = 567000
    xmax = 570600
    ymin = 4730500
    ymax = 4734100
    cell_size_x = 20
    cell_size_y = 20

  TRANSITION_ZONE
    size_left_(m) = 3600
    size_right_(m) = 3600
    size_bottom_(m) = 3600
    size_top_(m) = 3600

  BUFFER_ZONE
    size_left_(m) = 2000
    size_right_(m) = 2000
    size_bottom_(m) = 2000
    size_top_(m) = 2000
    cell_size_x = 600
    cell_size_y = 600

  VERTICAL
    ztop = 2350 (m above the lowest point)
    cell_distribution = geometric (options: linear / geometric)
    first_cell_size = 1
    number_of_cells = 30

  BUFFER
    smooth_buffer = yes
    elevation_buffer = -99. (use -99. for program estimation)

  GEOMETRY
    TOPOGRAPHY
      topo_file = Montecarrio.map (options: filename / none)
      format_topo_file = map (options: map)

  ROUGHNESS
    default_value = 0.03

```

Figure II.2: Example of inp file

APPENDIX III

RESULTS I: MESH CONVERGENCE OF CFDWIND1 FOR COMPLEX TERRAIN. WIND SPEED RATIOS AT WIND TURBINE POSITIONS

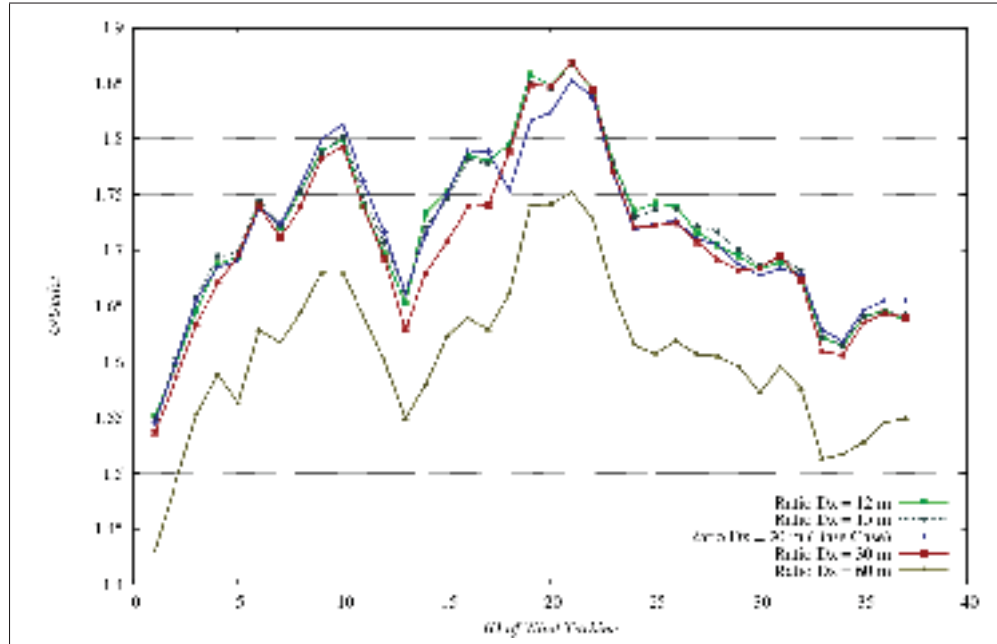


Figure III.1: Wind speed ratios ($U_{ref} = 8m/s$) in the wind turbine positions for different HORIZONTAL RESOLUTION

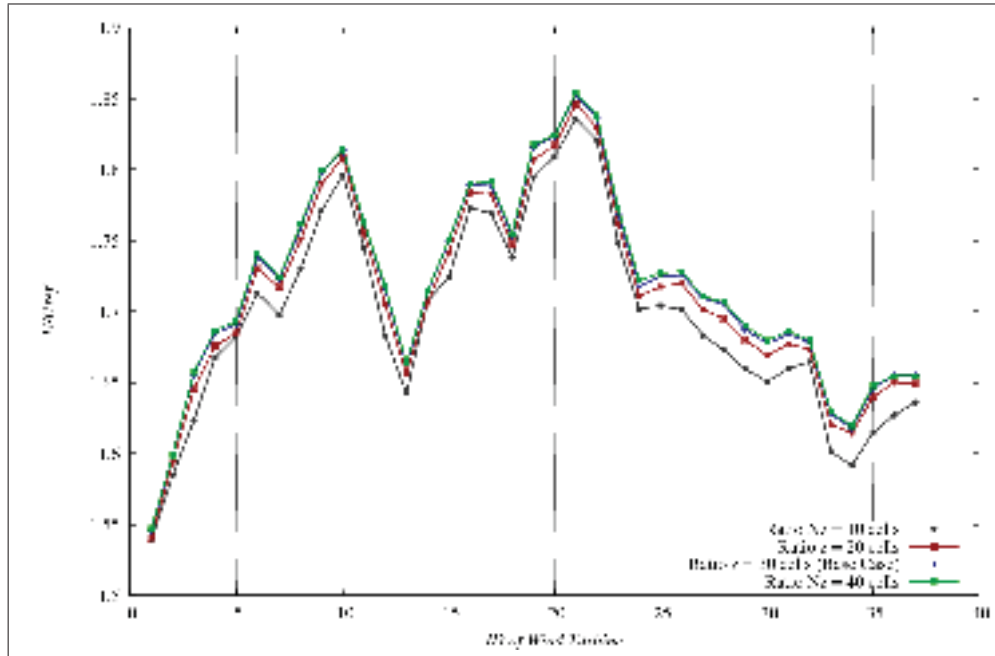


Figure III.2: Wind speed ratios ($U_{ref} = 8 \text{ m/s}$) in the wind turbine positions for different VERTICAL LEVELS

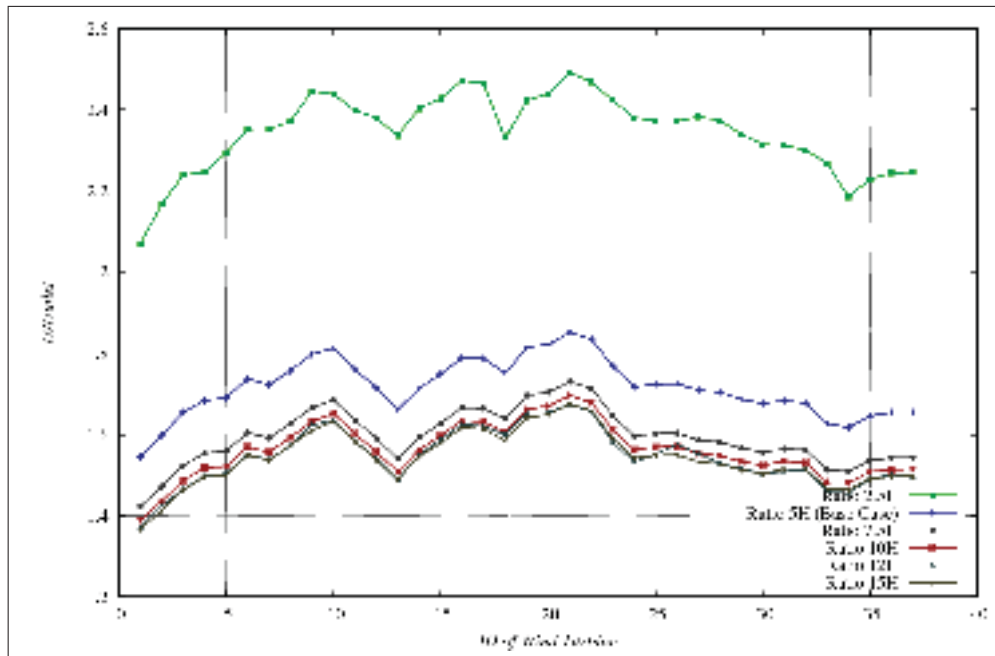


Figure III.3: Wind speed ratios ($U_{ref} = 8 \text{ m/s}$) in the wind turbine positions for different DOMAIN HEIGHTS

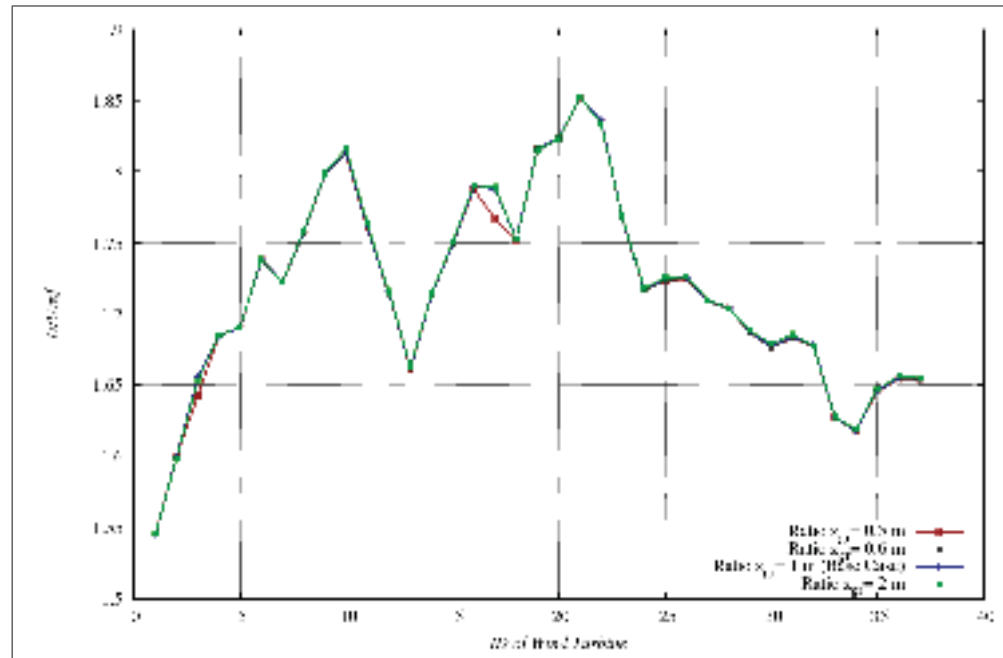


Figure III.4: Wind speed ratios ($U_{ref} = 8m/s$) in the wind turbine positions for different HEIGHT OF THE GROUND CELL

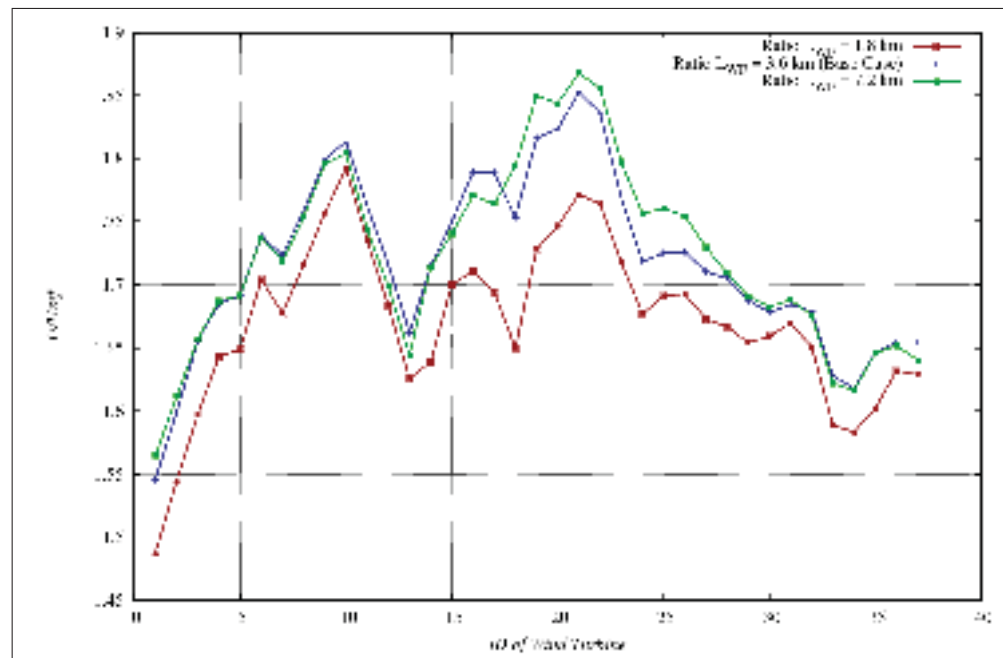


Figure III.5: Wind speed ratios ($U_{ref} = 8m/s$) in the wind turbine positions for different WIND FARM LENGTHS

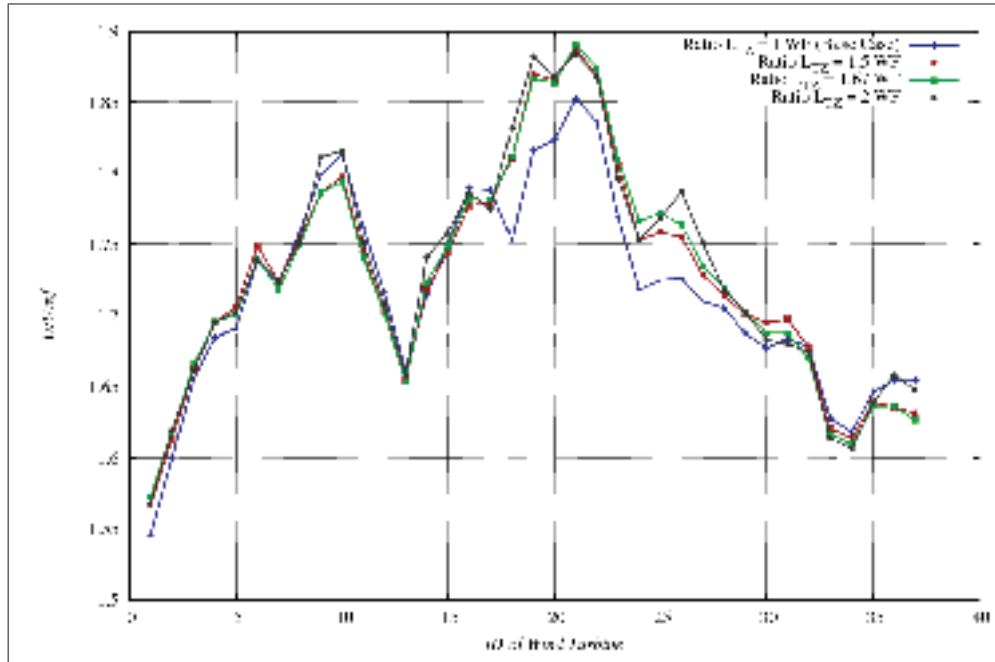


Figure III.6: Wind speed ratios ($U_{ref} = 8 \text{ m/s}$) in the wind turbine positions for different TRANSITION ZONE LENGTHS (BUFFER ZONE OF 2 KM)

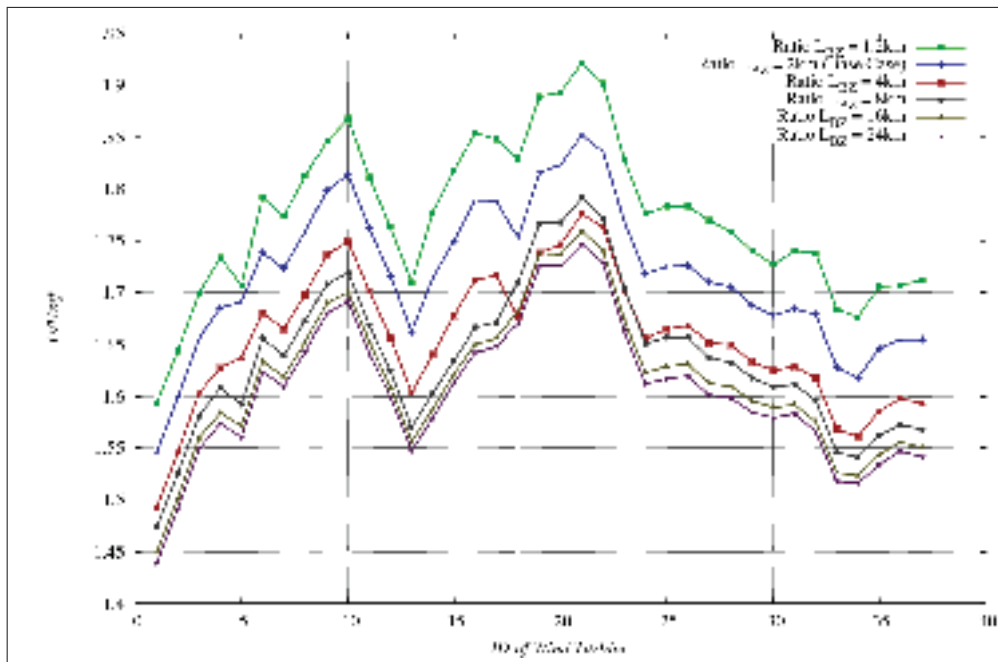


Figure III.7: Wind speed ratios ($U_{ref} = 8 \text{ m/s}$) in the wind turbine positions for different BUFFER ZONE LENGTHS

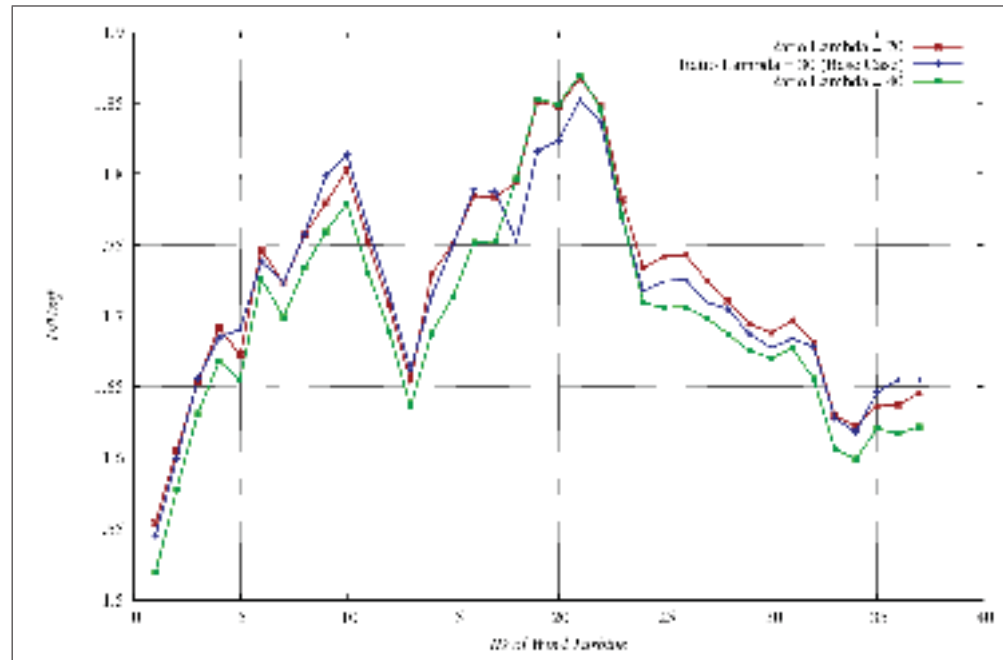


Figure III.8: Wind speed ratios ($U_{ref} = 8m/s$) in the wind turbine positions for different λ RATIO

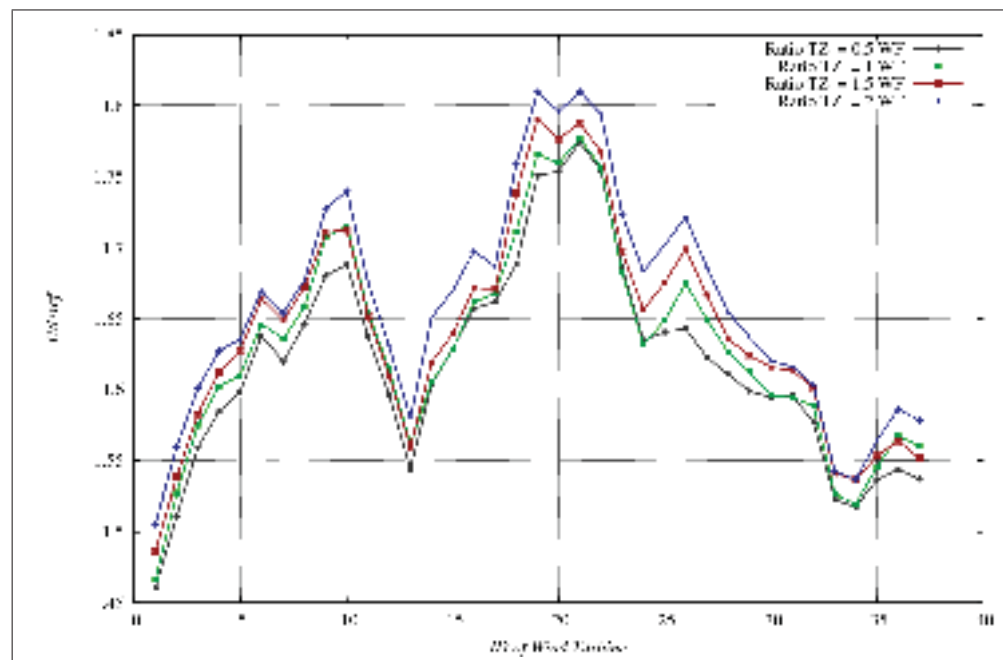


Figure III.9: Wind speed ratios ($U_{ref} = 8m/s$) in the wind turbine positions for different TRANSITION ZONE LENGTHS (BUFFER ZONE OF 8 KM)

APPENDIX IV

RESULTS II: MESH CONVERGENCE OF CFDWAKE1 FOR OFFSHORE. WIND SPEED RATIOS AT REFERENCE POSITIONS (U_{REF}) FOR THE CENTRAL ROW

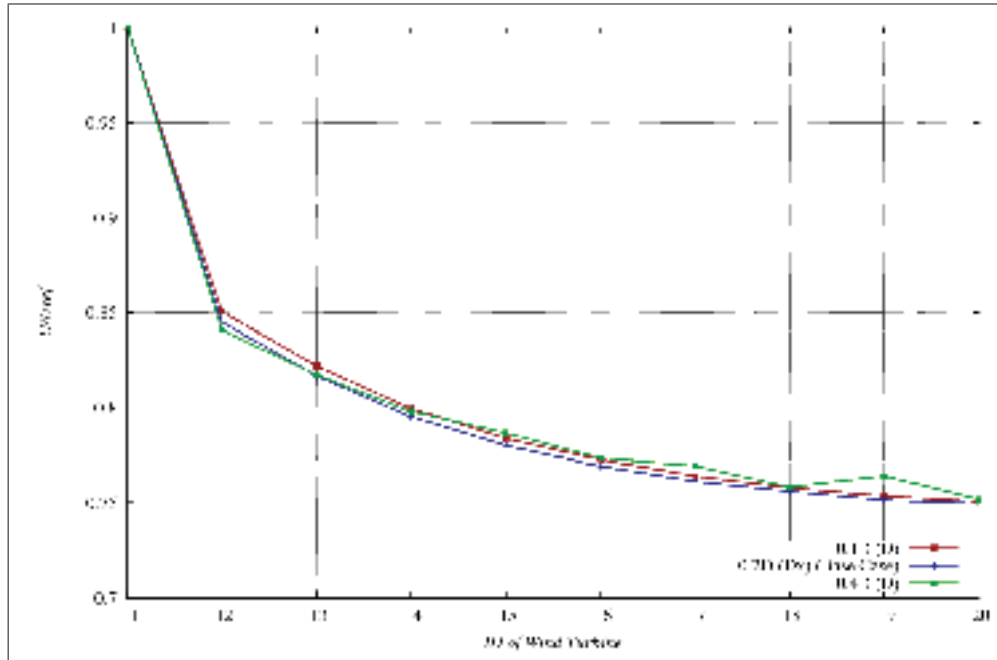


Figure IV.1: Wind speed ratios ($U_{ref} : U_{freestreamturbine}$) in the wind turbine positions of the central row for different HORIZONTAL RESOLUTION

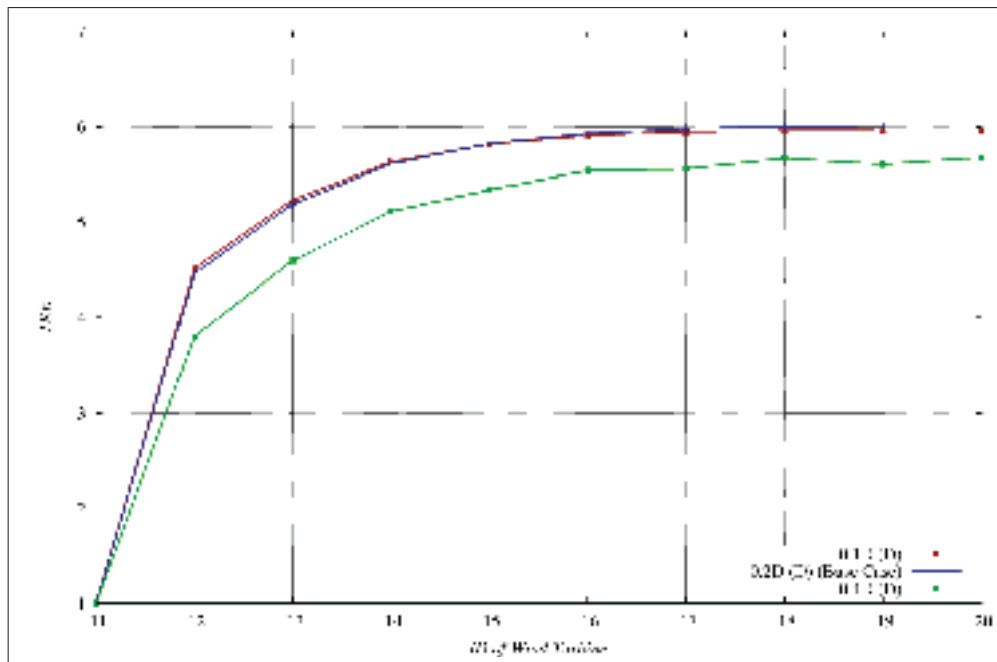


Figure IV.2: TKE ratios ($TKE_{ref} : TKE_{freestreamturbine}$) in the wind turbine positions of the central row for different HORIZONTAL RESOLUTION

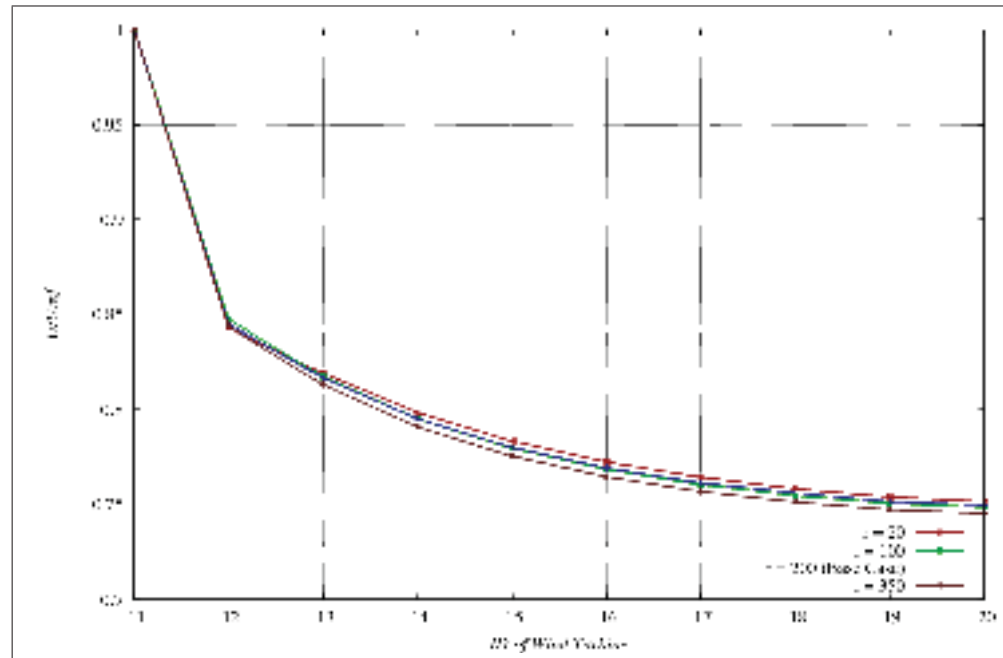


Figure IV.3: Wind speed ratios ($U_{ref} : freestreamturbine$) in the wind turbine positions of the central row for different VERTICAL EXPANSION RATIO

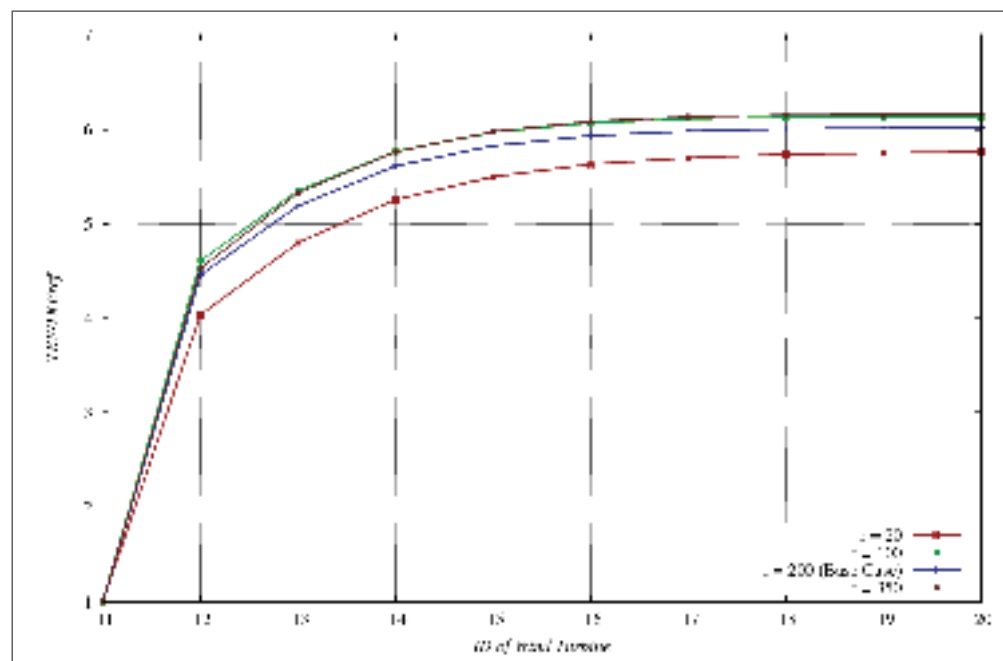


Figure IV.4: TKE ratios ($TKE_{ref} : freestreamturbine$) in the wind turbine positions of the central row for different VERTICAL EXPANSION RATIO

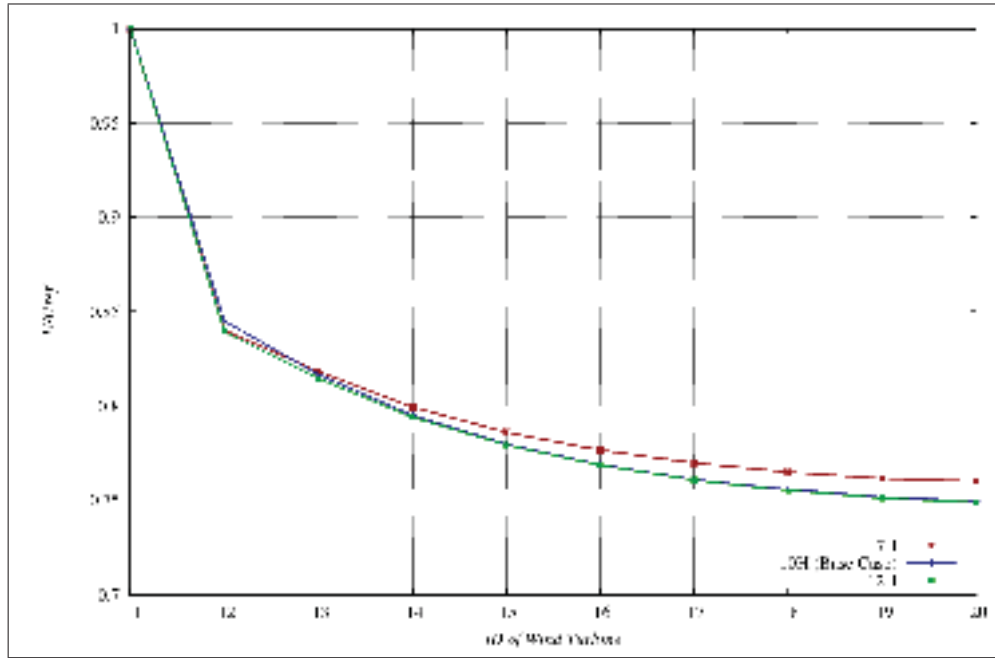


Figure IV.5: Wind speed ratios ($U_{ref} : freestreamturbine$) in the wind turbine positions of the central row for different DOMAIN HEIGHTS

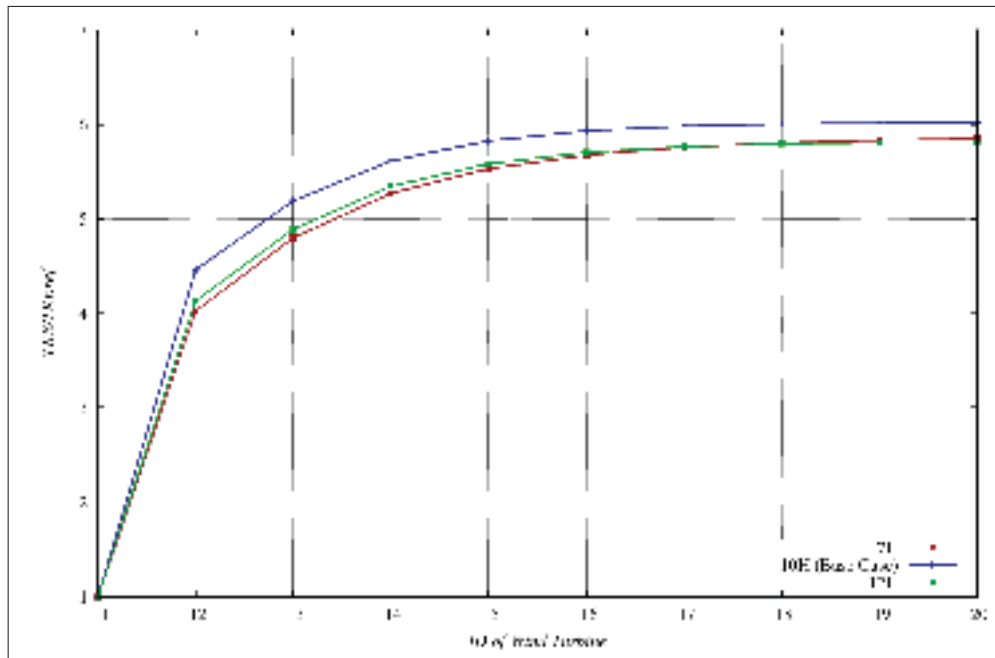


Figure IV.6: TKE ratios ($TKE_{ref} : freestreamturbine$) in the wind turbine positions of the central row for different DOMAIN HEIGHTS

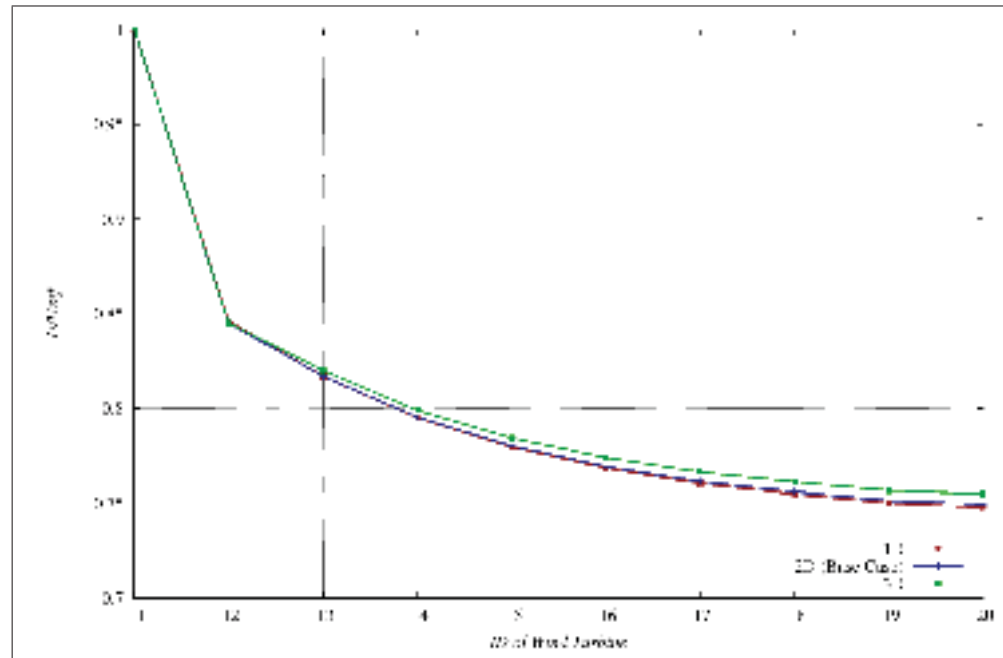


Figure IV.7: Wind speed ratios ($U_{ref} : \text{freestreamturbine}$) in the wind turbine positions of the central row for different UPSTREAM DISTANCE

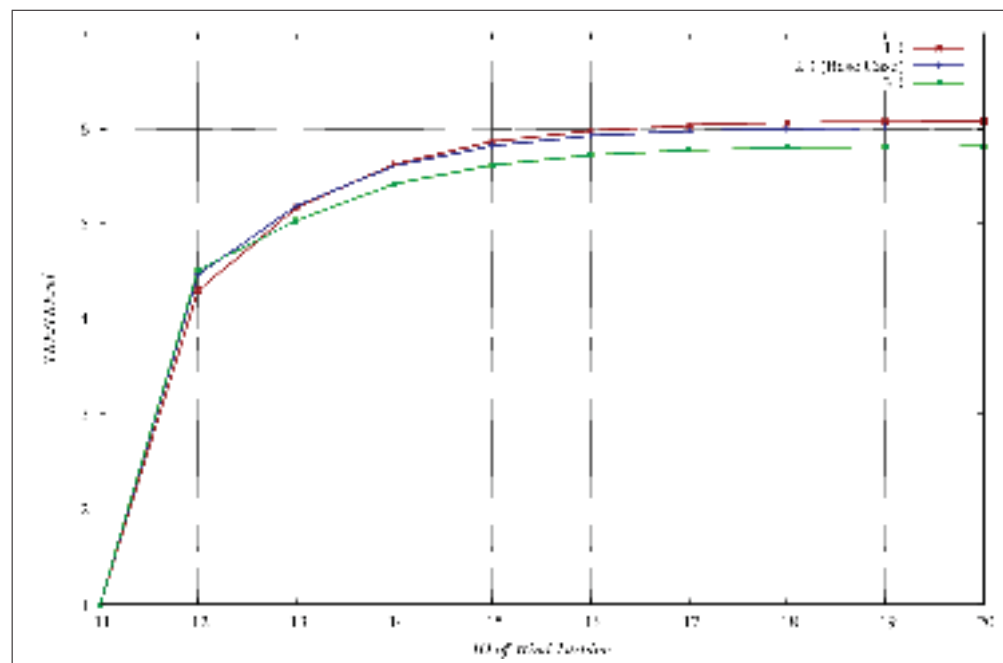


Figure IV.8: TKE ratios ($TKE_{ref} : \text{freestreamturbine}$) in the wind turbine positions of the central row for different UPSTREAM DISTANCE

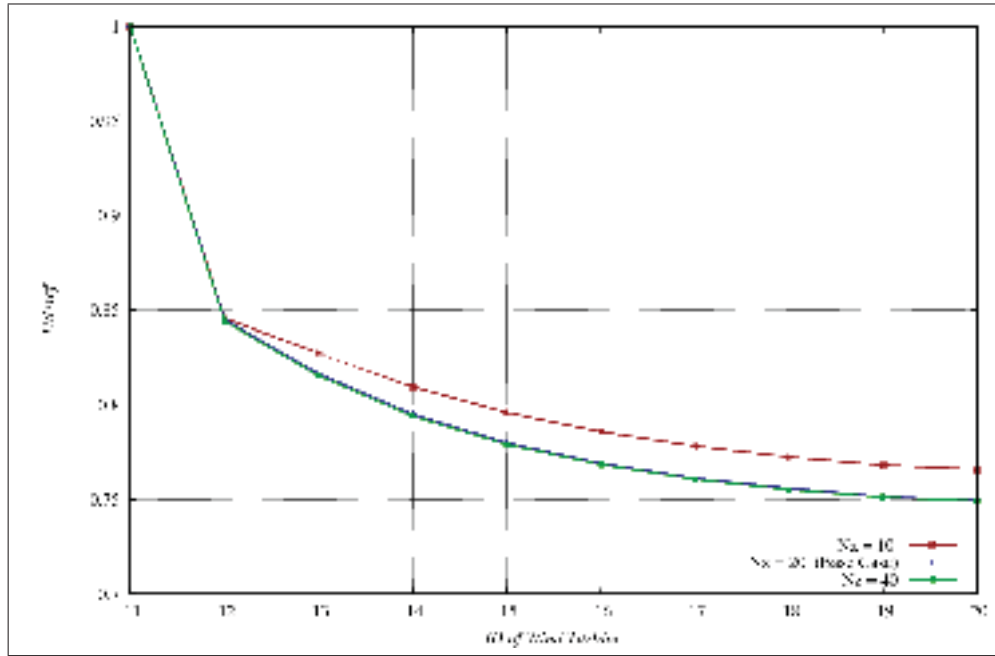


Figure IV.9: Wind speed ratios ($U_{ref} : freestreamturbine$) in the wind turbine positions of the central row for different NUMBER OF VERTICAL LEVELS

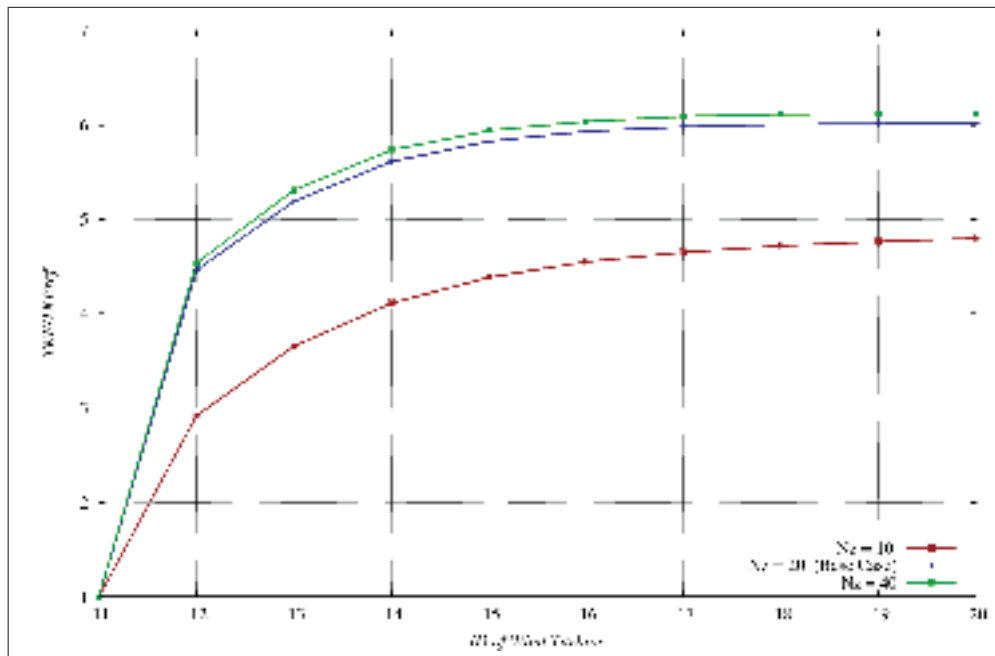


Figure IV.10: TKE ratios ($TKE_{ref} : freestreamturbine$) in the wind turbine positions of the central row for different NUMBER OF VERTICAL LEVELS

BIBLIOGRAPHY

- Anderson, J., 1995. *Computational Fluid Dynamics, The basics With Applications*. McGraw-Hill, Inc.
- Ansys, I. April 2009. *Ansys CFX Tutorials, Release 12.0*.
- Bakker, A. 2002. Lecture 10 - turbulence models. applied computational fluid dynamics. Power-Point presentation.
- Bechmann, A., J. Berg, M.S. Courtney, H.S. Jorgensen, J. Mann, and N.N. Sorensen. July 2009a. *The bolund experiment: Overview and background*. Technical report. Risø-DTU.
- Bechmann, A., J. Berg, M.S. Courtney, H.S. Jorgensen, J. Mann, and N.N. Sorensen. 2009b. The bolund experiment: Blind comparison of flow models.
- Blocken, B., T. Stathopoulos, and J. Carmeliet. 2007. "CFD simulation of the atmospheric boundary layer: wall function problems". *Atmospheric Environment*, p. 238-252.
- Bowen, A. and N.G. Mortensen. 1996. "Exploring the limits of WAsP, The Wind Atlas Analysis and Application Program". *European Union Wind Energy Conference*, p. 584-587.
- Cabezón, D., A. Iniesta, and I. Martí E. Ferrer. 2005. Comparing wasp and fluent for highly complex terrain wind prediction. J. Peinke, P. S. S. B., editor, *Proceedings of the Eurotech Colloquium*, p. 275-279. Springer.
- Cabezón, D., J. Sanz, and J. Van Beeck. 2007. Sensitivity analysis on turbulence models for the abl in complex terrain. *EWEK 2007 scientific proceedings*, Milano, Italy, 2007.
- Cabezón, D., Sumner J., García B., Sanz Rodrigo J., and Masson C. March 2011a. Rans simulations of wind flow at the bolund experiment. *EWEK 2011 scientific proceedings*, Brussels, Belgium, March 2011a.
- Cabezón, D., E. Migoya, and A. Crespo. 2011b. "Comparison of turbulence models for the computational fluid dynamics simulation of the wind turbine wakes in the atmospheric boundary layer". *Wind Energy*, p. 909-921.
- Carson, J. S. 2002. "Model Verification and Validation". *Proceedings of the Winter Simulation Conference*, p. 52-58.
- Elsamprojekt. 2000. *Horns rev offshore wind farm. environmental impact assessment, summary of eia report*. Technical report. EIA.
- Franke, J., A. Hellsten, H. Schlünzen, and B. Carissimo. 2007. *Best practice guideline for the cfd simulation of the flows in the urban environment*. Technical report. COST office.

- Frey, H., A. Mokhtari, and S.R. Patil. 2002. Identification and review of sensitivity analysis methods.
- IEA. 2010. *World Energy Outlook*.
- Jimenez, A., A. Crespo, E. Migoya, and J. Garcia. 2007. "Advances in large-eddy simulation of a wind turbine wake". *Journal of Physics: Conference Series*, p. 1-13.
- Jones, W. and B.E. Launder. 1972. "The prediction of laminarization with a two-equation model of turbulence". *Int. J. Heat Mass Transfer*, p. 301-314.
- Kasmi, A. E. and C. Masson. 2010. "Turbulence modeling of atmospheric boundary layer flow over complex terrain: A comparison of models at wind tunnel and full scale". *Wind energy*, p. 689-704.
- Kuo, K., 2005. *Principles of combustion*. 2nd edition. Wiley.
- Manwell, J., J.G. McGowan, and A.L. Rogers, 2009. *WIND ENERGY EXPLAINED, Theory, design and application*. 2nd edition. Wiley.
- Martinez, B. June 2011. Wind resource in complex terrain with openfoam. Master's thesis, Technical University of Denmark.
- Mokhtari, A., H.C. Frey, and J. Zheng. 2005. "Recommended Practice Regarding Selection, Application and Interpretation of Sensitivity analysis Methods Applied to Microbial Food Safety Process Risk Models". *Human and Ecological Risk Assessment*, p. 591-605.
- OpenCFD. July 2009. *OpenFOAM: The Open Source CFD Toolbox – User Guide v1.7*.
- Palma, J., F.A. Castro, L.F. Ribeiro, A.H. Rodrigues, and A.P.Pinto. 2008. "Linear and non-linear models in wind resource assessment and wind turbine micro-siting in complex terrain". *Journal of Wind Engineering and Industrial Aerodynamics*, p. 2308-2326.
- Panofsky, H., D.H. Lenschow H. Tennekes, and J.C. Wyngaard. 1977. "The characteristics of turbulent velocity components in the surface layer under convective conditions". *Boundary-Layer Meteorology*, p. 355-361.
- Patil, S. and H.C. Frey. 2004. "Comparison of Sensitivity Analysis Methods Based on Applications to a Food Safety Risk Assessment Model". *Risk Analysis*, p. 573-585.
- Pereira, R., R. Guedes, and C. Silva Santos. 2010. Comparing wasp and cfd wind resource estimates for the "regular" user.
- Politis, E. S., J. Prospathopoulos, D. Cabezón, K. S. Hansen, P. K. Chaviaropoulos, and R. Barthelmie. 2011. "Modelling wake effects in large wind farms in complex terrain: the problem, the methods and the issues". *Journal of Wind Energy*.

- Rethore, P.-E. 2009. *Wind turbine wake in atmospheric turbulence*. PhD thesis, Aalborg University, Department of Civil Engineering.
- Richards, P. and R. Hoxey. 1993. “Appropriate boundary conditions for computational wind engineering models using the k- ϵ turbulence model”. *Journal of Wind Engineering and Industrial Aerodynamics*, p. 145-153.
- Roache, P. October 2008. Validation: Definition or description. *Proceedings of the 3rd Workshop on CFD Uncertainty Analysis*, Lisbon, Portugal, October 2008.
- Sanz, J., D. Cabezon, I. Marti, P. Patilla, and J. van Beeck. 2008. Numerical cfd modelling of non-neutral atmospheric boundary layers for offshore wind resource assessment based on monin-obukhov theory. *EWEc scientific proceedings*, Brussels, Belgium, 2008.
- Sorensen, N. 1995. *General Purpose Flow Solver Applied to Flow over Hills*. PhD thesis, Technical University of Denmark.
- Spalart, P. 2009. “Detached-Eddy Simulation”. *Annual Review of Fluid Mechanics*, p. 181-202.
- Stangroom, P. 2004. *CFD Modelling of Wind Flow Over Terrain*. PhD thesis, University of Nottingham.
- Stull, R., 2009. *An Introduction to boundary layer meteorology*, volume 13 of *Atmospheric and Oceanographic Sciences Library*. Springer.
- Theodoropoulos, P. 2010. Validation and comparison between cfd and linear wasp model performance in vertical profile estimation using measurements from a 65m tall mast.
- Venayagamoorthy, S., J.R. Koseff, J.H. Ferziger, and L.H. Shih. 2003. “Testing of RANS turbulence models for stratified flows based on DNS data”. *Center for Turbulence Research. Annual Research Briefs*, p. 127-138.
- Versteeg, H. and W. Malalasekera, 2007. *An introduction to Computational Fluid Dynamics, The Finite Volume Method*. 2 edition. Pearson Education Limited.
- Wilcox, D., 1994. *Turbulence Modeling for CFD*. DCW Industries, Inc and La Cañada.
- Wolton, P. 2008. Wind farm wake prediction using cfd. Master’s thesis, University of Colorado.